

CONTRACT NAS8-20223

ACOUSTIC SCALE-MODEL TESTS OF HIGH-SPEED FLOWS PHASE II FINAL REPORT

DECEMBER 1966

prepared for

NATIONAL AERONAUTICS AND SPACE ADMINISTRATION
GEORGE C. MARSHALL SPACE FLIGHT CENTER
HUNTSVILLE, ALABAMA

prepared by

MARTIN COMPANY
A DIVISION OF MARTIN MARIETTA CORPORATION
DENVER, COLORADO

N67-33243

FACILITY FORM 902

(ACCESSION NUMBER)	(THRU)
10/19 RS 25	
(PAGES)	(CODE)
297	28
CR-87315 290	
(NASA CR OR TMX OR AD NUMBER)	(CATEGORY)

29B
Martin-CR-66-75

END

25
Contract NAS8-20223


29A CV

3 ACOUSTIC SCALE-MODEL TESTS OF
HIGH-SPEED FLOWS
PHASE II FINAL REPORT 6
- 1/4 - 4
9 December 1966 10 CV

Authors

6 E. B. Smith
W. L. Brown 9

Approved



L. F. Nicholson, Manager
Advanced Ground Systems Department

1 MARTIN COMPANY
A DIVISION OF MARTIN-MARIETTA CORPORATION
6 Denver, Colorado 3

FOREWORD

This report is submitted in accordance with Contract NAS8-20223, Acoustic Scale-Model Tests of High-Speed Flows, Phase II. This study has been administered by the Unsteady Aerodynamics Branch, National Aeronautics and Space Administration, George C. Marshall Space Flight Center, Huntsville, Alabama.

The following Martin Company personnel other than the authors were primarily responsible for the indicated work areas during the course of the contract work:

D. Dowell - Propulsion System and Facility;

P. E. Bingham - Test Engineer.

CONTENTS

	<u>Page</u>
Foreword	ii
Contents	iii
Summary	viii
Nomenclature	ix and x
I. Introduction	1
II. Test Plan	2
A. Program Firings	2
B. Test Fixture	4
C. Acoustic Measurements	4
III. Propulsion System and Engine Performance	8
A. Propulsion System	8
B. Engine Performance	19
IV. Data Acquisition and Analysis Systems	29
A. Data Acquisition System and Procedures	29
B. Data Reduction System and Procedures	35
V. Results of Program Firings	39
A. Analysis Procedure	39
B. Results	41
VI. Discussion of Data and Data Comparison	44
A. Overall Acoustic Power Level	47
B. Acoustic Power Spectrum	49
C. Directivity Index	56
D. Apparent Source Location	59
E. Near Field	62
VII. Conclusions	68
VIII. Recommendations	70
IX. References	71
X. Bibliography	73 thru 75

Appendix A -- Data Tabulation	A-1 thru A-32
---	---------------------

Figure

II-1	Far-Field Measurement Locations	5
II-2	Near-Field Measurement Locations	6
III-1	Engine Assembly Schematic	12
III-2	Engine Case and Igniter	13
III-3	Propellant System Schematic	15
III-4	Engine Thrust Stand	16
III-5	Firing Sequence	18
III-6	Engine Chamber Pressure Time History, Firing No. 9	21
III-7	Engine Chamber Pressure Time History, Firing No. 10	22
III-8	Engine Chamber Pressure Time History, Firing No. 11	23
III-9	Twelve-Engine Cluster, Firing No. 9	24
III-10	Twelve-Engine Circular Cluster, Engine Cant Angle = 15 deg, Firing No. 10	25
III-11	Twelve-Engine Circular Cluster, Engine Cant Angle = 0 deg, Firing No. 11	26
III-12	Multiple-Engine Cluster Configurations	27
IV-1	Far-Field Microphone System Installation	30
IV-2	Block Diagram of Data Reduction System	32
IV-3	Block Diagram of Acoustic Data Acquisition System	36
IV-4	Signal-to-Noise Ratio 1/3-Octave Band	38
V-1	1/3-Octave Band Power Spectrums of Four Program Firings	43
VI-1	Comparison of Acoustic Efficiency, η	48
IV-2	Correlation of Acoustic Power Spectrums	51
VI-3	Comparison of Nondimensional Power Spectrums	52
IV-4	Correlation and Comparison of Octave Band Power Spectrums	53

VI-5	Power Spectra Correlation Using Subsonic Parameters	55
IV-6	Comparison of the Overall Directivity Indices	58
IV-7	1/3-Octave Band Directivity Index Comparison for Selected Frequencies	60
IV-8	Apparent Source Location Data Compared with Other Results	61
IV-9	Near-Field SPL Spectra at 16 D _e from NEP	64
IV-10	Near-Field SPL Spectra at the NEP for the Twelve-Engine Firings	66
IV-11	Near-Field SPL Spectra at the NEP	67
A-1a	SPL Distribution Traverse Microphone Program Firing No. 2	A-14
A-1b	SPL Distribution Traverse Microphone Program Firing No. 2	A-15
A-1c	SPL Distribution Traverse Microphone Program Firing No. 2	A-16
A-2a	SPL Distribution Traverse Microphone Program Firing No. 3	A-17
A-2b	SPL Distribution Traverse Microphone Program Firing No. 3	A-18
A-2c	SPL Distribution Traverse Microphone Program Firing No. 3	A-19
A-3a	SPL Distribution Traverse Microphone Program Firing No. 4	A-20
A-3b	SPL Distribution Traverse Microphone Program Firing No. 4	A-21
A-3c	SPL Distribution Traverse Microphone Program Firing No. 4	A-22
A-4a	SPL Distribution Traverse Microphone Program Firing No. 5	A-23
A-4b	SPL Distribution Traverse Microphone Program Firing No. 5	A-24
A-4c	SPL Distribution Traverse Microphone Program Firing No. 5	A-25
A-5a	SPL Distribution Traverse Microphone Program Firing No. 8	A-26

A-5b	SPL Distribution Traverse Microphone Program Firing No. 8	A-27
A-5c	SPL Distribution Traverse Microphone Program Firing No. 8	A-28
A-6a	SPL Distribution Traverse Microphone Program Firing No. 9	A-29
A-6b	SPL Distribution Traverse Microphone Program Firing No. 9	A-30
A-7a	SPL Distribution Traverse Microphone Program Firing No. 10	A-31
A-7b	SPL Distribution Traverse Microphone Program Firing No. 10	A-32

Table

II-1	Program Firings	3
III-1	Calculated Engine Performance Data	9
III-2	Engine Performance Summary	10
III-3	Program Firings Run Summary	11
V-1	Atmospheric Attenuation (α) in db/120 ft	40
VI-1	Engine Performance Data Comparison	45
VI-2	Data Summary for Present Work	46
VI-3	Effects of Clustering on Overall Acoustic Power Level	49
A-1	Program Firing Test Log	A-1
A-2	1/3-Octave-Band Sound Level in Decibels (in db re. 10^{-13} watts)	A-2
A-3	1/3-Octave-Band Sound Pressure Levels in Decibels (db re: 0.0002 μ bar)	A-3
A-4	1/3-Octave-Band Sound Pressure Levels in Decibels (db re: 0.0002 μ bar)	A-4
A-5	1/3-Octave-Band Sound Pressure Levels in Decibels (db re: 0.0002 μ bar)	A-5
A-6	1/3-Octave-Band Sound Pressure Levels in Decibels (db re: 0.0002 μ bar)	A-6
A-7	1/3-Octave-Band Sound Pressure Levels in Decibels (db re: 0.0002 μ bar)	A-7

A-8	1/3-Octave-Band Sound Pressure Levels in Decibels (db re: 0.0002 μ bar)	A-8
A-9	1/3-Octave Band Sound Pressure Levels in Decibels (db re: 0.0002 μ bar)	A-9
A-10	1/3-Octave-Band Sound Pressure Levels in Decibels (db re: 0.0002 μ bar)	A-10
A-11	1/3-Octave Band Sound Pressure Levels in Decibels (db re: 0.0002 μ bar)	A-11
A-12	1/3-Octave-Band Sound Pressure Levels in Decibels (db re: 0.0002 μ bar)	A-12
A-13	1/3-Octave-Band Sound Pressure Levels in Decibels (db re: 0.0002 μ bar)	A-13

SUMMARY

The purpose of this contract was to conduct a scale-model test program to determine the acoustical field generated by high-chamber-pressure, hydrogen-fueled engines in various cluster configurations. A total of thirteen acoustic measurements were taken during eleven program firings. These eleven firings were composed of three single-engine firings, three five-engine cluster firings, two eight-engine clusters, and three twelve-engine clusters. The acoustic measurements were divided -- four in the near-field and eight in the far-field so as to be able to calculate the power spectrum and the far-field characteristics as well as obtain the near-field data. Engine data obtained for each firing include mixture ratio, propellant weight flow, total thrust, and chamber pressure. These data were acquired to describe the source characteristics. The acoustic data were analyzed in 1/3-octave bands for study over a frequency range from 50 to 10,000 cps.

The power spectrum, acoustic efficiency, and the directivity indices were calculated from the far-field sound pressure level spectra. The near-field decay upstream of the engine exhaust plane and the apparent source location were measured with the near-field data.

The characteristics of the acoustic fields were compared where possible with the data from other investigators, using information obtained from undeflected free jets only.

The data tabulation from all eleven program firings is included in Appendix A.

NOMENCLATURE

A_t	engine throat area
C_F	thrust coefficient
c_o	speed of sound
c_p	specific heat at constant pressure
D_c	overall diameter of cluster at nozzle exit plane
d_e	engine exit diameter
D_e	effective exit diameter of a cluster
D_5	diameter parameter from Ref 9
DI	directivity index
D_t	engine throat diameter
f	frequency (usually the center frequency of each 1/3-octave band)
F_g	thrust
I_{sp}	specific impulse
M_e	exit Mach number
MR	mixture ratio O_2/H_2
MW	molecular weight
N	number of nozzles in the cluster
NEP	nozzle exit plane
P_c	chamber pressure
p_e	exit static pressure
PSL	power spectrum level in db re. 10^{-13} watts
PWL	acoustic power level in db re. 10^{-13} watts

r	source-to-receiver distance
RH	relative humidity
SPL	sound pressure level in db, re. 0.0002 μ bar
T_c	combustion temperature
T_e	exit static temperature
u	engine exit velocity
u_5	velocity parameter from Ref 9
W_a	acoustic power
W_m	jet exhaust mechanical power
x	downstream distance from nozzle exit plane
α	atmospheric absorption
γ	ratio of specific heats
ϵ	engine area ratio
η	acoustic conversion efficiency
η_1	I_{sp} efficiency (measured)
θ	angle from exhaust stream axis
ρ_e	density of exhaust gases at the exit
ρ_o	density of ambient air
$\dot{\omega}_o$	oxygen weight flow
$\dot{\omega}_f$	hydrogen weight flow
$\dot{\omega}_p$	total propellant weight flow

I. INTRODUCTION

The noise field generated by a high-thrust rocket engine can contribute significantly to the total dynamic environment of the launch vehicle, producing at times stringent, structural design requirements. This acoustic environment may be important for both the liftoff and flight portions of the vehicle firing. In addition, man does not function at peak efficiency in a high-noise environment, so the rocket-generated noise field is important in the design and operation of man-rated systems. A less important but still significant factor is the propagation of rocket noise to areas surrounding the launch or static test area, which interferes with the normal activities of man. For these reasons, it is important to obtain a good understanding of the mechanism by which rocket engines (and clusters of engines) generate acoustic energy and the manner in which the acoustic propagation takes place. The general area of aerodynamically produced noise has been investigated theoretically but with limited success. The experimentally produced results have been used much more extensively to solve the real engineering problems.

The work reported in this document was undertaken with the objective of expanding the fund of knowledge concerning rocket engine noise -- specifically, noise generated by various cluster configurations. How the noise field is altered both in distribution and in spectrum content when changing from a single engine to a cluster has not been completely described in the past.

A total of eleven test firings were made during this program with eight tests conducted during Phase I and three firings made during Phase II. The eight firings of Phase I include three repeatability firings made on a single engine and a five-engine cluster, and single firings of two eight-engine cluster configurations. The results of these firings are reported and discussed in Ref 1.

The Phase II testing was made up of three twelve-engine cluster configurations, each different from the other. The results of these tests are described in this report. This report also contains the discussion and comparison of all the data produced during both phases of the study. In addition, all data from both phases is tabulated in Appendix A.

II. TEST PLAN

At the beginning of the test program, a document, "Program Firing Plan," was written and issued to indicate the general purpose and scope of the test firings as well as the detailed information required for coordinating the testing. The firing schedule was included along with a description of the engine configurations. A list of all measurements gave positions, ranges, and readout equipment required. Finally a detailed description was given of all necessary calibration and data reduction procedures.




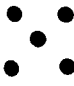
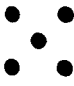
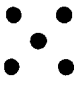
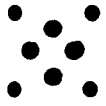
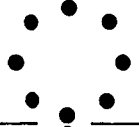

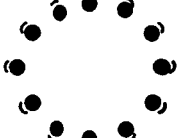
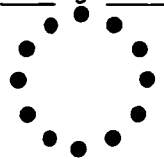
Most of the details of the "Program Firing Plan" are included in other chapters of this report. A summary of the test plan is given in this chapter to acquaint the reader with the general scope of the program firings and the data acquisition and analysis. This plan covers both Phase I and Phase II firings.

A. PROGRAM FIRINGS

The eleven program firings are listed in Table II-1, which also presents the engine configuration and measurement list. One basic engine design was used throughout the tests with multiple engine clusters composed of five, eight, or twelve basic single engines. All firings were horizontal with no deflector present. Firings 1 thru 3 were repeatability firings of the single-engine configuration. Firings 4 thru 6 were repeatability firings of the five-engine cluster, which is similar to the Saturn V cluster configuration. Firing 7 was an eight-engine cluster similar to the S-IB clustering, and Firing 8 was an eight-engine circular cluster. Firing 9 was a twelve-engine cluster, Firing 10 a twelve-engine circular cluster with engines canted 15 deg, and finally Firing 11 was a twelve-engine circular cluster with 0 deg engine cant. The orientation of the multiple engines is also shown in Table II-1 with acoustic measuring plane at right angles to the vertical axis.

Engine instrumentation includes chamber pressure in each chamber, total thrust, two temperatures and pressures required for propellant weight flow and mixture ratio calculations, and four pressures in the propellant supply lines. The acoustic measurements were distributed between the far-field and near-field as shown in Table II-1 for all firings. High-speed movies were taken of each firing to be used for general flow visualization and any required system troubleshooting.

Table II-1 Program Firings

PHASE	TEST CONFIGURATION	ENGINE MEASUREMENT	ACOUSTIC MEASUREMENT	
			NEAR-FIELD	FAR-FIELD
I	1 Single-Engine 	10	4	9
	2 Single-Engine 	10	4	9
	3 Single-Engine 	10	4	9
	4 Five-Engine Cluster 	14	4	9
	5 Five-Engine Cluster 	14	4	9
	6 Five-Engine Cluster 	14	4	9
	7 Eight-Engine Cluster 	17	4	9
	8 Eight-Engine Cluster Circular 	17	4	9
II	9 Twelve-Engine Cluster 	21	4	9
	10 Twelve-Engine Circular Cluster Canted 15° 	21	4	9
	11 Twelve-Engine Circular Cluster 	21	4	9

B. TEST FIXTURE

The engines were designed to burn gaseous oxygen and hydrogen at a mixture ratio of 3:1 and a chamber pressure of 1200 psia. Engine run time was set at a minimum of 3.0 seconds of steady-state operation but generally exceeded this time. Single-engine thrust on the order of 400 lb was calculated with a total propellant weight flow of 1.0 lb per sec. The calculated exit Mach number was 3.5 for a fully expanded area ratio of 10. Other pertinent engine and exhaust gas data are given in Table III-1.

Each configuration was mounted on a thrust stand firing horizontally with the engine centerline six ft from the ground plane. The single engine and the clusters were mounted on a thrust plate designed to measure total engine thrust. The firing was controlled automatically by a control console that provided a programed sequence of events.

C. ACOUSTIC MEASUREMENTS

The far-field microphones were on poles six ft above the ground plane on a 120-ft radius measured from the engine exit. The far-field positions are shown in Fig. II-1. The measuring plane was flat, sloping gently from the 160-deg to the 20-deg position and is composed of bare packed earth. The near-field acoustics measurements were taken at three locations near the engine and at the boundary of the exhaust stream by a traversing microphone. These near-field data points are shown in Fig. II-2. The diameter used in positioning the three microphones on the stand was an effective exit diameter that is an equivalent flow diameter of the clusters.

All acoustic data were acquired using the Bruel and Kjaer 1/4-in. condenser microphone systems, connected by coaxial cable to the signal conditioning equipment, and a 14-channel CEC magnetic tape recorder. The frequency range was 50 to 10,000 cps. An electrical system calibration for each data channel was made prior to the test series. An end-to-end amplitude calibration was made before each firing using the B&K Pistonphone. In addition, each microphone was calibrated by the reciprocity method and the electrostatic actuator twice during the test series.

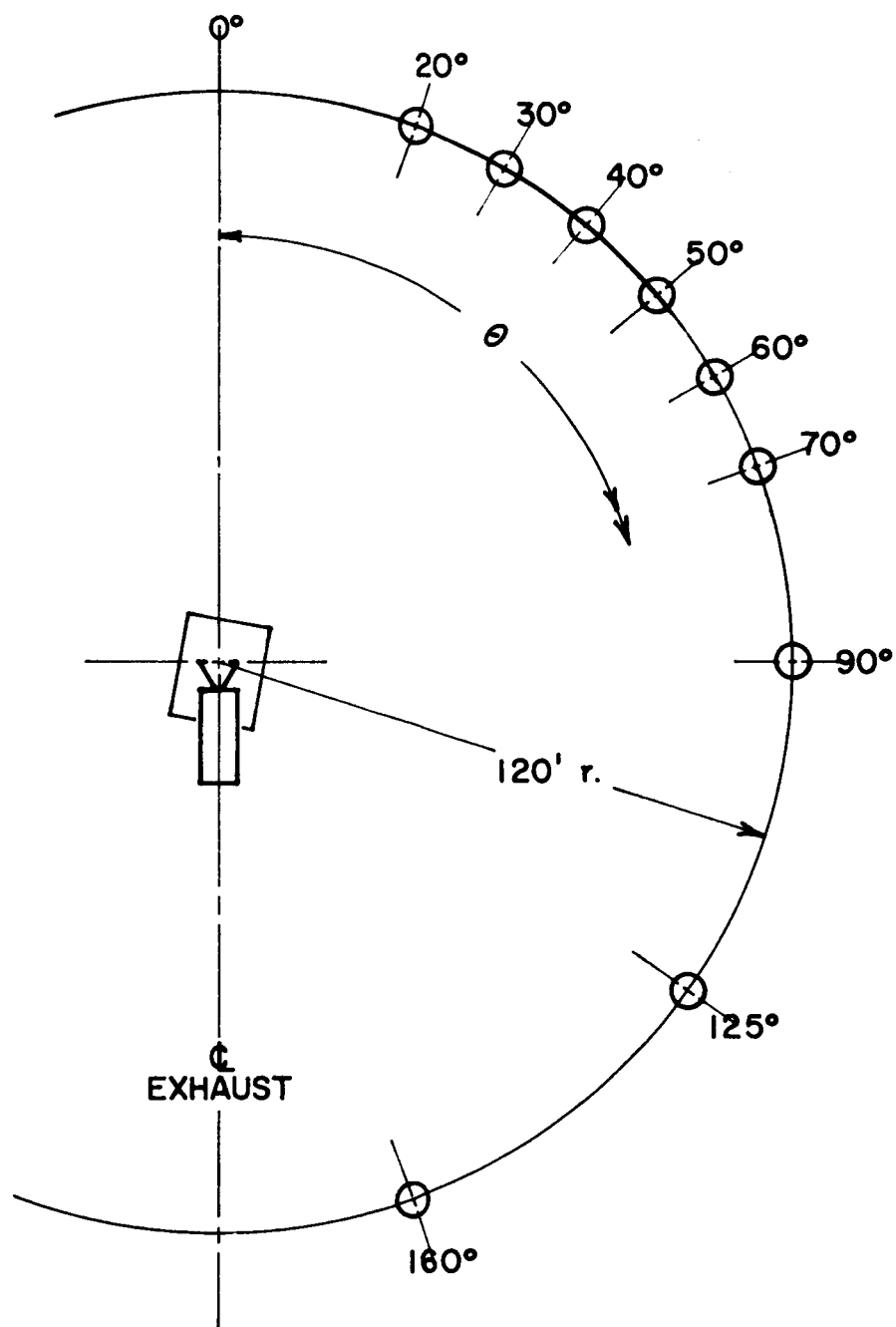


Fig. II-1 Far-Field Measurement Locations

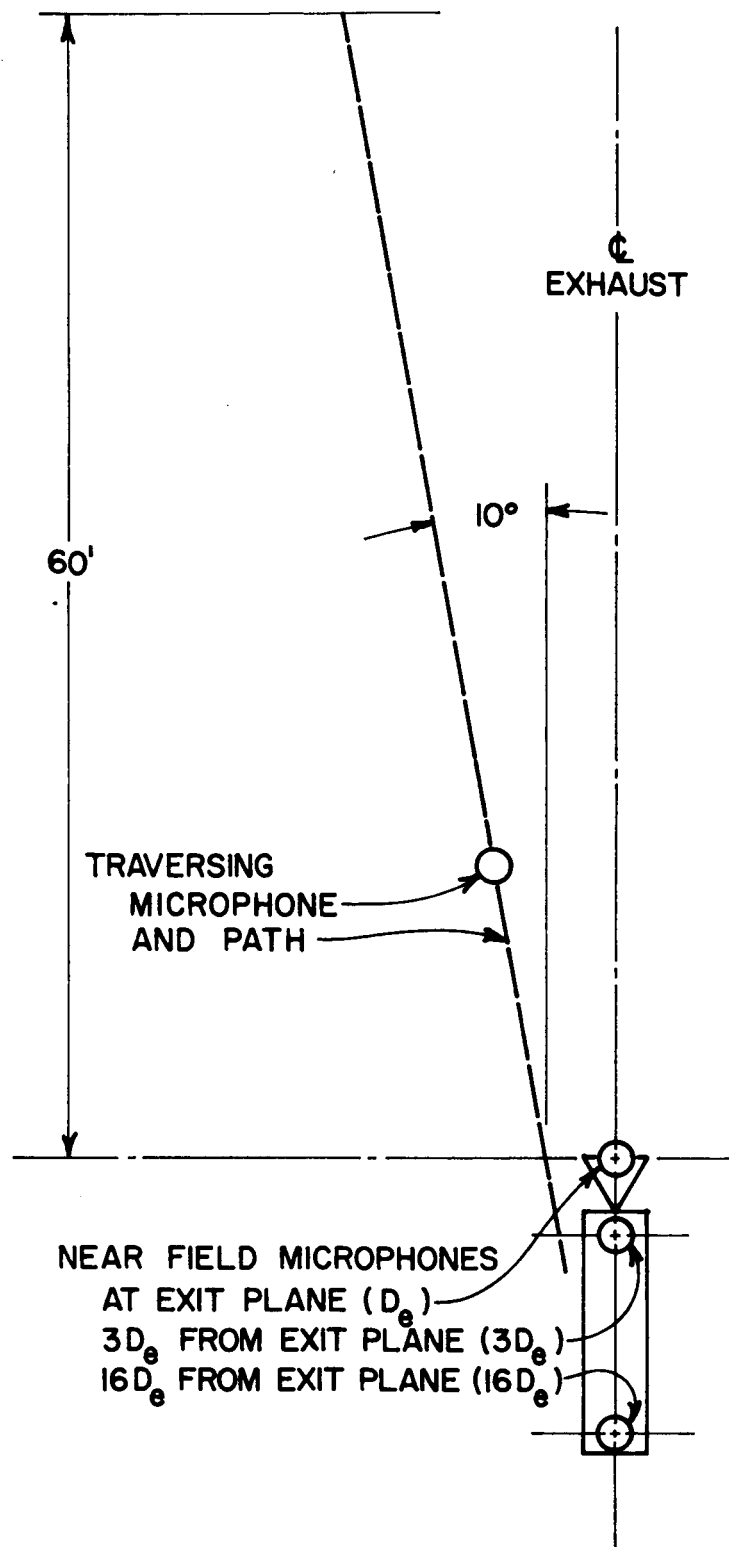


Fig. II-2 Near-Field Measurement Locations

All acoustic data were reduced to overall time histories to aid in selecting the data sample to be analyzed and to review general data quality. A 1/3-octave band analysis was then made of the resulting tape loops using the B&K 1/3-octave analyzer. The traversing microphone data were analyzed in 1/3-octave band time histories, to be later converted to sound pressure level as a function of distance.

III. PROPULSION SYSTEM AND ENGINE PERFORMANCE

This chapter provides a general description of the facility and propulsion system and documents the engine performance for the Phase II test firings. The details of the test fixture are given in Ref 1. The engine performance for the Phase I firings is also given in detail in Ref 1, while the pertinent performance results are summarized in Tables III-2 and III-3 for both the Phase I and Phase II firings.

A. PROPULSION SYSTEM

1. Engine Design

The basic engine that is mounted on the thrust plate is composed of the thrust chamber case, graphite liner and throat, injector plate, back plate, and igniter. Fig. III-1 shows in schematic form the engine assembly, while Fig. III-2 is a picture of the case with the igniter in place. The engine case was made of stainless steel with Rokide Z coating on the nozzle walls. The graphite liner is wrapped in a glass phenolic material and must be replaced with each firing. The graphite throat suffers some throat erosion as evidenced by the decaying chamber pressure **shown later. The engine case is reusable requiring only refurbish** of the Rokide Z coating after a few firings. The injector plate has a single port O_2 injector in the center with a multiple port H_2 injector on the periphery. Seventy-five percent of the fuel flow is directed at an angle toward the oxidizer stream and twenty-five percent flows axially along the thrust chamber walls for film cooling. The back plate holds the propellant supply lines from the manifold. The igniter is an **automobile spark plug (Champion N-3)** with a modified gap (Ref 1). Separate transformers for each engine provided 10,000 vac at 0.023 amp to the igniters. These transformers operated from 115-vac power. Details of the engine design and the checkout firings are contained in Ref 1. The engine geometry and performance are given in Tables III-1, III-2, and III-3.

Table III-1 Calculated Engine Performance Data

Computer Program Input	Propellants	Gaseous Hydrogen and Gaseous Oxygen
	Mixture Ratio, MR	3:1
	Nozzle Expansion Ratio, A_e/A_t	10.0
Computer Program Output	Chamber Pressure, P_c	1200 psia
	Nozzle Exit Pressure, p_e	11.8 psia
	Exit Mach No., M_e	3.5
	Exit Static Temperature, T_e	1800°R
	Exit Density, ρ_e	0.00496 lb/cu ft
	Specific Heat at Constant Pressure (Exit), c_p	1.02 Btu/lb °R
	Molecular Weight, MW	8.04
	Combustion Temperature, T_c	4844°R
	Specific Heat Ratio, γ	1.32
	Specific Impulse, I_{sp}	415 sec
Other Data	Thrust Coefficient, C_F	1.60
	Thrust (100% Efficiency), F_g	415 lb
	Exit Velocity, u	12,900 fps
	Propellant Flow, \dot{w}_p	1.00 lb/sec
	Nozzle Exit Diameter, d_e	1.56 in.
	Nozzle Throat Diameter, D_t	0.494 in.
	Ambient Pressure in Denver	11.8 psia

Table III-2 Engine Performance Summary

Phase	Firing No.	$\dot{\omega}_f$ (lb/sec)	$\dot{\omega}_o$ (lb/sec)	$\dot{\omega}_p$ (lb/sec)	Thrust/Engine (lb)		I _{sp} (sec)			Maximum P _c (psia)	C _F [†]	C _F ^{**} Efficiency	$\dot{\omega}_o/\dot{\omega}_f$
					Measured	Calculated	Measured	Calculated [†]	η_1				
I	1	0.256	0.776	1.032	*	404 [†]	*	391	94.5	1307	1.57 ^{††}	98.1	3.03
	2	0.253	0.772	1.025	*	396 [†]	*	386	93.1	1302	1.57 ^{††}	98.1	3.05
	3	0.257	0.825	1.082	436		403		97.2	1357	1.63	102	3.20
	4	0.252	0.796	1.048	408		389		93.9	1341	1.54	96.5	3.16
	5	0.258	0.804	1.062	408		384		92.6	1329	1.56	97.5	3.11
	6	0.252	0.761	1.013	394		389		93.8	1321	1.52	95.0	3.02
	7	0.252	0.775	1.027	392		382		92.1	1262	1.58	98.6	3.07
	8	0.255	0.774	1.029	411		400		96.5	1298	1.61	100.7	3.03
II	9	0.232	0.727	0.959	352	369 [†]	368	385 [†]	89	1192	1.50	94	3.14
	10	0.245	0.725	0.970	361	382 [†]	372	394 [†]	90	1237	1.48	93	2.96
	11	0.230	0.725	0.955	367	381 [†]	384	399 [†]	93	1231	1.51	94	3.15

*No thrust data on Firings 1 and 2.

†Values based on average C_F = 1.57, Firings 3 thru 8.‡Assumes A_T = 0.197 sq in.**Ideal C_F = 1.60.

††Average from Firings 3 thru 8.

Note: Performance data are average values per engine for cluster firings and an average over approximately three sec for each run.

Table III-3 Program Firings Run Summary

Run No.	No. of Engines	Camera Coverage	Atmospheric Conditions			Event Timing (sec from start)					Steady-State Run Time (sec)	Fuel Pressure (psia)		O ₂ Pressure (psia)	
			Wind (mph)	Temperature (°F)	Barometer (In. Hg)	Fuel Start	Oxygen Start	Ignition	CO ₂ Off	OH ₂ Off		Set at Regulator	Actual at Engine	Set at Regulator	Actual at Engine
PHASE I	1	High Speed and Still Color	2	60	24.15	0.55 to 0.60	1.1 to 1.2	1.8	5.7	7.9	4.3	1565	1680	1680	1680
	2	High Speed Color	2	62	24.01	0.92 to 1.07	1.5 to 1.6	1.62	5.72	7.82	4.0	1565	1700	1720	1700
	3	High Speed Color	5	49	23.70	0.52 to 0.60	1.15 to 1.25	1.30	6.0	8.2	4.5	1565	1790	1720	1790
	4	High Speed Color	6	57	24.15	1.57 to 1.70	2.17 to 2.32	2.24 to 2.45	6.95	8.96	4.3	1620	1740	1690	1740
	5	High Speed Color and Still Color	4	49	23.82	1.6 to 1.75	2.2 to 2.35	2.31 to 2.37	7.04	9.2	4.5	1620	1720	1650	1720
6	5	High Speed Color	5 to 8	37	24.04	1.66 to 1.79	2.2 to 2.34	2.33 to 2.46	7.1	9.3	4.4	1620	1630	1650	1630
7	8	High Speed Color	5	46	24.10	1.61 to 1.74	2.12 to 2.27	2.20 to 2.40	6.95	8.8	4.3	1700	1645	1660	1645
8	8	High Speed Color	5	39	24.00	1.64 to 1.80	2.14 to 2.30	2.26 to 2.40	7.04	9.12	4.4	1700	1625	1660	1625
PHASE II	9	High Speed Color	4 to 13	83	24.33	3.25	3.67	3.76 to 3.96	7.23	9.07	3.0	1840	1622	1750	1622
	10	High Speed Color	3	86	24.17	3.27	3.67	3.80 to 3.88	7.15	9.05	2.6	1840	1612	1750	1612
	11	High Speed Color	2	81	24.37	3.22	3.61	3.74 to 3.93	8.06	9.90	3.0	1840	1617	1750	1617

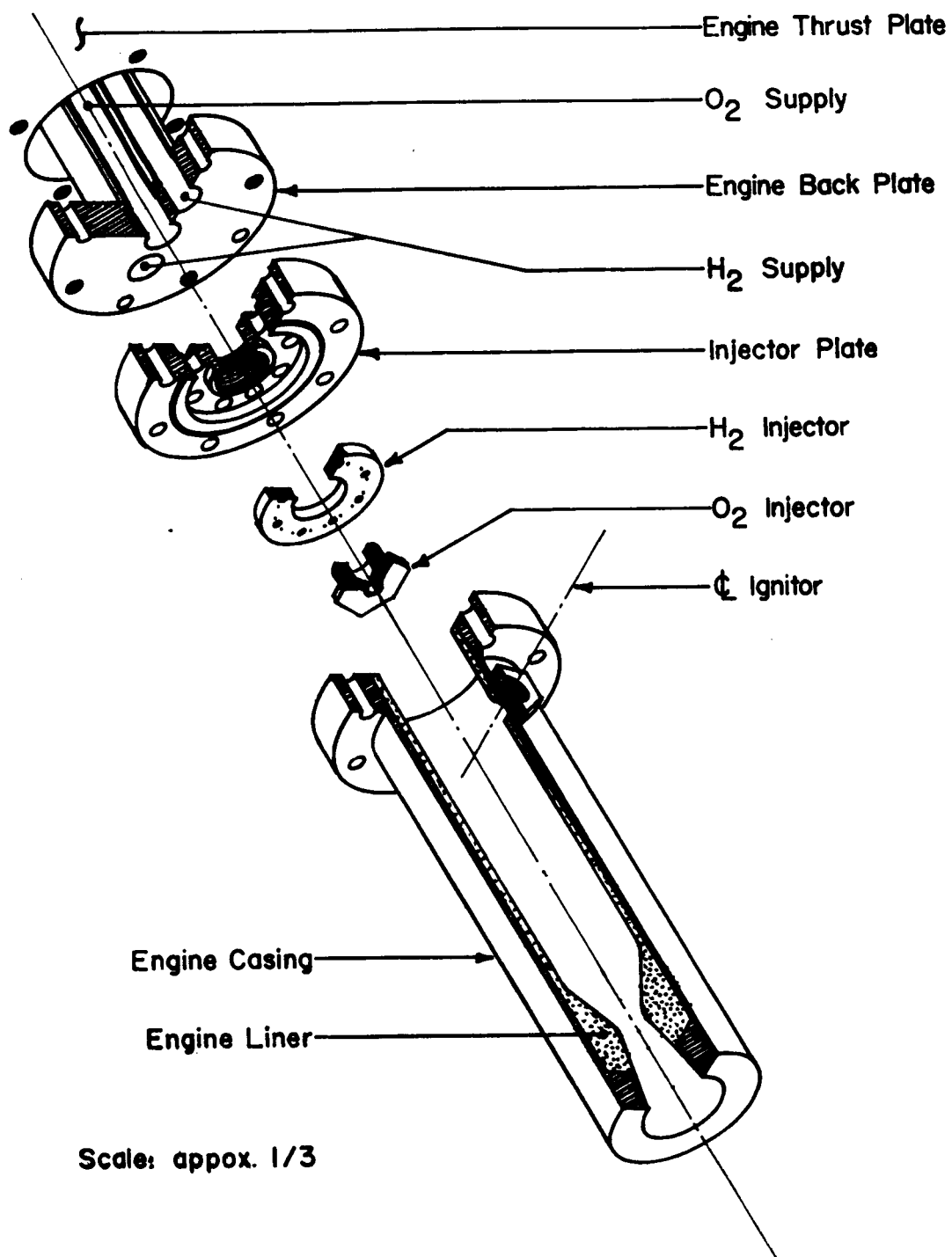


Fig. III-1 Engine Assembly Schematic

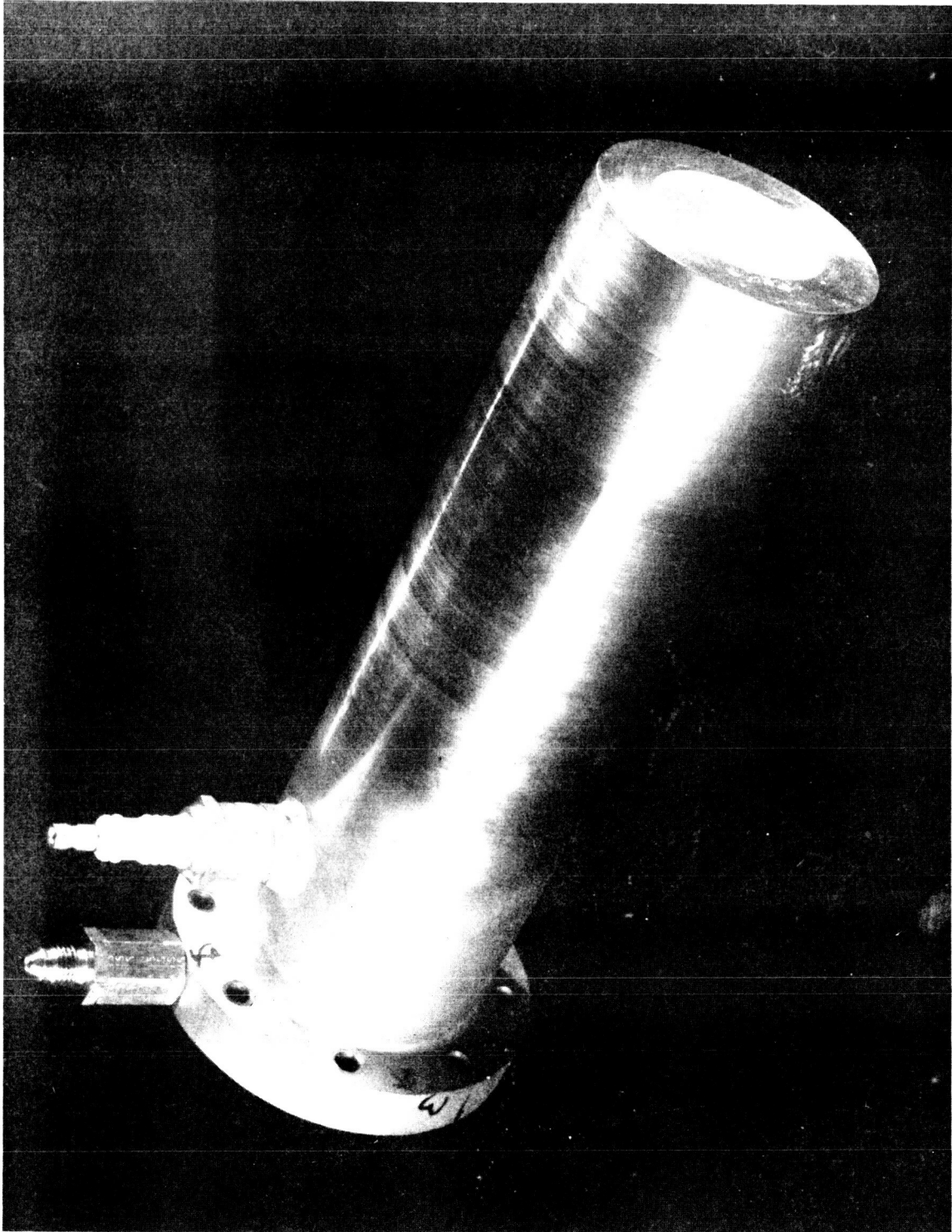


Fig. III-2 Engine Case and Igniter

2. Propellant Supply and Transfer System

A schematic of the propellant supply and transfer system is shown in Fig. III-3. The GO_2 storage consists of 72 standard K bottles manifolded together with a storage pressure of 2400 psig. Loading provisions permit the gas supply to be replenished by commercial delivery. The GH_2 storage is composed of high pressure steel cylinders with a total water volume of 58.5 cu ft. The maximum allowable storage pressure is 2900 psig. Liquid hydrogen is loaded into a vacuum jacketed sphere with a capacity of 5.5 cu ft. The sphere is then opened to the storage tanks and the liquid gases off into the storage system. The hydrogen system is located in an earth revetment 70 ft from the test area for safety reasons. Both propellants are transferred to the thrust stand through 1 1/2-in. stainless steel lines and controlled and regulated by remotely controlled valves and pressure regulators as shown in Fig. III-3.

On the thrust stand, the propellants are transferred to the engine injectors via two cylindrical manifolds and a set of toroidal manifolds. The latter permit individual flexible hoses to supply propellant from the toroidal manifold to each engine. Figure III-4 is a view of the thrust stand and acoustic measuring field. Figure III-9 shows the thrust stand supply lines and manifold system.

A thrust plate, on which the engines are mounted, is connected to the thrust readout by a steel shaft. This shaft is supported from the thrust mount by bearings which permits free horizontal motion. The thrust plate is isolated mechanically from the rest of the thrust stand by use of flexible supply hoses.

There were two principal changes to the propellant supply and transfer system from the Phase I configuration. The hydrogen storage capacity was increased by 27% in order to have adequate fuel for a three-second firing. The flow capacity in the oxygen system was increased by adding a 1 1/2-in. regulator in parallel with the existing regulator. Both of these changes were necessary because of the increased propellant flow rates required by the twelve-engine clusters.

3. Control and Firing Sequence

The control console was specifically designed to operate the described propellant system. It consists basically of a timer and an array of stepper switches that automatically operate the necessary valves during a firing. Valve timing can easily be altered

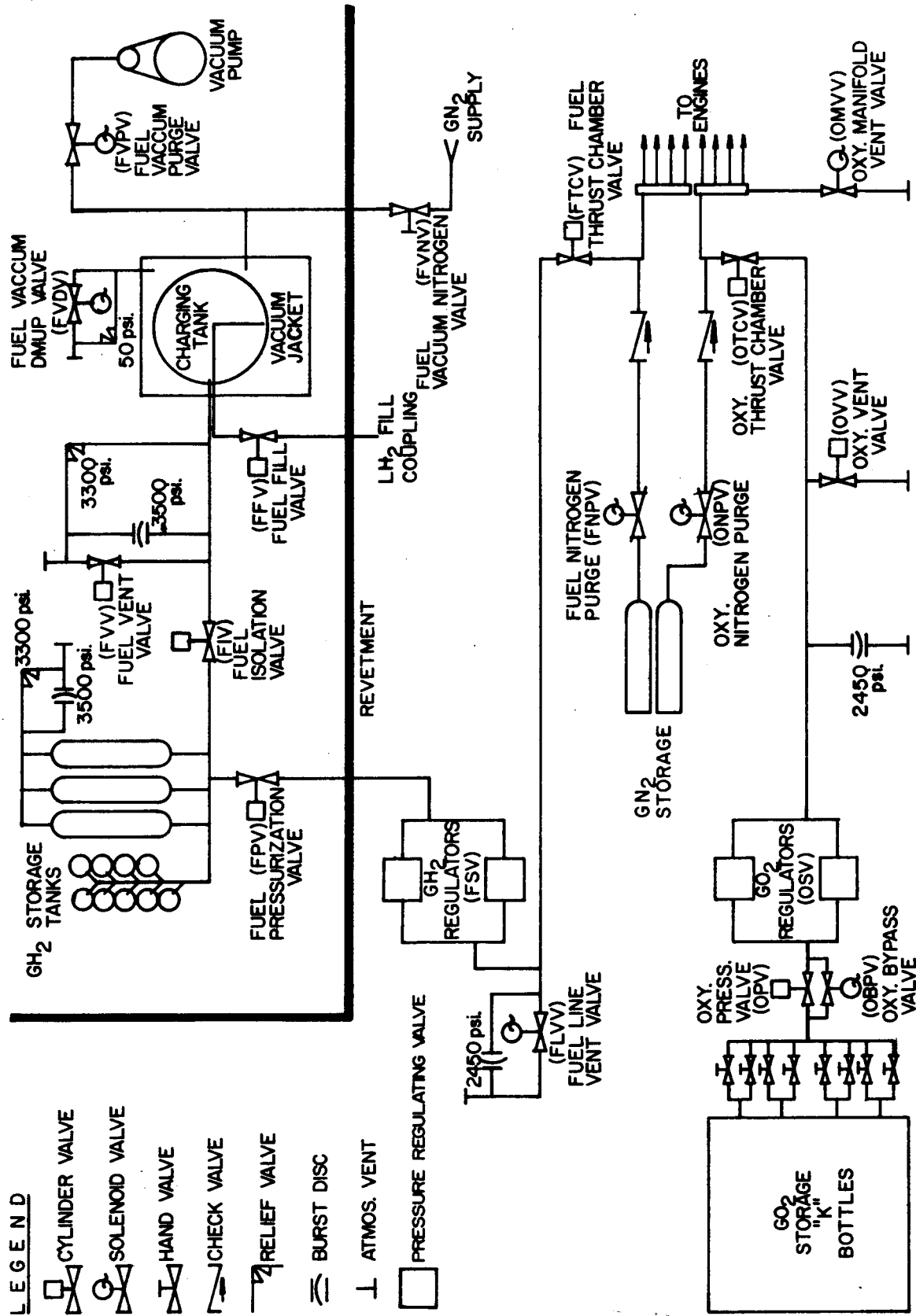


Fig. III-3 Propellant System Schematic



Fig. III-4 Engine Thrust Stand

for each function by a patch panel. In addition to the automatic control capability, the console provides for command shutdown and contains appropriate position lights for all valves. The control console is operated by 28-vdc power.

The actual sequence of valves during firing was automatically controlled by the test console. Figure III-5 represents the sequence of events during a typical firing. Before the fire switch is actuated, a nitrogen purge was established in the fuel manifold system and engine to ensure that all air was eliminated before hydrogen entered the system. This purge was continued throughout the run and during post-test; however, a check valve prevented hydrogen flow into the purge system during the 6-sec period of fuel flow. The automatic timer opened the fuel thrust chamber valve; 0.5 sec later it closed the oxygen manifold vent and opened the oxygen thrust chamber valve. At this point ignition occurred, and immediately thereafter the power supply to the ignition system was manually shut off. This was done to reduce the ignition system operating time, since the electronic interference from the spark system was reflected in both the acoustic and engine data. During actual firing, the oxygen purge valve was manually opened permitting nitrogen purge of the system as soon as propellant pressure dropped.

This sequencing provided approximately 3.5 sec of engine operation during which a minimum of 3 sec of steady-state data was obtained. Hydrogen flow continued for 2 sec after oxygen shutoff to ensure a fuel-rich shutdown, and a N_2 purge of both systems then continued for several minutes.

This sequence of events is only slightly different from those in the Phase I firings.

4. Engine Instrumentation

The thrust was measured using the readout of a standard load cell in the thrust mount. Isolated mechanically by the supply flex lines, the mount transmits engine thrust along a central shaft which was supported in pillow blocks. These bearings carry the load of the engines and engine mounting plate and permit the movement of the shaft. A calibration fixture has been made using a hydraulic cylinder for the load input and an external calibrated load cell to measure the input force. Readout was with (as with all present engine instrumentation) a CEC oscillograph.

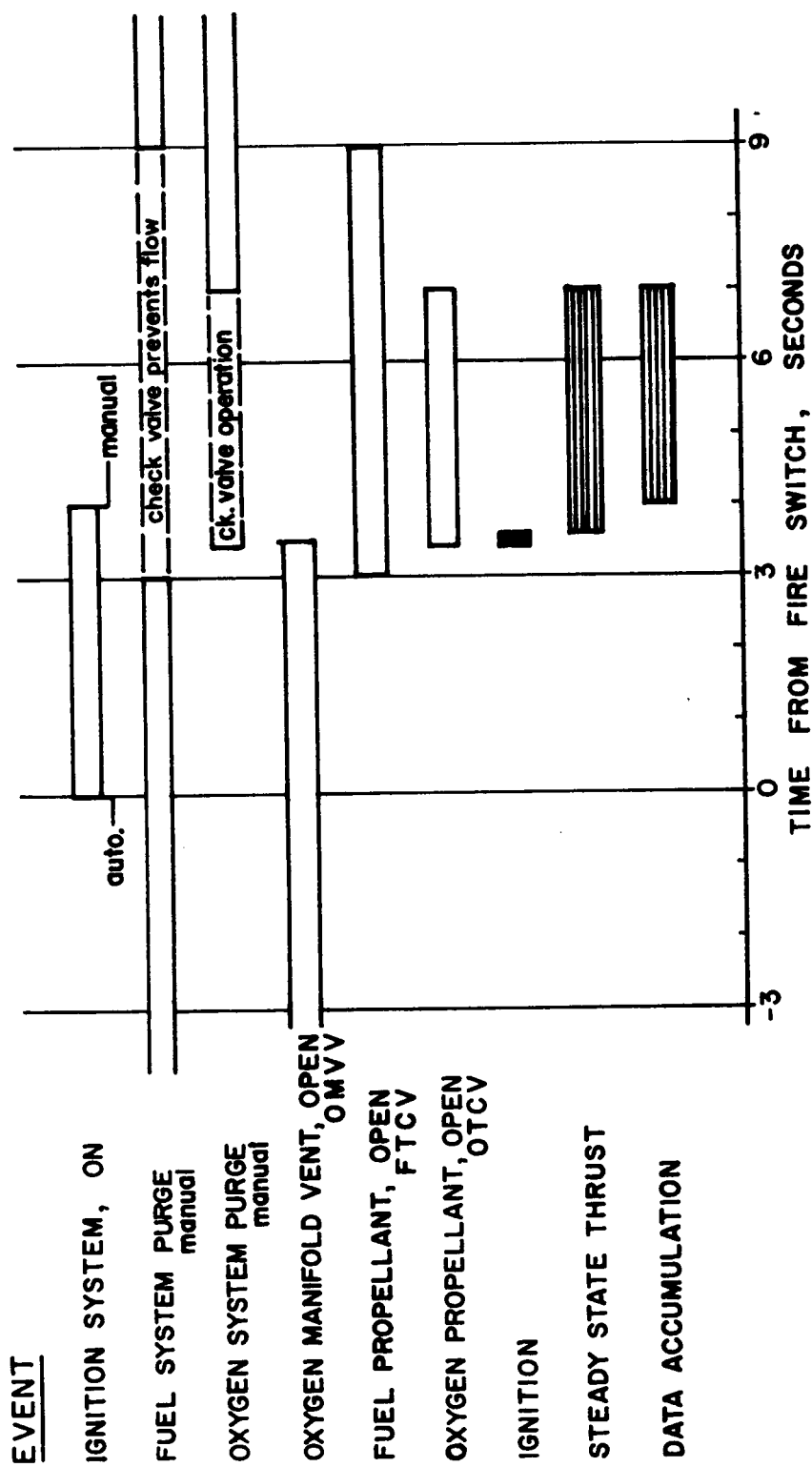


Fig. III-5 Firing Sequence

The propellant weight flow was calculated by measuring the temperature and pressure in the propellant manifolds upstream of the choked venturis.

Engine chamber pressure was instrumented by a tap immediately downstream of the injector face. A short length of tubing filled with silicon grease isolated the transducer from the engine chamber. The line pressure was also recorded upstream and downstream of the regulator in both propellant supply lines. All pressure transducers were calibrated using a dead weight calibrator producing an end-to-end system calibration.

An events recorder was used to both set the start sequence before firing and to record the actual valve timing during the firings.

B. ENGINE PERFORMANCE

The Phase II program firings were conducted in August and September of 1966. Tables III-1, III-2, and III-3 are summary tables of facility and engine performance data. Table III-1 contains engine exhaust data useful in the acoustic data correlation. These tables contain the data for both the Phase I and Phase II firings since the acoustic data correlation and comparison will make use of the data gathered during both phases.

In Table III-2, it should be noted that there is a difference in the measured I_{sp} and thrust coefficient values between the Phase I and Phase II firings. Since these are identical engine and injector configurations, no difference in specific impulse and thrust coefficient would be expected.

The most reliable measurements based on experience and repeated calibration are the propellant weight flow and chamber pressure measurements. The thrust measurement depends critically on the thrust stand calibration under simulated firing conditions, i.e., with propellant feed lines pressurized, and is therefore considered the less reliable absolute measurement. Since the initial throat area can be determined accurately, the calculated thrust in Table III-2 for the Phase II firings has been determined by using the initial throat area, the measured peak chamber pressure, and the average thrust coefficient determined from Firings 3 thru 8. The agreement between this calculated thrust and the measured

thrust from the Phase I firings is good when consideration is made for the chamber pressures. The calculated specific impulse is then obtained by using this calculated thrust and the measured propellant weight flow. Again, these calculated impulse values are in fair agreement with the measured I_{sp} from the Phase I firings.

For the calculations involving thrust and specific impulse in Chapter VI, the measured values have been used for the Phase I firings, and these calculated values were used for the Phase II firings. Table III-2 does contain all the measured data for reference.

The chamber pressure was measured in each engine during the firings and the traces of pressure as a function of time are shown in Fig. III-6, III-7, and III-8 for Firings 9, 10, and 11. The decay in chamber pressure is due to throat erosion during the duration of the firing. The acoustic data do not vary significantly during the firing indicating no dependence on chamber pressure per se.

Figures III-9, III-10, and III-11, show the three twelve-engine cluster configurations tested during the Phase II effort mounted on the thrust stand. The nozzle spacing at the exit was held constant for each of the cluster configurations. Figure III-12 is a sketch showing the dimensions of the nozzle spacing for all program firing configurations. All the cluster configurations had similar exit plane spacing, which was fixed mainly by the engine flange diameter.

A brief description of each of the Phase II firings is given below.

1. Program Firing No. 9

This test used the twelve-engine cluster configuration. Results were satisfactory in all respects, with approximately 3.0 seconds of steady-state data obtained. Because of the proximity of the inner diameter of engines to the outer it was not possible to install chamber pressure instrumentation in the four innermost engines. Data were not valid for two of the remaining engines.

Figure III-6 presents a time history of the chamber pressure data obtained during this run. The average maximum chamber pressure for these engines was 1192 psi. No damage to engine hardware was sustained other than the normal erosion of the graphite nozzle liner.

PROGRAM FIRING N° 9

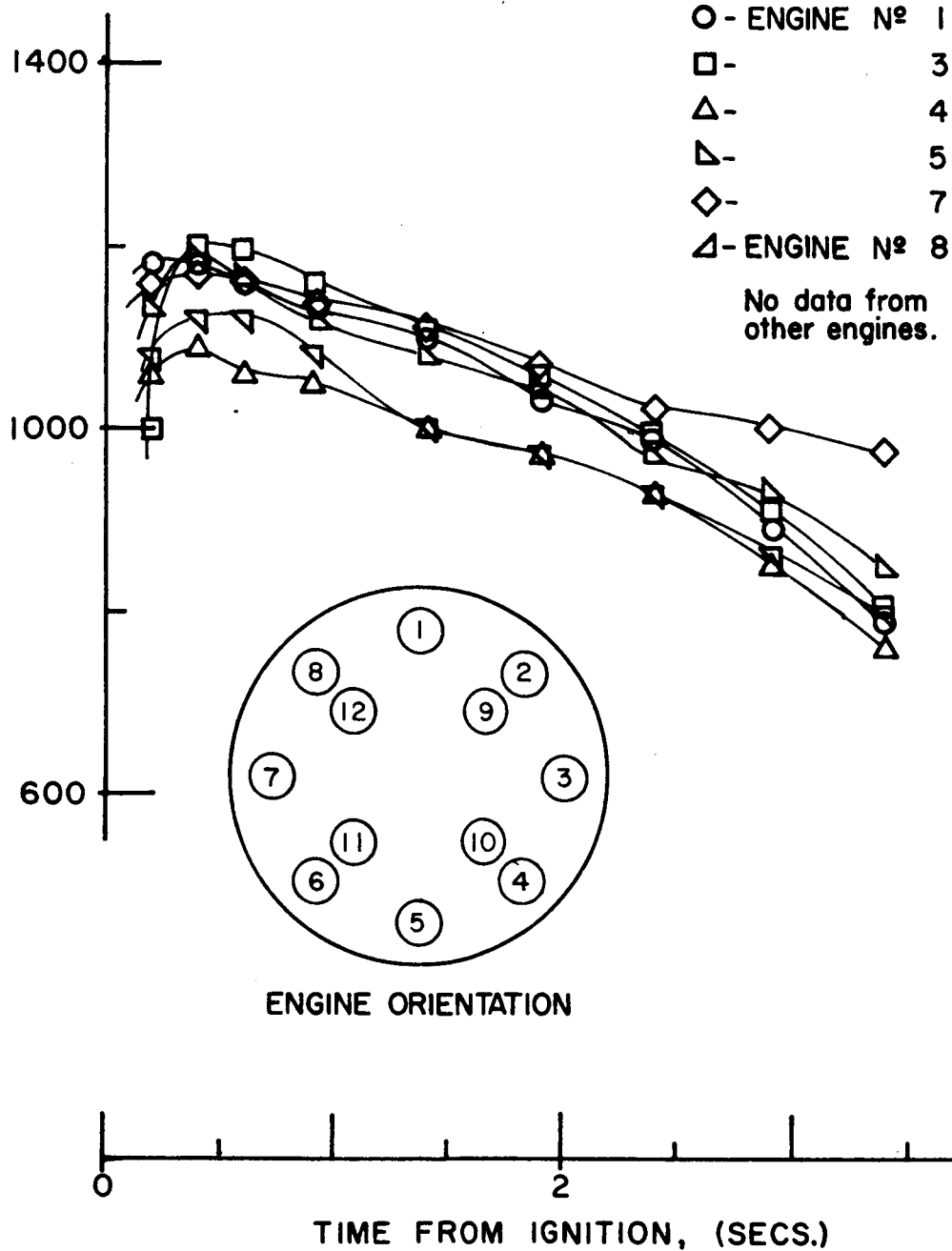
ENGINE CHAMBER
PRESSURE, P_c ,
(PSIG)

Fig. III-6 Engine Chamber Pressure Time History, Firing No. 9

PROGRAM FIRING Nº 10

ENGINE CHAMBER
PRESSURE, P_c ,
(PSIG)

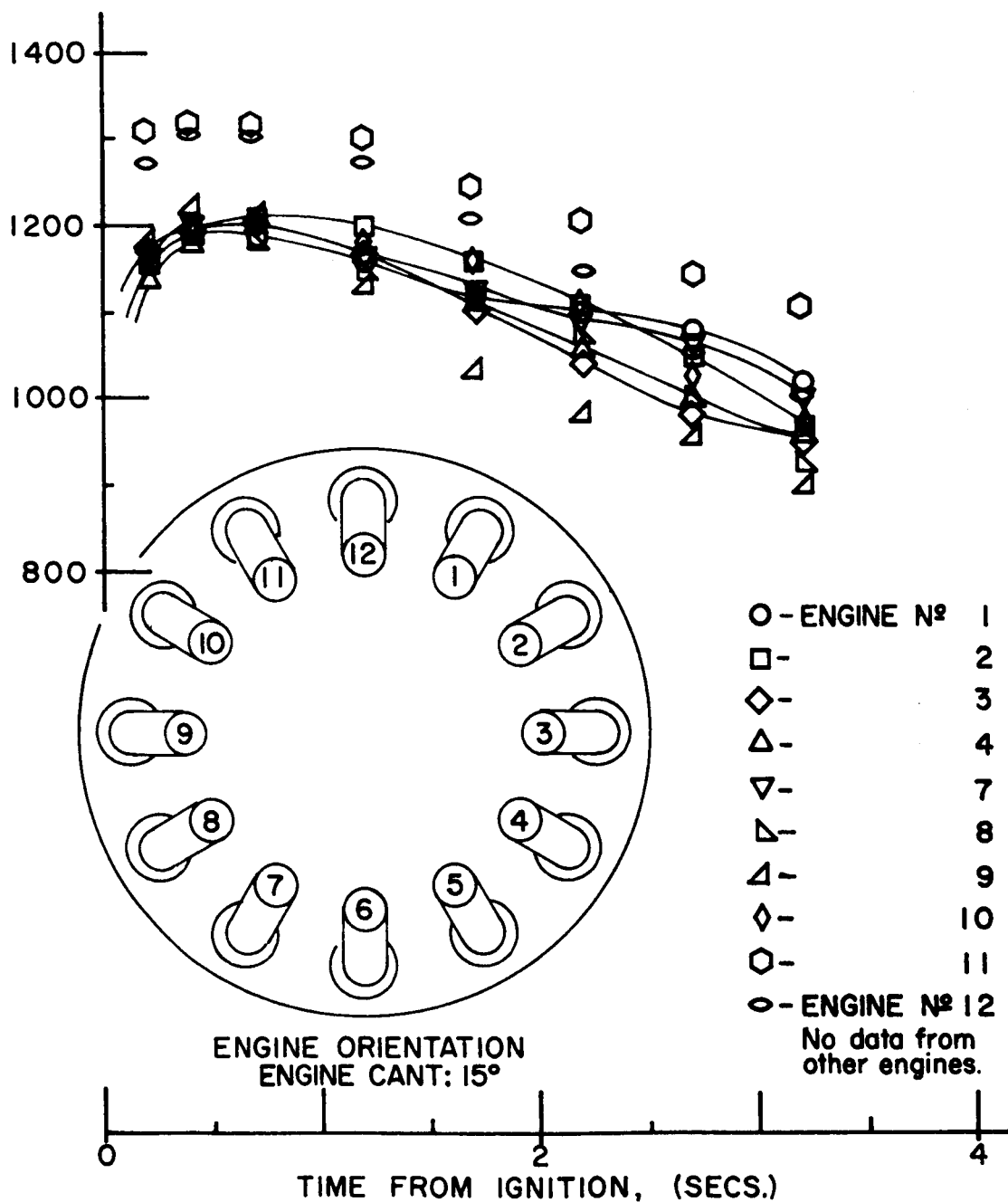


Fig. III-7 Engine Chamber Pressure Time History, Firing No. 10

PROGRAM FIRING N° 11

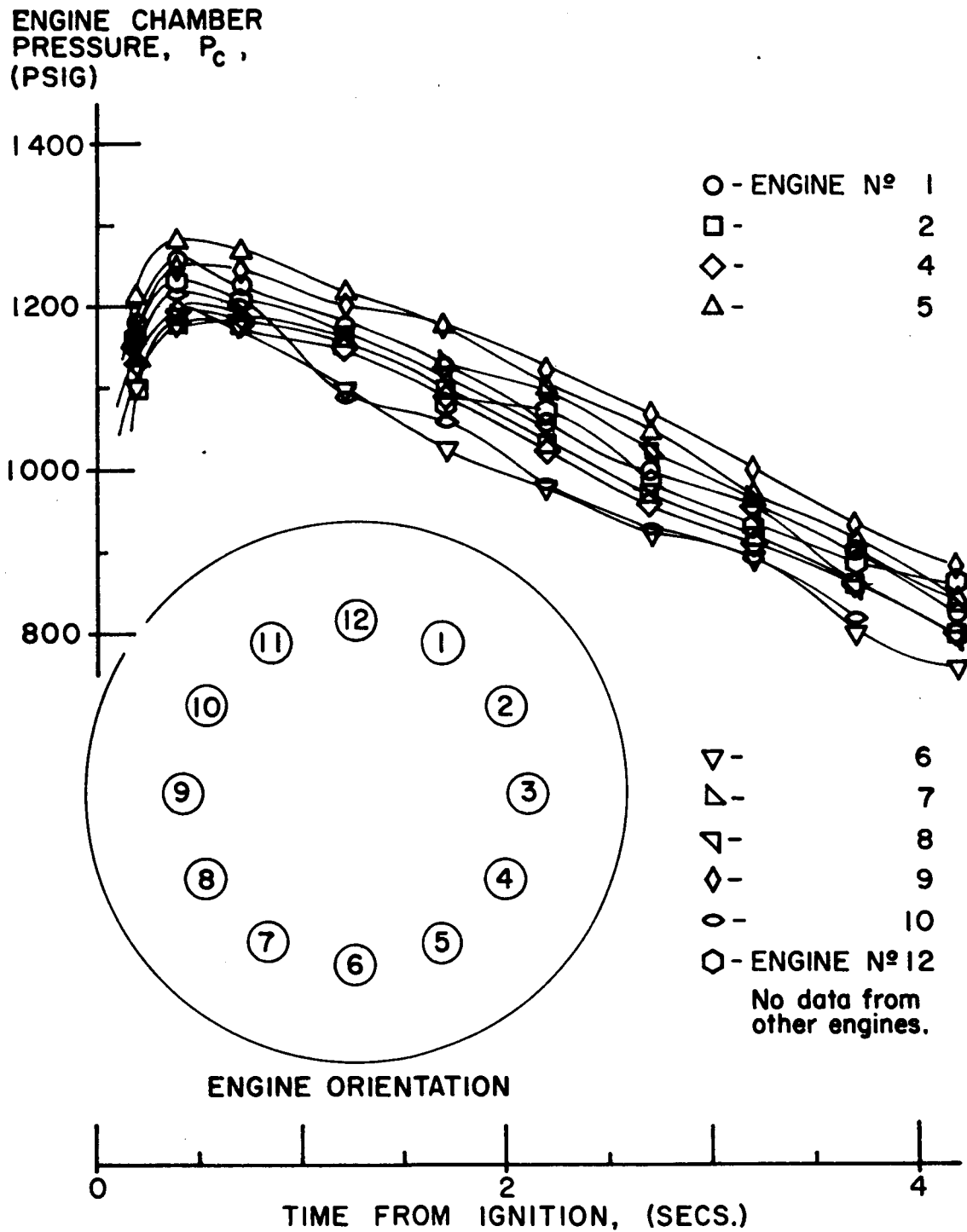


Fig. III-8 Engine Chamber Pressure Time History, Firing No. 11

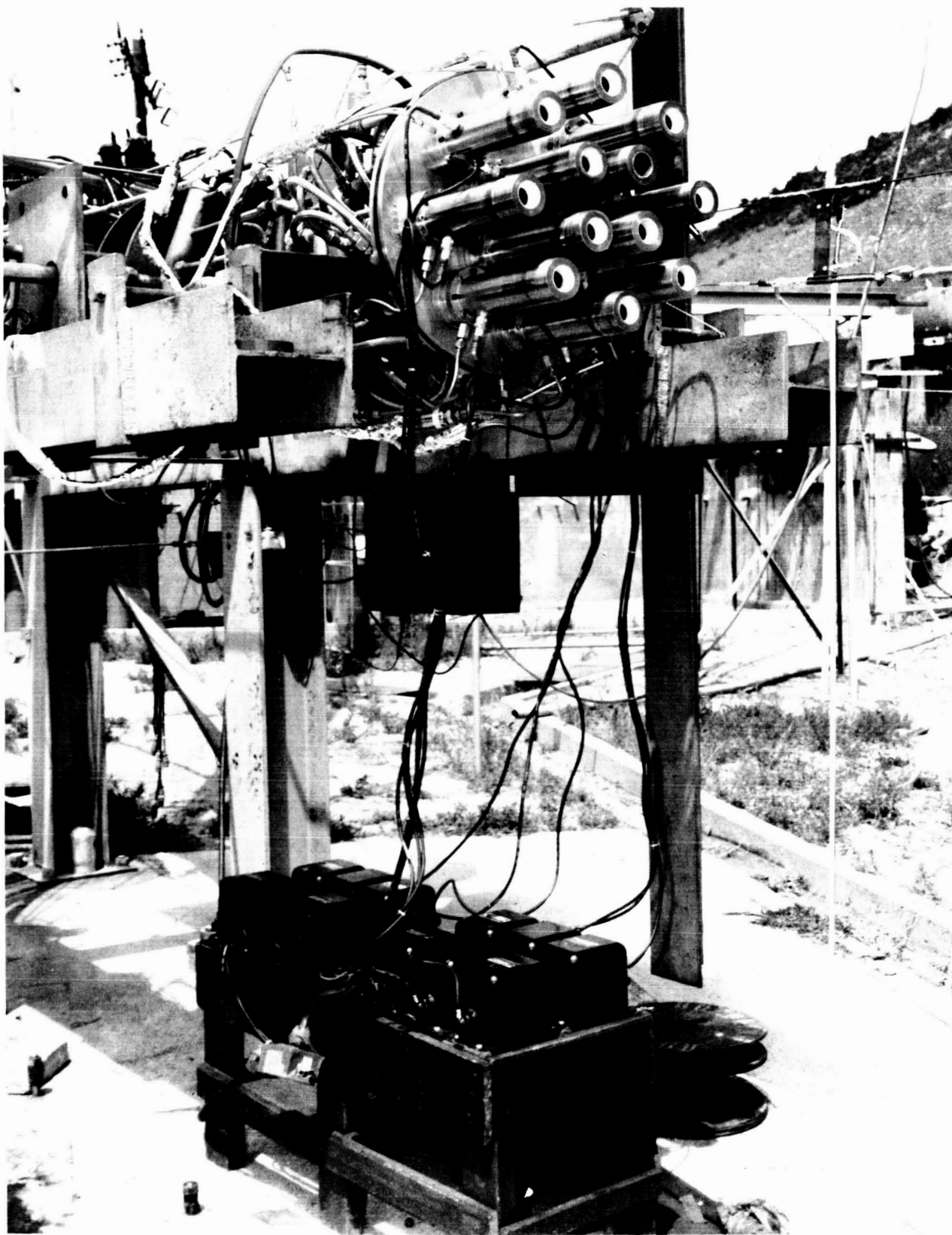


Fig. III-9 Twelve-Engine Cluster, Firing No. 9

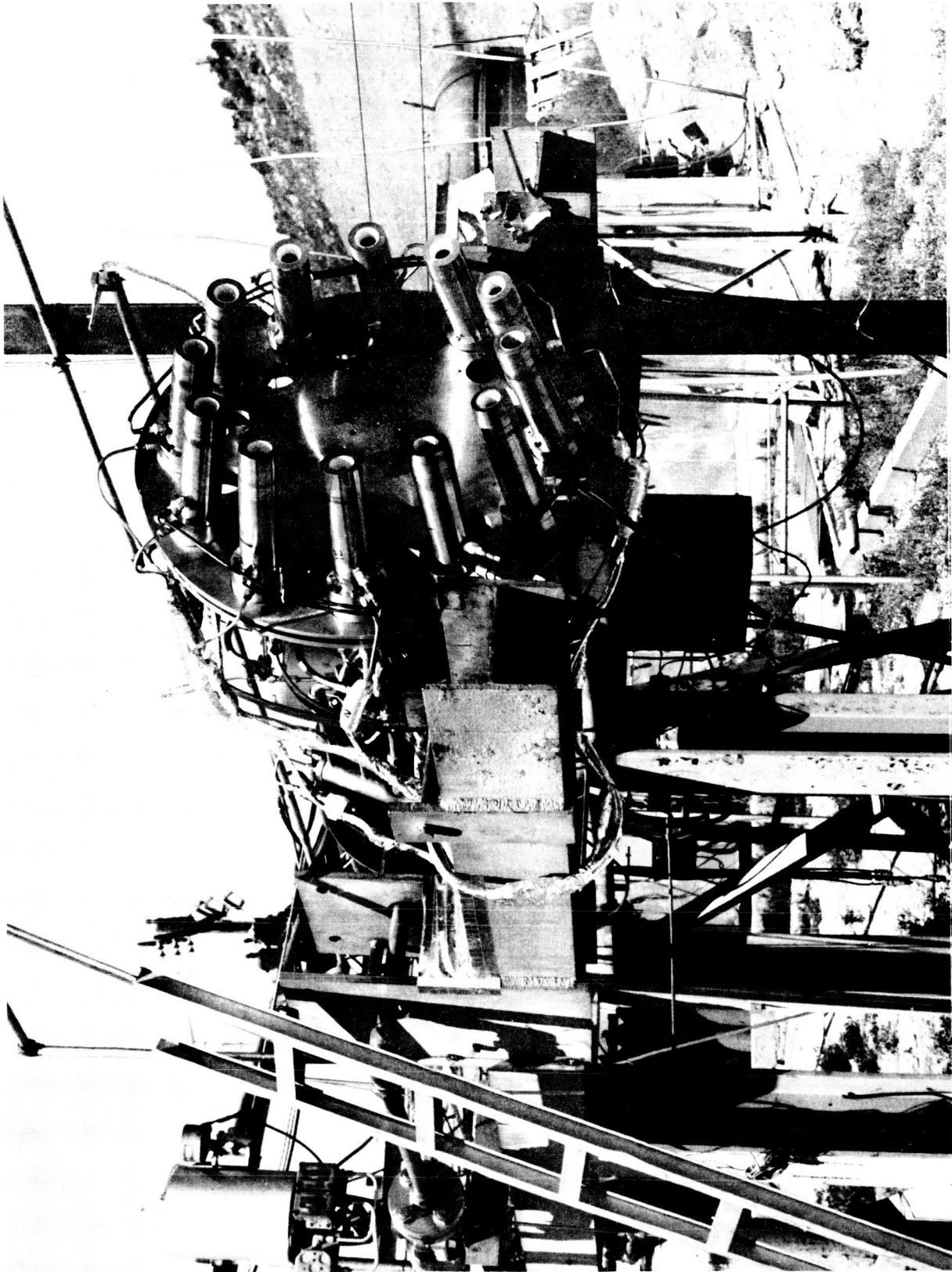


Fig. III-10 Twelve-Engine Circular Cluster, Engine Cant Angle ≈ 15 deg,
Firing No. 10

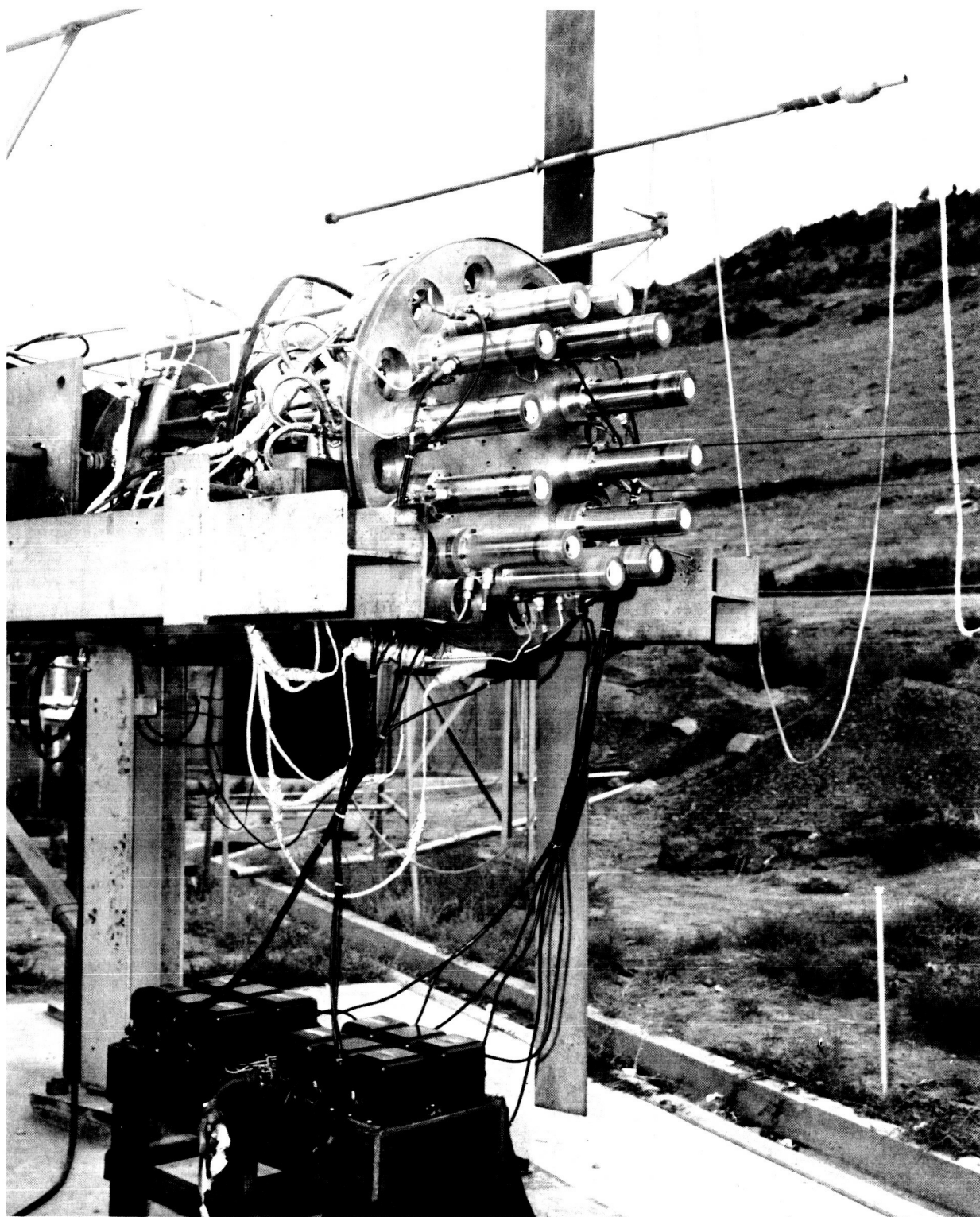


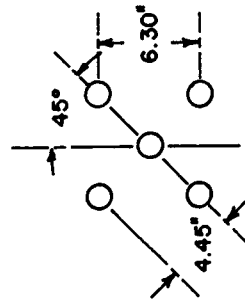
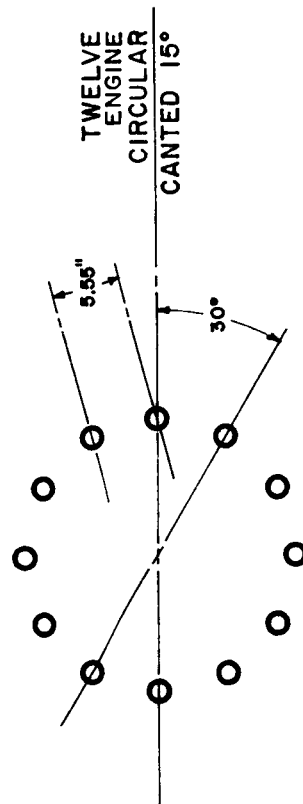
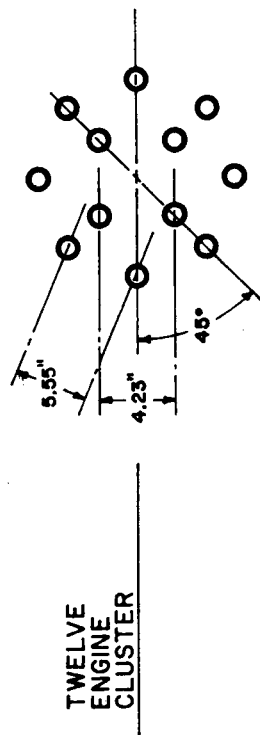
Fig. III-11 Twelve-Engine Circular Cluster, Engine Cant Angle = 0 deg,
Firing No. 11

Engine exit diameter = 1.56 inches.

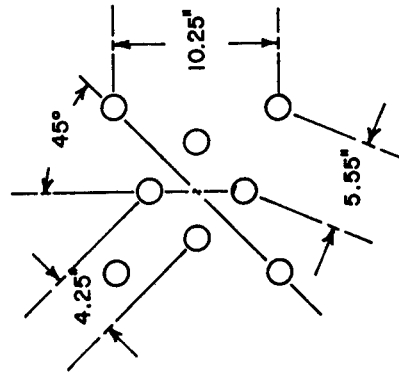
Scale: 1/8

Scale: 1/10

Engine exit diameter = 1.56 inches.



EIGHT ENGINE SATURN IB



EIGHT ENGINE CIRCULAR

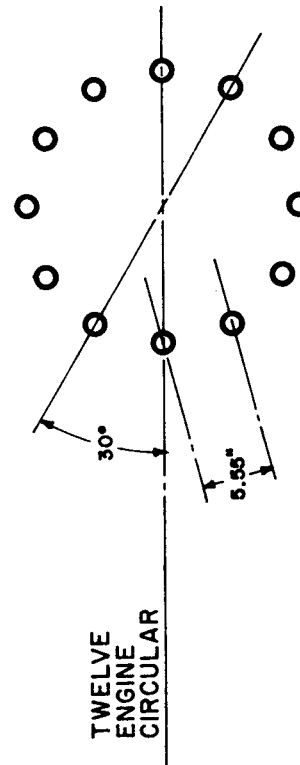
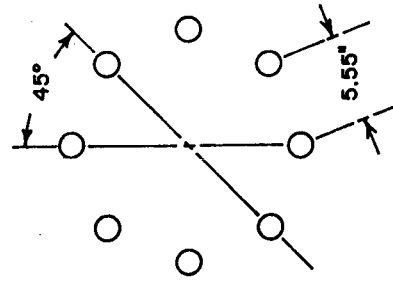


Fig. III-12 Multiple-Engine Cluster Configurations

2. Program Firing No. 10

This firing was the circular cluster with all engines canted 15 deg toward the centerline of the thrust plate. Results were again satisfactory. No hardware damage was observed, and good agreement with results of Firing No. 9 was indicated. Approximately 2.6 seconds of data were obtained prior to shutdown.

Figure III-7 presents the chamber pressure data on this run. Consistent results are noted with the average maximum pressure equal to 1237 psi.

3. Program Firing No. 11

This test used the twelve-engine circular configuration with all engines on centerline. Results were again satisfactory, and no significant damage was noted. Engine chamber pressure data (Fig. III-8) indicate an average maximum of 1231 psi. Thrust chamber valve closing was extended one sec for this run to increase the period of steady-state run time as much as possible.

IV. DATA ACQUISITION AND ANALYSIS SYSTEMS

This chapter describes the acoustic data acquisition and reduction systems, including calibration procedures. The systems, although not unusual, meet the program requirements for reliability and accuracy. The data handling is described to familiarize the reader with the steps involved.

A. DATA ACQUISITION SYSTEM AND PROCEDURES

The acoustic measurement points were divided into nine far-field and four near-field measurements. The far-field data were taken at nine angular positions (see Fig. II-1) on a 120-ft radius measured from the engine exit plane. The microphones were mounted on 6-ft high poles with fiberglass mounts at an angle of incidence equal to 0 deg. In Fig. IV-1, a typical far-field measurement point is shown. The microphone power supply is located in the box mounted on the lower part of the pole.

The near-field positions included three pickups mounted along the engine centerline and upstream of the engine exit and one microphone that traverses outside of and parallel to the engine exhaust stream. Figure II-2 shows the location of these near-field points. The exit plane position was fixed for all firings, with the 3-D_e and 16-D_e positions moved for different cluster configurations based on the effective cluster diameter. (Effective diameter was calculated by multiplying the square root of the number of engines by the exit diameter of a single engine.) At these three positions, the microphones were mounted at grazing incidence.

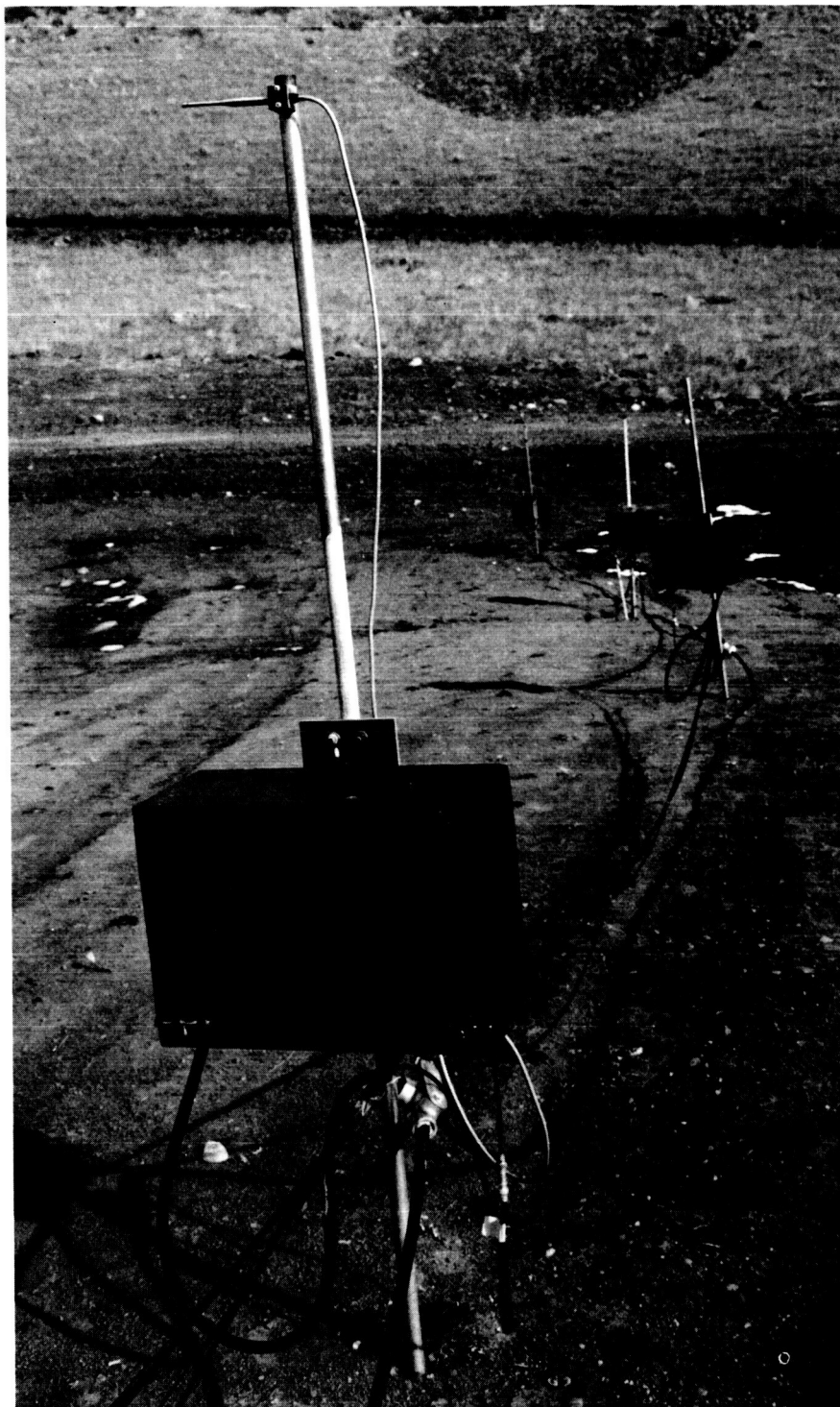


Fig. IV-1 Far-Field Microphone System Installation

Martin-CR-66-75

The traversing microphone was 22 in. to the side of the cluster centerline when positioned axially at the engine exit plane. The sensing element was 8 in. above the centerline of the cluster at all times. This latter position was necessary to minimize the view angle of the microphone diaphragm and thereby reduce radiation heating to a minimum. The traverse microphone started 11 in. upstream of the engine exit plane and ran along an angle of 10 deg (ref the cluster centerline) at a speed of approximately 3.5 fps. The motion was supplied by a 28-vdc motor and pulley system mounted on a stand 60 ft from the engine. The carriage holding the microphone remained in an upright position during travel. The extension cable connecting the microphone to the power supply was suspended from a cable above the thrust stand and was paid out as the microphone traverse required.

A high-speed movie camera (~125 frames/sec) recorded each firing from a point just downstream of the exit and 15 ft to the side of the stand. This film coverage was used for general flow visualization and propulsion system performance and as a calibration method for the traversing microphone.

A block diagram of the acoustic data acquisition system is shown in Fig. IV-2. The $\frac{1}{2}$ -in. Bruel and Kjaer microphones have a usable frequency range from about 20 cps to 100 kcps, being down approximately 3 db at the lower frequency and less than that at the higher frequency according to the manufacturer's specifications. The frequency range of interest for this program was from 50 to 10,000 cps so the microphone frequency response has no problem in covering this range. The total measurement system frequency response was fixed at the high end by the tape recorder response (0 to 10,000 cps at 60 in./sec) and the Dana amplifiers (0 to 10,000 cps), and at the low end by the microphones. The resulting system frequency response was 50 to 10,000 cps, flat within \pm one db. The total dynamic range usually achieved was about 40 db. This is set mainly by the low signal output from the mikes to the Dana amplifiers.

The acoustic calibration procedures consisted of: (1) microphone system calibrations performed by the primary standards laboratory; (2) system electrical calibrations performed in the field; and (3) prefiring and postfiring acoustic calibrations to establish the absolute system gain.

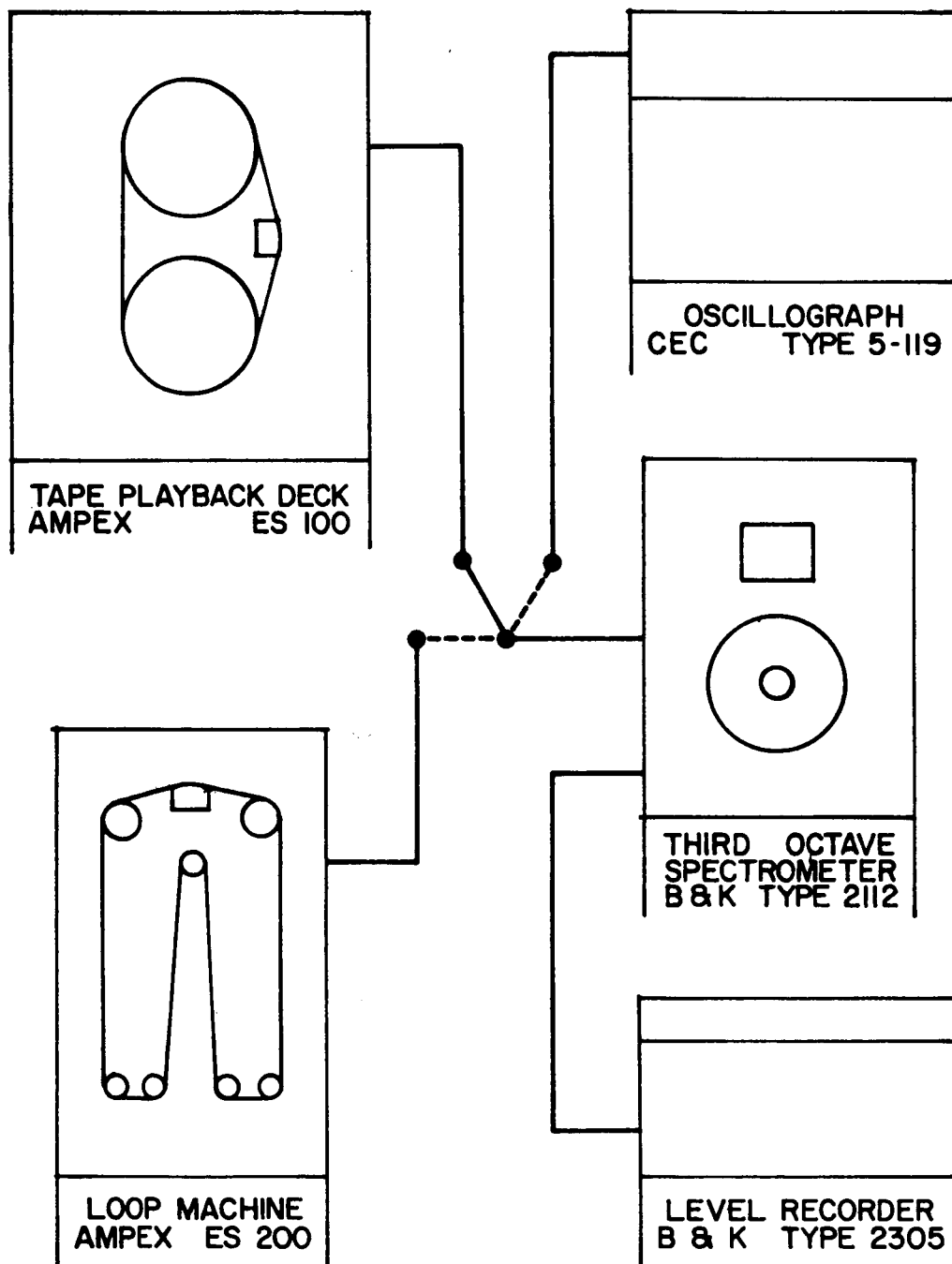


Fig. IV-2 Block Diagram of Data Reduction System

The primary standards laboratory made a microphone frequency response calibration twice during the Phase I firings and once during Phase II using the Bruel and Kjaer electrostatic actuator and covering the frequency range from 20 to 10,000 cps. The absolute sensitivity was determined by the reciprocity technique using a secondary laboratory standard microphone. This was done twice during the program. The differences between both calibrations were on the order of 0.5 db.

The electrical system was calibrated by inserting an accurately measured sine-wave signal into each cathode follower and recording this signal on magnetic tape as the frequency was varied in discrete steps. An analysis of the tape playback gave the signal deviation as a function of frequency. This system calibration produced corrections on the order of ± 0.5 db over the frequency measuring range.

Prefiring and postfiring calibrations were made using the Bruel and Kjaer pistonphone corrected for the barometric pressure. In some cases, the direct output from a channel was too high or too low to be recorded directly on the tape. In these cases, a signal substitution method was used by accurately measuring the microphone system output for the known input, i.e., the pistonphone. Prefiring and postfiring calibrations were always within ± 0.5 db.

The tape recorder oscillators were set up before each firing to ensure maximum dynamic range. The condition of each system was determined before each firing by observing the calibration signal on an oscilloscope, looking for general waveshape distortion and 60-cycle noise. The tape system distortion and cross-talk were measured only at the beginning of the program and were found to be at acceptable levels. The distortion measurements were used to determine the maximum signal that could be fed into the recorder before a significant amount of distortion was produced. In rocket engine noise measurements, since the expected levels can only be estimated, the tendency is to push the signal level high to maintain a good signal-to-noise ratio. The danger in this lies in a resulting signal level that overdrives the tape electronics and produces clipping with attendant distortion. The dynamic range of all channels was checked when set up at the highest expected gain settings. All channels proved to have an overall signal-to-noise ratio in excess of 33 db. In most cases, the signal-to-noise ratio during a firing exceeded this value.

Reduction of the traverse microphone data results in a 1/3-octave band SPL as a function of time. It is necessary to convert this to a SPL as a function of distance from the nozzle exit plane to obtain the apparent source location data. If the microphone travels at a constant speed, a correlation of the start and stop positions with time would fix the time and distance scales. Calibration using a 1/100-sec electrical timer and a measuring tape proved that the speed of travel had both linear and nonlinear regions. As a result, two methods of fixing the time and distance relationship were used -- the high-speed firing movie, and the velocity calibration curves and a start/stop signal on the magnetic tape.

The first method was accomplished by setting striped poles in line with the camera and at specified axial distances from the nozzle exit plane (0, 2.5, and 5 ft). Since the camera film speed can be obtained accurately, the number of frames were counted between successive pole crossings to determine the traverse position relative to ignition. This method is most accurate in the region of 0 to 5 ft from the nozzle exit plane.

The second method was accomplished by placing a spike on the voice channel of the magnetic tape at the microphone start and stop times. This spike was generated by the same circuitry that was used to actually provide power to the dc motor driving the traversing carriage. Since a previous calibration had been made of the microphone position as a function of time, the time scale can be converted to a distance scale.

An important part of the data acquisition program was to acquire meteorological data pertinent to the objectives of the tests. For example, a contract requirement was that no testing should be done with winds in excess of 5 knots. A roof-mounted anemometer was used to obtain local wind velocity and direction both of which were recorded on a potentiometric recorder at the time of test.

The local Martin Company weather station provided dry-bulb temperature, dew point and/or relative humidity, and barometric pressure corrected to the laboratory altitude at the time of each test firing. The weather station is located about $\frac{1}{2}$ mile from the test site on a hilltop. There was evidence from the Phase I data that the atmospheric acoustic attenuation which was calculated based on the station weather data was high. For this reason the wet and dry bulb temperature and the barometric pressure were measured at the test site during the Phase II firings.

This weather information permitted the calculation of engine performance and atmospheric acoustic attenuation as well as ensuring that the contract requirement concerning wind velocity was met.

B. DATA REDUCTION SYSTEM AND PROCEDURES

The primary data reduction system used is shown in block diagram form in Fig. IV-3. The Ampex ES 100 was used to play back all tapes for the overall time histories and to reduce the traversing microphone data. The Ampex ES 200 loop machine was used for all 1/3-octave band analyses of each data sample. The Bruel and Kjaer audiofrequency spectrometer was used for both the overall and 1/3-octave band analyses. The data were recorded on the Bruel and Kjaer level recorder. For most of the tests, an unfiltered oscillographic record was made of each data channel using the CEC Type 5-119 oscillograph. The data reduction system correction is included in the previously described system electrical response.

The data reduction procedures consisted of two steps. The data were played back unfiltered and recorded on the Bruel and Kjaer level recorder and the CEC oscillograph as overall rms time history and waveform history, respectively. Examination of these records was made to determine the general quality of the signal and to detect if any clipping or other distortion was present. Correlation of this record with the engine performance data permitted a data sample to be selected during the steady-state portion of the test. Since the prefire noise was also recorded, the overall signal-to-noise ratio was measured at this time. The sample times were between 2.5 and 4.0 sec for all runs and are listed in Table A-1 in Appendix A. After the data sample was selected, the 1/3-octave band analysis was performed on all acoustic measurements except the traversing microphone. The 1/3-octave analyzer was set at a scan rate of one 1/3-octave band in 4 sec. This scan rate ensured that all data from the sample would be used.

ONE OF THIRTEEN SIMILAR CHANNELS.

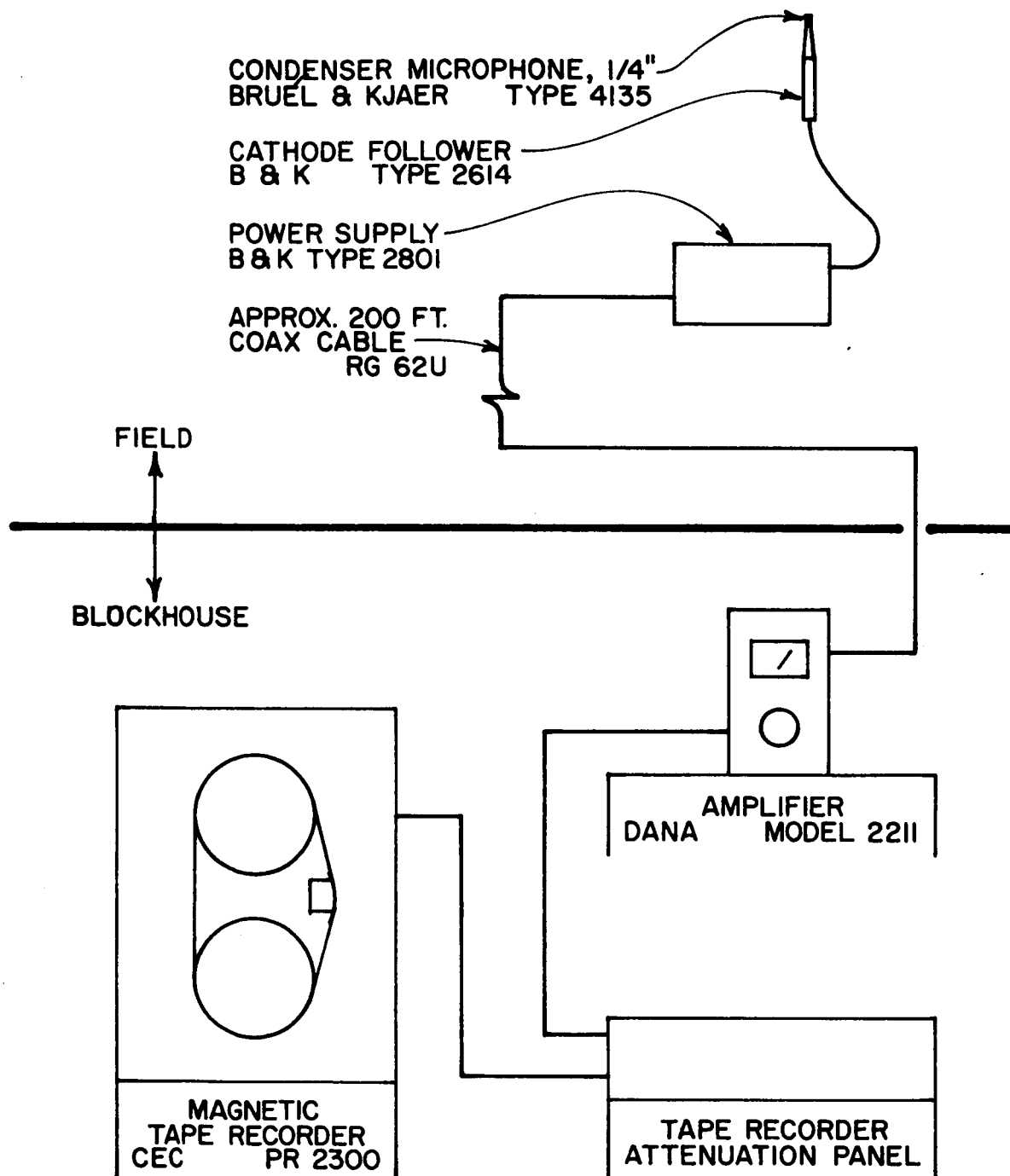


Fig. IV-3 Block Diagram of Acoustic Data Acquisition System

The statistical accuracy of a broadband data analysis is a function of the sample time and bandwidth. For constant percentage bandwidth analysis, the lowest frequency band is the most unreliable. Confidence limits have been calculated from Ref 2 for the lower 1/3-octave bands and a sample time of 3 sec. The results are that 90% of the data in the 50-cps band should lie within -1.1 and +1.3 db of the measured value. Since most of the data samples used are for longer sample times, this range will decrease. For example, a 4-sec data sample will give limits for the 50-cps band of from -1.0 to +1.1 db for 90% of the data.

One run was used to determine the 1/3-octave band signal-to-noise ratio, and some results are seen in Fig. IV-4. This is the worst case and shows that 64 cps is the only band that comes even close to a bad signal-to-noise ratio.

The traversing microphone data reduction was analyzed in 1/3-octave bands as a function of time. The marking channel on the Bruel and Kjaer level recorder was used to record the start and stop signals from the tape. Various events can be easily detected on the overall trace on the level recorder. The traverse microphone is stationary during the start transients and is activated only after the engines are running. The events in the start sequence can be identified and assist in the checking of the traverse microphone position. The level recorder speed is an important variable in determining the microphone position and, for this reason, was checked by playing an accurate one-pps signal on the marking channel and running the tape at an indicated speed of 30 mm/sec. This check showed that the level recorder tape speed was accurate and stable.

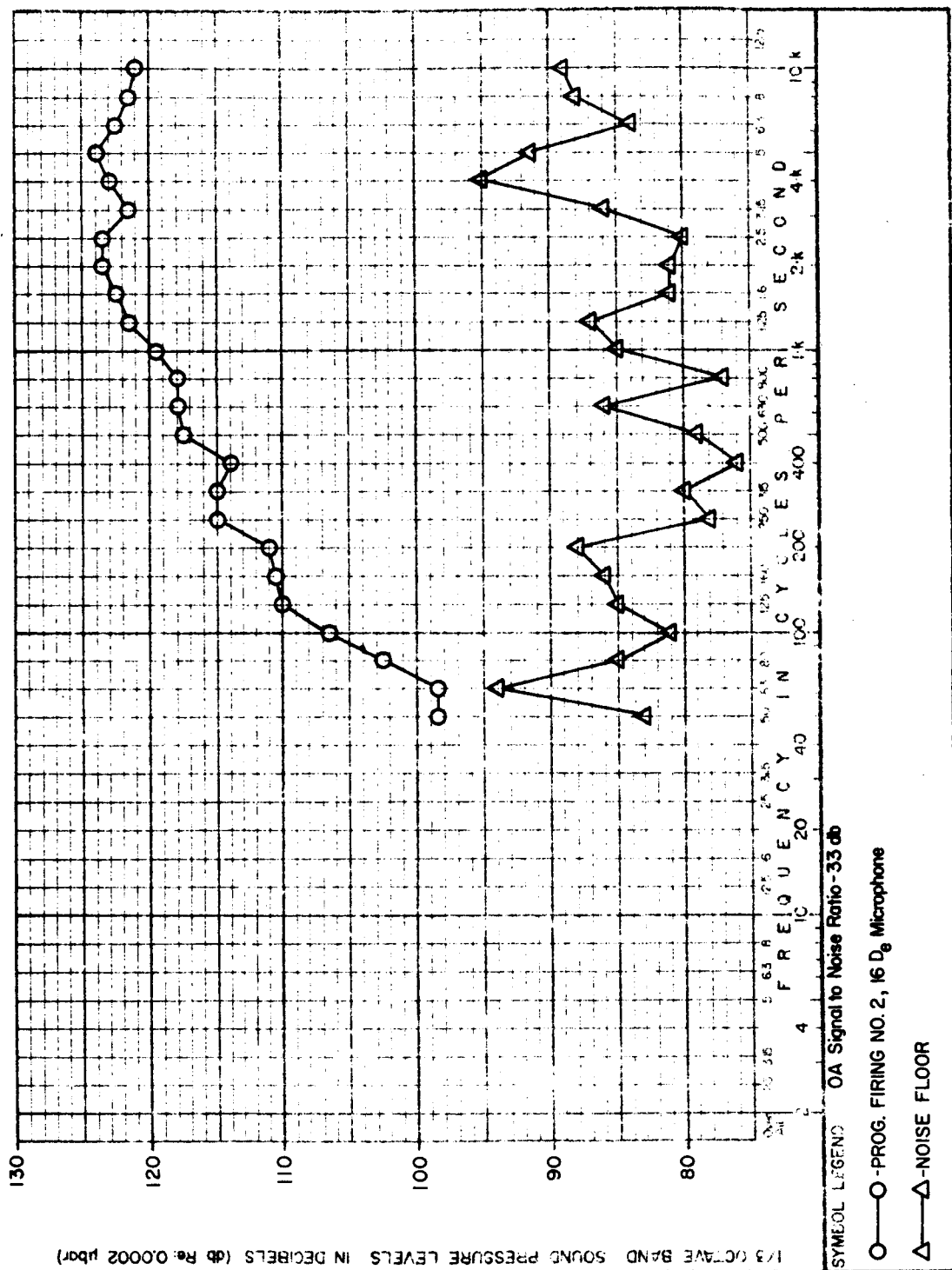


Fig. IV-4 Signal-to-Noise Ratio 1/3-Octave Band

V. RESULTS OF PROGRAM FIRINGS

A. ANALYSIS PROCEDURE

The 1/3-octave band sound pressure levels were tabulated from the level recorder traces by taking an average value in each band where some variation in time was present. These data were then corrected for the microphone and electrical system responses. For the frequency range of interest, the sum of these two corrections was important only in the lowest and highest frequency bands and only rarely had a maximum value as high as 1.0 db. In addition, the far-field data were corrected for the atmospheric attenuation. This correction for a measuring radius of 120 ft is ordinarily small if the relative humidity exceeds 50%. In this program, due to the low prevailing relative humidity of the area, the atmospheric attenuation (α) is unusually large. The procedure to obtain the attenuation values given in Table V-1 was as follows. The absolute humidity was calculated from the weather data given for each test in Table A-1 of Appendix A. The experimentally determined data from Ref 3 were then used to determine the attenuation. Reference 3 gives a graphic relationship between absolute humidity and attenuation (α) when the maximum attenuation for a given frequency is known to occur at a given absolute humidity. (This calculation contains an altitude correction due to the fact that a measured dry-bulb temperature and dew point were used in obtaining the value of absolute humidity.) The temperature and dew point were supplied by the weather station located at the laboratory where the measurements were made.

The wind condition at the time of firing is noted in Table A-1 in Appendix A. It will be noted that for Firing 9, the wind speed is listed as 4-13 mph. The wind was less than 4 mph previous to the firing with the 13-mph upper limit due to a gust before the firing was completed. Since an examination of the data (SPL as a function of time) did not indicate any marked effect due to the gust, it has been assumed that the wind was local and did not alter the sound field appreciably.

The acoustic power level spectrum was calculated for each firing by integrating the intensity over a hemisphere using the measured far-field sound pressure levels. A value of $\rho_0 c_0$ was determined for each firing to use in this calculation and was generally on the order of 33.5 rayls.

TABLE V-1 ATMOSPHERIC ATTENUATION (α) in db/120 ft

FREQUENCY CPS	Program Firing Number										
	1	2	3	4	5	6	7	8	9	10	11
630	0.2	0.2			0.3		0.2	0.3			
800	0.3	0.4		0.2	0.6	0.5	0.4	0.5			
1000	0.4	0.6	0.2	0.3	0.9	0.9	0.7	0.8			0.2
1250	0.6	0.8	0.3	0.5	1.3	1.2	1.0	1.1	0.2	0.2	0.2
1600	0.9	1.2	0.5	0.7	1.6	1.6	1.5	1.5	0.3	0.3	0.3
2000	1.3	1.7	0.8	1.0	2.0	2.0	2.0	1.9	0.4	0.4	0.4
2500	1.7	2.3	1.4	1.3	2.3	2.4	2.4	2.4	0.5	0.5	0.6
3150	2.4	3.0	2.0	1.9	2.6	2.7	3.0	3.0	0.6	0.7	0.9
4000	3.2	3.6	2.6	2.5	2.9	3.0	3.4	3.5	0.8	0.9	1.4
5000	4.8	4.3	4.2	4.1	3.2	3.2	3.7	3.8	1.1	1.3	2.0
6300	6.4	5.1	6.4	6.2	3.6	3.9	4.4	4.5	1.5	2.0	2.8
8000	6.9	5.3	7.9	7.9	3.6	3.9	4.5	4.7	2.3	3.0	4.3
10000	8.4	6.3	10.2	10.2	4.3	4.6	5.4	5.5	3.4	4.3	6.3

The traversing microphone data results are given in Appendix A in terms of SPL as a function of distance from the nozzle exit plane. In addition, to determine an effective source distance, the peak in each curve was noted, and two distances recorded where the SPL was one db below the peak on each side. This represents to some extent the definition in determining an apparent source location and results in an area for each source rather than a fixed point.

B. RESULTS

The acoustic data have been tabulated and summarized in Appendix A. These tables give the results for all eleven program firings, tabulating the 1/3-octave band power spectra, the sound pressure level spectra, and the sound pressure distribution along the exhaust stream boundary.

There were 13 acoustic measurements planned for each of the 11 program firings for a total of 143 measurement points. Of the 143 planned measurements, nine were unsuccessful due to equipment malfunction. Five of these nine were far-field data needed to calculate the acoustic power spectrum. To supply the missing data for the power level calculation, the 1/3-octave band sound pressure levels were plotted for the firing, and the missing data points were interpolated or extrapolated as necessary. Data obtained in this manner are so noted in the tables of Appendix A.

The traversing microphone data were not obtained on four of the firings for three different reasons. The calibration tone was lost on two firings, the traversing mechanism seized on one firing, and the microphone was damaged on Firing 11.

The first six program firings were made in two groups of three identical configurations to obtain a measure of the repeatability of the overall system. Reference 1 contains a discussion of these data. The major results are that the repeatability of the far-field SPL spectra is ± 3 db for 95% of the points, and for the power spectra, it is ± 2 db for 98% of the 1/3-octave bands.

The discussion of results and comparison with other similar work is contained in Chapter VI. The one set of curves in Fig. V-1 will serve to illustrate several points. These are the 1/3-octave band power spectrum curves for Firings 1, 4, 7, and 10. The "dip" in the spectrum at 315 to 400 cps for Firings 1, 4, and 7 and at 800 cps for Firing 10 are attributed to a ground attenuation phenomenon discussed in detail in Appendix A of Ref 1. This absorption is a function of source and receiver geometry and the specific impedance of the ground plane. The theory in Ref 1 shows that the maximum attenuation occurs at an increasing value of the frequency as the impedance increases. The trend is borne out by the data of Fig. V-1 and the observation of the change in the ground conditions between the Phase I and Phase II firings. The ground during the Phase I firings was generally soft with a low specific impedance (actual values are given in Ref 1). In preparation for the Phase II firings (9 thru 11), the measuring plane was scraped and packed resulting in a "hard" surface with undoubtedly a higher specific impedance. This effect makes the data interpretation difficult but, in most cases of the study in Chapter VI, it is easily identifiable.

The spectrums in Fig. V-1 also illustrate the marked change in the spectrum shape resulting from the cluster configurations. The sharp rise in the low frequency noise results in a shift of the peak of the spectrum to lower frequencies for the larger clusters. The high frequency components, after an increase between the single engine and the five-engine cluster, do not further increase in magnitude for the larger clusters.

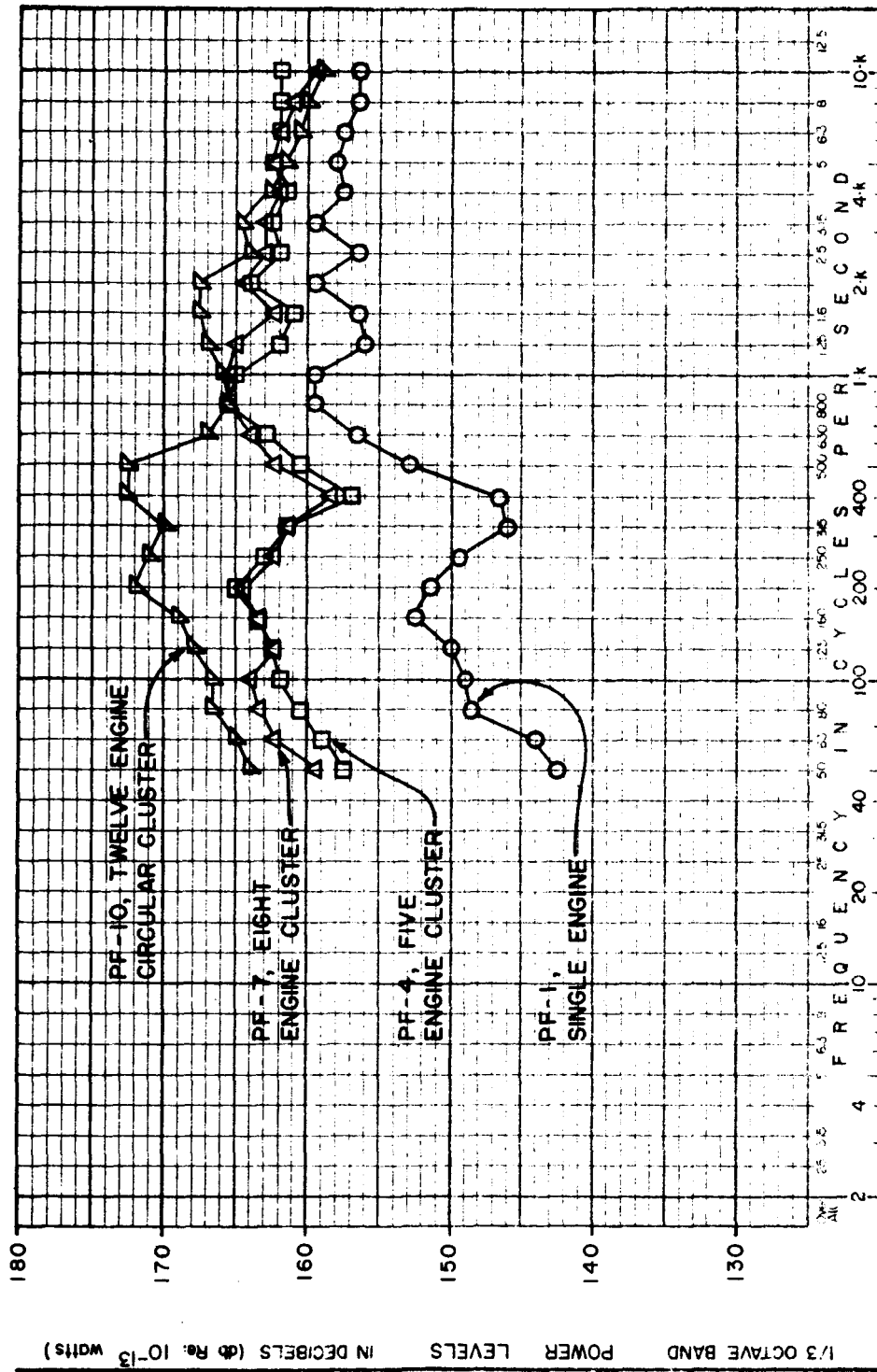


Fig. V-1 1/3-Octave Band Power Spectrums of Four Program Firings

VI. DISCUSSION OF DATA AND DATA COMPARISON

The noise source produced by high-speed gas flow is a complicated phenomenon. In spite of the fact that much theoretical and experimental work has been done in this field, it is not now possible to accurately predict the noise source characteristics or resulting acoustic field using the obtainable aerodynamic data of the exhaust stream. A step in this area has been taken (Ref 4) where the acoustic power spectrum of a subsonic jet has been calculated using aerodynamic variables of the exhaust. Specifically, the mean velocity distribution in the exhaust is coupled with an apparent source location to calculate the acoustic power spectrum.

In the absence of a similar method for rocket exhaust sources, the approach of developing correlation parameters has been used most often. Many parameters, such as the "generalized power spectrum," have been produced in an effort to provide the means with which to predict the acoustic characteristics of rocket motor exhausts not previously measured or perhaps even built. In addition to providing a means of extrapolating, the correlation parameters can also give a qualitative insight into the basic noise source mechanism.

The acoustic power spectrum and the directivity are source characteristics necessary to define the far acoustic field. These, coupled with the "apparent source location" in the stream, have been used with some success in defining the near/field environment. Finally, the correlation of the near-field acoustic environments along the upstream axis of the flow is a useful parameter.

This chapter contains a discussion of the data gathered during both Phase I and Phase II of this contract. This discussion is combined with a comparison of these data, information produced by other researchers, and some suggested correlation parameters.

Tables VI-1 and VI-2 are tabulations of the engine performance data for the present work and for the various sources used in the correlation study. Most of the data are included in the referenced reports; however, some has been estimated in order to make use of the acoustic data. It should be emphasized that the data selected for comparison were obtained, as in the present work, from undeflected high speed exhausts. The discussion is broken into five main areas -- the overall acoustic power level, the acoustic power spectrum, the directional effects, the apparent source location, and the near sound field.

Table VI-1 Engine Performance Data Comparison

Reference	Authors	Thrust (lb)	Exit Velocity (fps)	Exit Diameter (in.)	Exit Mach No.	Exit Density (lb/cu ft)	Weight Flow (lb/sec)	Mechanical Power (watts)	Gas Constant, R, lb ⁻¹ °R	Overall Acoustic Power Level (db)	Acoustical Efficiency (%)	Comments
Present Work	Smith & Brown	400	12,600	1.56	3.5	0.00496	1.0	3.5×10^6	192	170	0.3	Gaseous O ₂ /H ₂ Engines
11	Manhart GN ₂ Tests	16,600	5,400	30	3.3	0.00373	100	6.2×10^7	772	180	0.16	Nuclear Rocket
	KIWI B-4E	41,750	19,500	30	3.7	0.00072	69	5.5×10^8	772	190	0.18	Nuclear Rocket
12	Mayes Nozzle F	1,650	6,600	2.88	2.59		8.05	7.4×10^6		176	0.54	Solid Rocket Motor
6	Morgan Rocket	430	8,300	2.33	3.12	0.0065	1.67	2.6×10^6	54	173.5	0.87	Solid Rocket
	Helium "A"	162	7,900	1.47	3.12	0.0065	0.66	1.03×10^6	387	174	2.4	Cold Helium Jet
10	Cole Rocket C	100,000	*	*		0.0387	*	42×10^7	62	195	0.75	Solid Rocket
	Rocket F	34,000	*	*		0.0146	*	15.7×10^7	62	190	0.64	Solid Rocket
13	Cole	1,000	5,850	2.6	3.05 (Est)		89	4×10^6	54 (Est)	170	0.25	Solid Rocket Motor
18	Mull		2,000 (Est)	1.2	2.87				53			Cold Air (80°F) Jet

*Classified Information.

Table VI-2 Data Summary for Present Work

Program Firing	Configuration	Overall Acoustic Power Level (db)	Δdb (From Table VI-3)	W_M (10^3 watts)	W_A (10^3 watts)	η (%)	F_g (lb)	u (10^3 fps)	D_e (in.)	D_c (in.)	D_5 (in.)	u_5 (10^3 fps)
1	•	169.5		3.45	8.8	0.25	404	12.6	1.56	1.56	15	2.63
2	•	170		3.36	9.7	0.29	398	12.4	1.56	1.56	15	2.63
3	•	171.5		3.84	13.8	0.36	436	13.0	1.56	1.56	15	2.63
4	••	176	-1	17.4	40.8	0.23	2040	12.5	3.5	10.4	16.3	1.56
5	••	176	-1	17.1	41.3	0.24	2040	12.4	3.5	10.4	16.3	1.56
6	••	176	-1	16.7	40.7	0.24	1970	12.5	3.5	10.4	16.3	1.56
7	•••	177	-2	26.2	52.5	0.20	3136	12.3	4.4	16	22.4	1.42
8	•••	177	-2	28.7	52	0.18	3288	12.9	4.4	16	22.4	1.42
9	••••	181	+1	37.2	126	0.34	4430	12.4	5.4	16	20.3	2.14
10	•••••	181.5	+1	39.4	141	0.36	4590	12.7	5.4	22.8	--	--
11	••••••	178	-2.5	40	63	0.18	4580	12.9	5.4	22.8	27.7	1.39

Notes: 1. $M_e = 3.5$.2. $p_e = 11.8$ psia.3. $\rho_e = 0.00496$ lb/cu ft.4. $d_e = 1.56$ in.

A. OVERALL ACOUSTIC POWER LEVEL

The acoustic efficiency of an exhaust stream is defined as the ratio of the acoustic power to the mechanical power of the exhaust. This parameter has been proven useful in correlating the efficiency as a function of mechanical power, as in Ref 5. Guest used data over a thrust range of 4000 to 1.5×10^6 lb and showed that the efficiency (η) increases with mechanical power, approaching a constant value of 0.6% for mechanical powers on the order of 10^{12} watts.

The results of the present work are shown in a different form in Fig. VI-1 (also in Table VI-2) along with data from the indicated sources. Here, the total acoustic power is plotted as a function of the stream mechanical power with lines of conversion efficiency (η) drawn in. The results of the present work, ranging in thrust from 400 to 4600 lb, lie along the 0.25% efficiency line. Guest's curve indicates an efficiency of about 0.2% for mechanical powers on the order of 10^7 watts. It is obvious from Fig. VI-1 that there is considerable scatter of the data over a wide range of mechanical power. For example, efficiencies as high as 2.4% were obtained by Morgan (Ref 6) at a mechanical power of 10^6 watts. This is an order of magnitude higher than would be expected based on the trend established by the other data.

There is also some scatter between the various cluster configurations of the present work. The changing efficiency here can be interpreted another way, namely as an effect of clustering. Table VI-3 gives the measured power level of each cluster and the power level which would be expected if the clusters exhibit the same efficiency as the single engine. The difference is a measure of the effect on the total acoustic power of clustering a number of engine modules. That the reduced power level (e.g., -2.5 db for Firing 11) is an effect due to clustering is supported by the few investigators who have worked with clustered nozzles. Measured results in Ref 7 and 8 confirm this result, while the theoretical work of Potter and Crocker in Ref 9 recognize the effect as being due to shielding of the "inner" acoustic sources of the cluster.

STREAM MECHANICAL POWER,

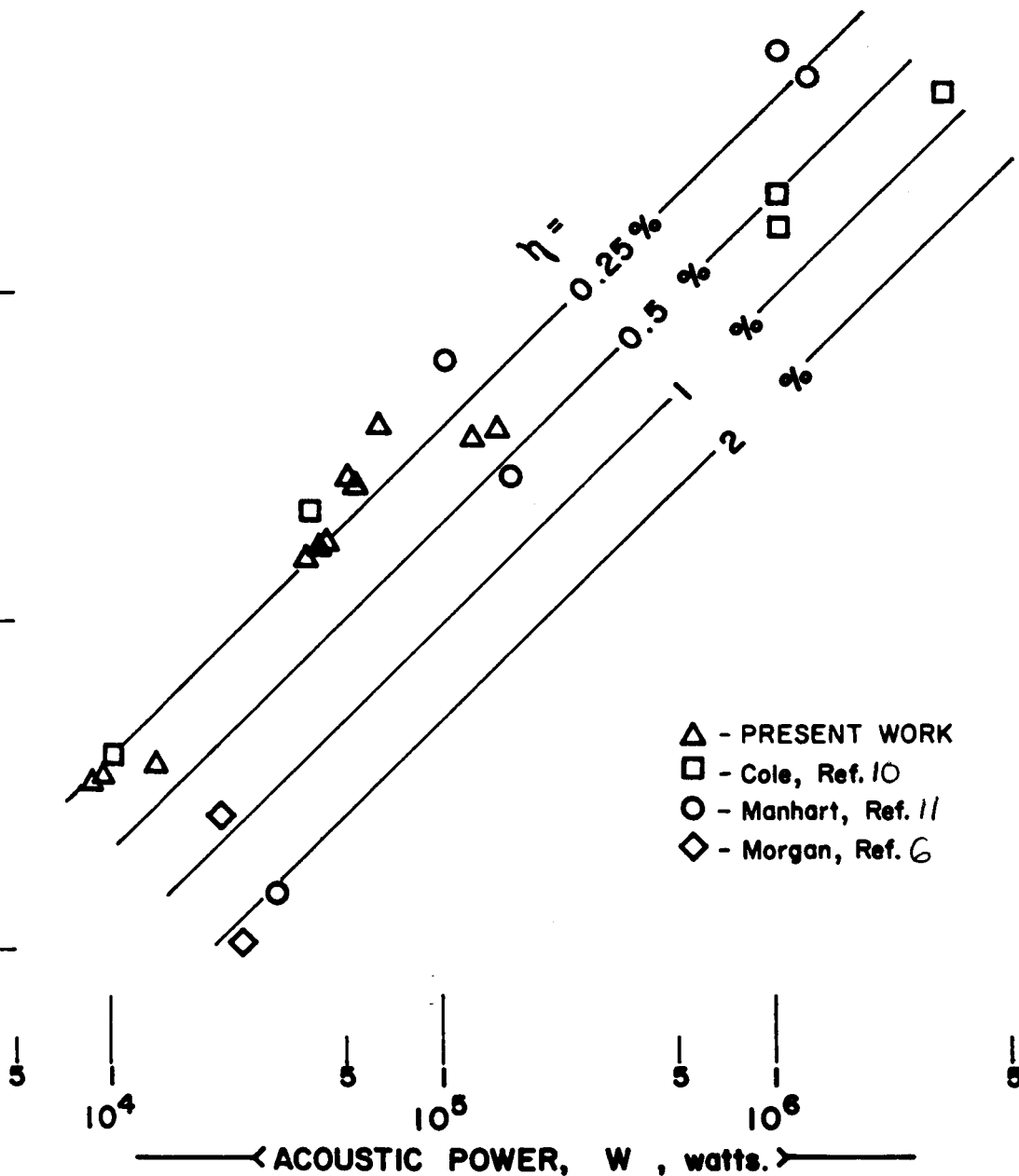
 W_M , watts. 10^9 10^8 10^7 10^6 Fig. VI-1 Comparison of Acoustic Efficiency, η

Table VI-3 Effects of Clustering on Overall Acoustic Power Level

Firing	Configuration	Measured Overall Acoustic Power Level (db)	Overall Acoustic Power Level of the Single Engine (+ 10 log ΔW_m)	Δ Power Level (db)
1-3	Single Engine	170	170	--
4-6	Five-Engine Clusters	176	177	-1
7-8	Eight-Engine Clusters	177	179	-2
9	Twelve-Engine Clusters	181	180	+1
10	Twelve-Engine, Circular, Canted	181.5	180.5	+1
11	Twelve-Engine, Circular	178	180.5	-2.5
<u>Note:</u> ΔW_m = the increase in mechanical stream power of the given cluster over a single engine.				

B. ACOUSTIC POWER SPECTRUM

The present work offers the opportunity to explore the effect that clustering has on the acoustic power spectrum. Since the data used to determine the various generalized power spectrums, such as Ref 10 and 11, are produced by single nozzles, the question arises as to the characteristic diameter to be used in correlating clustered engines. In the past, an equivalent diameter has been used and is defined as the diameter of a single nozzle with the exit area equal to the total cluster exit area or, $D_e = \sqrt{N} d_e$.

This diameter may not represent any real physical dimension in the exhaust stream but is the diameter of an equivalent single engine flow area.

Figure VI-2 shows the power spectrum correlation of the present work using this effective diameter. The ordinate in the figure is one proposed by Cole in his correlation of power spectrum data in Ref 10. The data used here are the 1/3-octave power spectrum levels and are the actual data points. The effect of the ground attenuation discussed previously is evident in the "dip" in the data points. This correlation gives a fair collapse of the data, but the resulting curve does not agree with Cole's generalized spectrum which peaks at a Strouhal number of 0.025 and at +11 db on the ordinate

The bottom plot in Fig. VI-2 uses the diameter of the cluster as the characteristic diameter with the result that the data again correlates, but the agreement with Cole's curve is not very good. This cluster diameter is measured between the outer edges of the outside engines in each cluster and comes closer to representing an actual stream dimension than the effective diameter. To compare with other investigators, the plot of Fig. VI-3 is used, which is from Manhart (Ref 11) and contains data from Cole (Ref 10), Morgan and Young (Ref 6), and the present work. This correlation technique does not work well as can be seen from the figure. Table VI-1, which contains the performance data for these references, shows a wide range of thrust, velocity, and nozzle diameter covered in the attempted correlation in Fig. VI-3. The magnitude of the factor U_e / D_e seems to be involved in the data scatter, indicating that the basic correlating parameters are not correct over this range of variables.

A different approach is used in the result shown in Fig. VI-4. The ordinate is simply the octave band power level relative to the overall power level. The abscissa is again the Strouhal number using an effective diameter. The correlation of the present work is very good in Fig. VI-4 (most of the points below the curve result from the ground attenuation). Comparing this with the other work in the lower part of the figure shows the agreement to be good on the ordinate but poor on the abscissa. The shapes of the curves are similar but seem to be scattered along the abscissa. Two other sources of data are added on this plot -- that of Mayes (Ref 12) and another report by Cole (Ref 13).

Martin-CR-66-75

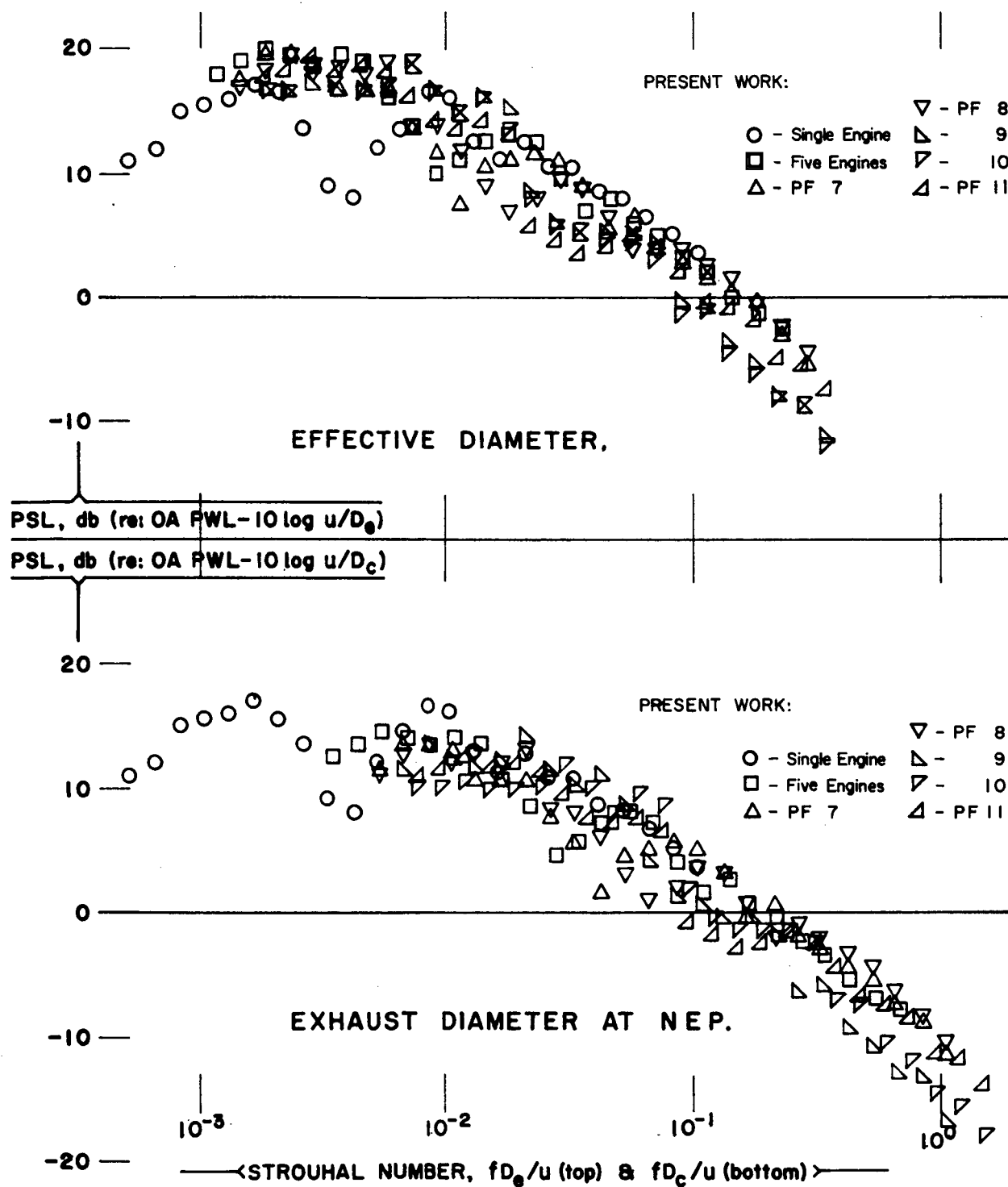


Fig. VI-2 Correlation of Acoustic Power Spectrums

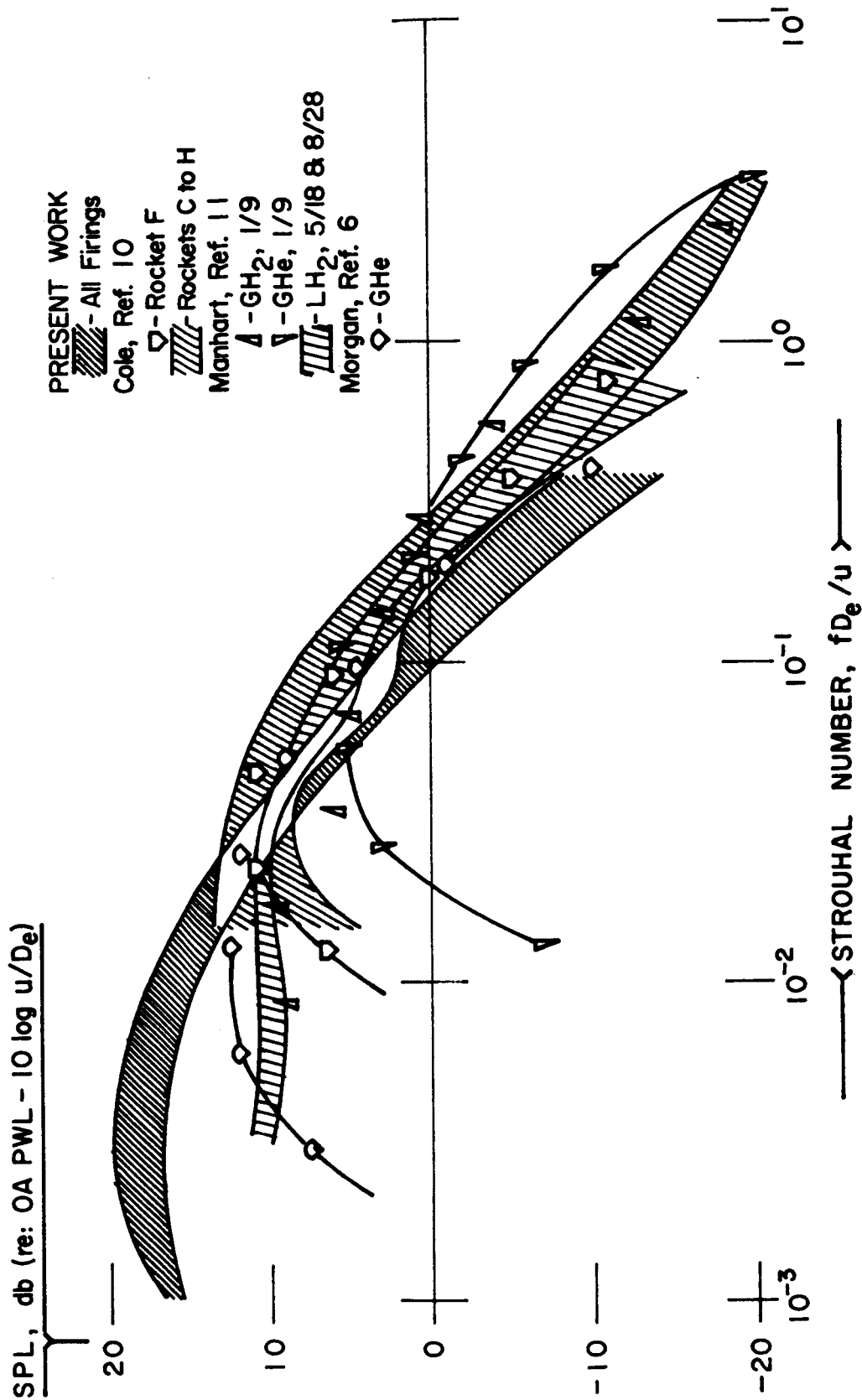


Fig. VI-3 Comparison of Nondimensional Power Spectrums

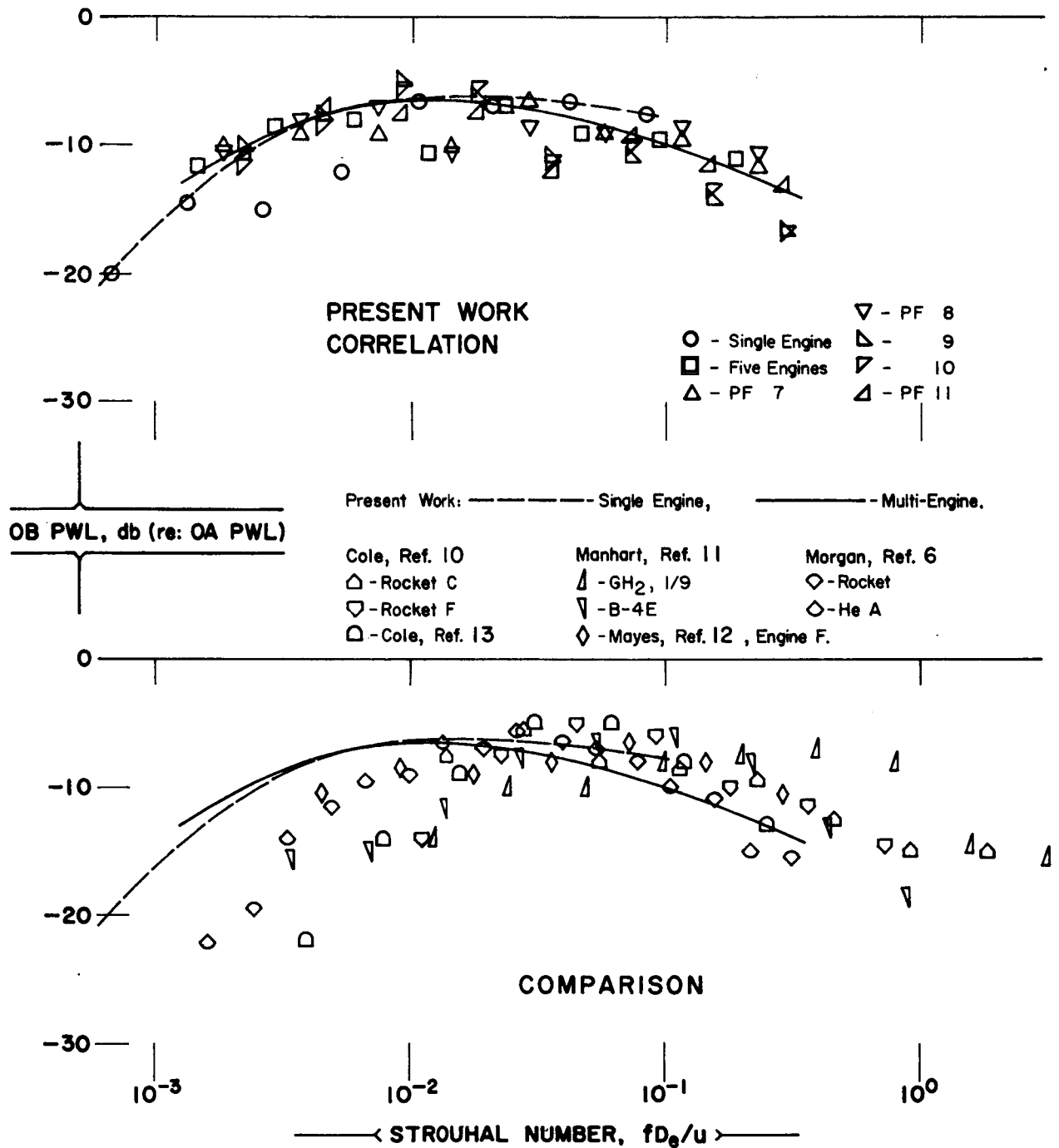


Fig. VI-4 Correlation and Comparison of Octave Band Power Spectrums

The failure of these parameters to correlate the data indicates that the acoustic source characteristics in rocket exhausts are not defined adequately by the correlation factors involving the exit velocity and by the various diameters which were used. Other correlation parameters were tried using the various combinations of variables proposed by other investigators. None were satisfactory in correlation of all the data and few seem to have any relationship to the physical situation involved.

Potter and Crocker (Ref 9) have demonstrated some success by considering a cluster of rockets to produce two regions of flow each of which has a distinctive acoustic identity. One region near the engine exit is composed of the individual flows in the cluster. This region has a characteristic velocity and diameter equal to the engine exit velocity and diameter. The second flow region exists where the individual exhaust streams have mixed to produce a flow which has a large diameter and a subsonic velocity. When the contribution from these two flow regions to the power spectrum are compared, it is seen that the large diameter subsonic flow is the major contributor to the low frequency part of the spectrum, and the individual flows produce the major effect in the high frequency end of the spectrum. The subsonic portion produces the "peak" in the overall power spectrum.

Using a method developed by Potter and Crocker, the velocity (U_5) and the diameter (D_5) were calculated for the clusters of the present work. This velocity and diameter are those at the exit of a nozzle which would produce the combined flow. Using these velocities and diameters, the spectra shown in Fig. VI-5 were calculated. The single-engine subsonic velocity and diameter were determined from the nondimensional curves of Anderson and Johns (Ref 14). For an exit Mach number of 3.5, the end of the supersonic core is found at x/d_e equal to 42. Taking the temperature decay curves and the known exit temperature, the stream static temperature at the core tip was calculated to be 860°R. Since the Mach number is 1.0 at this point, the stream velocity (U_5) was determined to be equal to 2630 fps. The spreading characteristics of the stream are also given by Ref 14 for a number of rocket motors. The effective stream diameter at the end of the supersonic core was determined by the radial velocity distribution at this point. Taking points on the radial velocity distribution curve where the velocity is 10% of its centerline value resulted in a diameter (D_5) of 15 in.

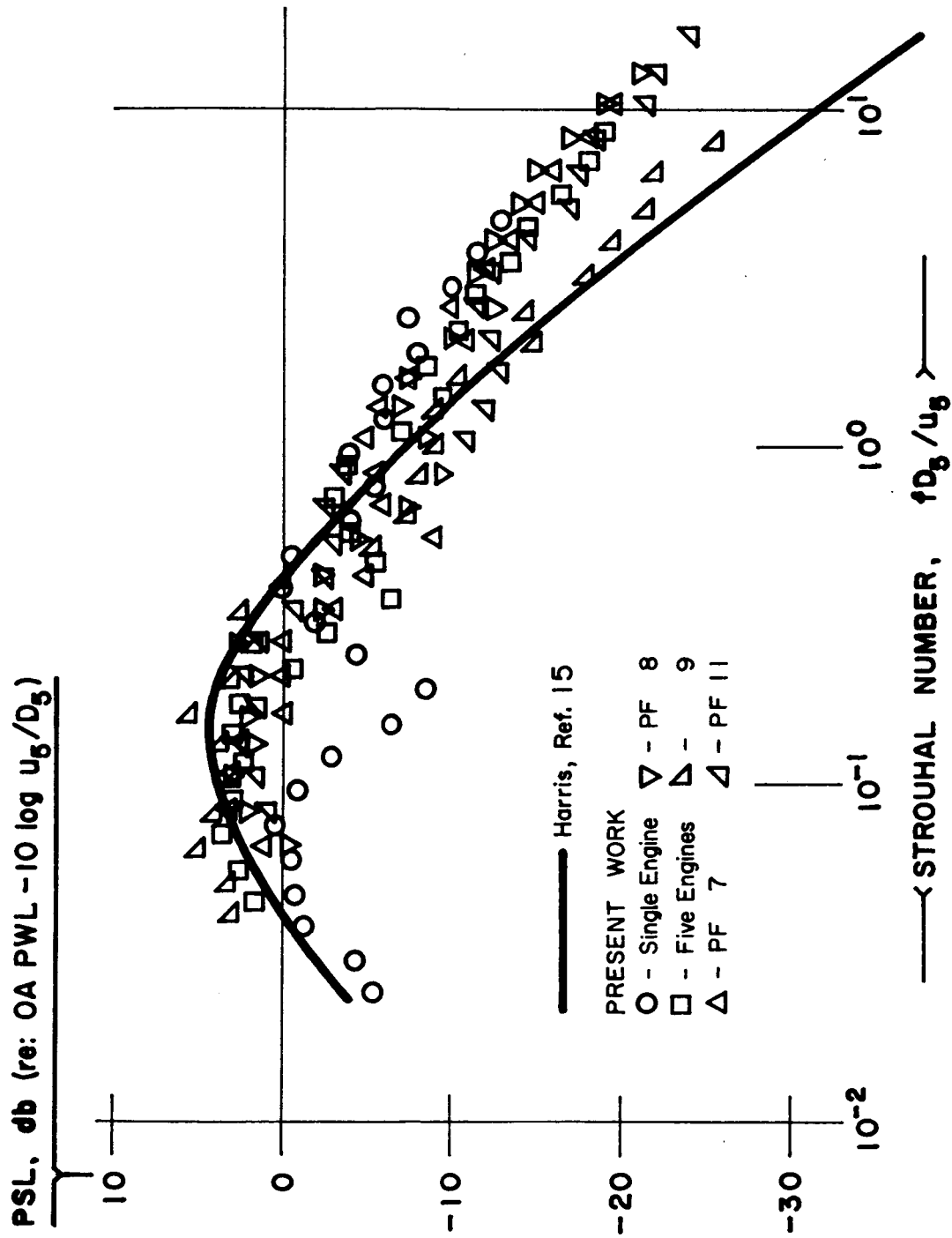


Fig. VI-5 Power Spectra Correlation Using Subsonic Parameters

Using these subsonic velocities and equivalent diameters result in good correlation of the spectra in Fig. VI-5. The heavy line on Fig. VI-5 is from Harris (Ref 15) and is the generalized spectrum for subsonic air jets and jet engines. The agreement is very good except at the Strouhal numbers above the peak. This part of the spectrum is undoubtedly influenced by the flow noise produced near the nozzle exit in the unmixed region. The peak Strouhal number is about 0.25, and the peak occurs on the ordinate at a value of about +4 db.

The procedure for the calculation of the subsonic velocity and diameter are not well defined. For example, the temperature decay in the stream depends critically on the amount of afterburning in the exhaust as well as the thermodynamic properties in the flow. It is also difficult to fix a diameter since the flow has a developed turbulent flow profile at this point.

Potter and Crocker (Ref 9) make certain assumptions in developing the equations for the determination of the "mixed" velocity and diameter of a cluster of rocket motors. It is not known how closely the present cluster plumes conform to these assumptions, mainly because of lack of information on the afterburning in the exhaust.

The success demonstrated by Potter and Crocker and apparent correlation observed with the present data is sufficient evidence to warrant further investigation in this area. Another conclusion which might be drawn is that the major sources of noise in the supersonic rocket exhaust stream may very well be in the highly turbulent subsonic region of the flow.

C. DIRECTIVITY INDEX

The directivity index is a measure of the departure of the source directional characteristics from that of a point source. It is determined by comparing the measured SPL at a point in the far-field with the average SPL at the same distance from the source. These values can be obtained from each 1/3-octave band for every firing by using the tabulated data in Appendix A. The difference between the power level and the average SPL is approximately 50 db for the 120-ft radius and the existing atmospheric conditions.

For comparison, the data which have been plotted in Fig. VI-6 represent the smoothed curve through the overall directivity index data points for each cluster configuration. One curve only is used for the three single-engine firings and one for the three five-engine cluster firings because of similarity. The symbols at the top of Fig. VI-6 are for identification only and are not data points. The plot shows that the peak of the overall directivity indices shifts to angles closer to the exhaust axis as the number of engines in the cluster increases. A more meaningful condition is that the peak in the directivity index curve shifts toward small angles as the spectrum content is dominated by lower frequency components. A later figure will demonstrate that lower frequency components peak at smaller angles than the higher frequencies; consequently, the shift in the overall directivity index curves is not surprising.

Comparing these results with the data of Cole (Ref 10 and 13) and Morgan (Ref 6), the lower plot in Fig. VI-6 is the result. In general, the shape of the curves is similar, but the single-engine data from the present work is shifted to higher angles. Morgan's single engine is about the same size but produces a much different directivity index curve. The directivity index at angles close to the exhaust axis seem to exhibit the greatest scatter. It's difficult to say whether this is the result of measurement scatter, a characteristic of the source directivity (i.e., sensitivity of the source directivity index at this angle), or some other as yet unrecognized phenomena. Some of the other data available for comparison were not used because of anomalies within the whole body of the data.

Lee and Semrau proposed in Ref 16 that the directivity patterns for a given 1/3-octave band were the same for different jet engine nozzle configurations whose overall directivity index curves were quite different. They demonstrated with a limited amount of data that this proposal had some merit. This concept, if proven true, would be a useful directivity correlation technique since the overall directivity would be a function mainly of the distribution of energy in the power spectrum. In other words, if in two different spectrums the 1/3-octave band directivity indices are the same at a given frequency, then the one which has the greater intensity will influence the overall directivity index more than the other.

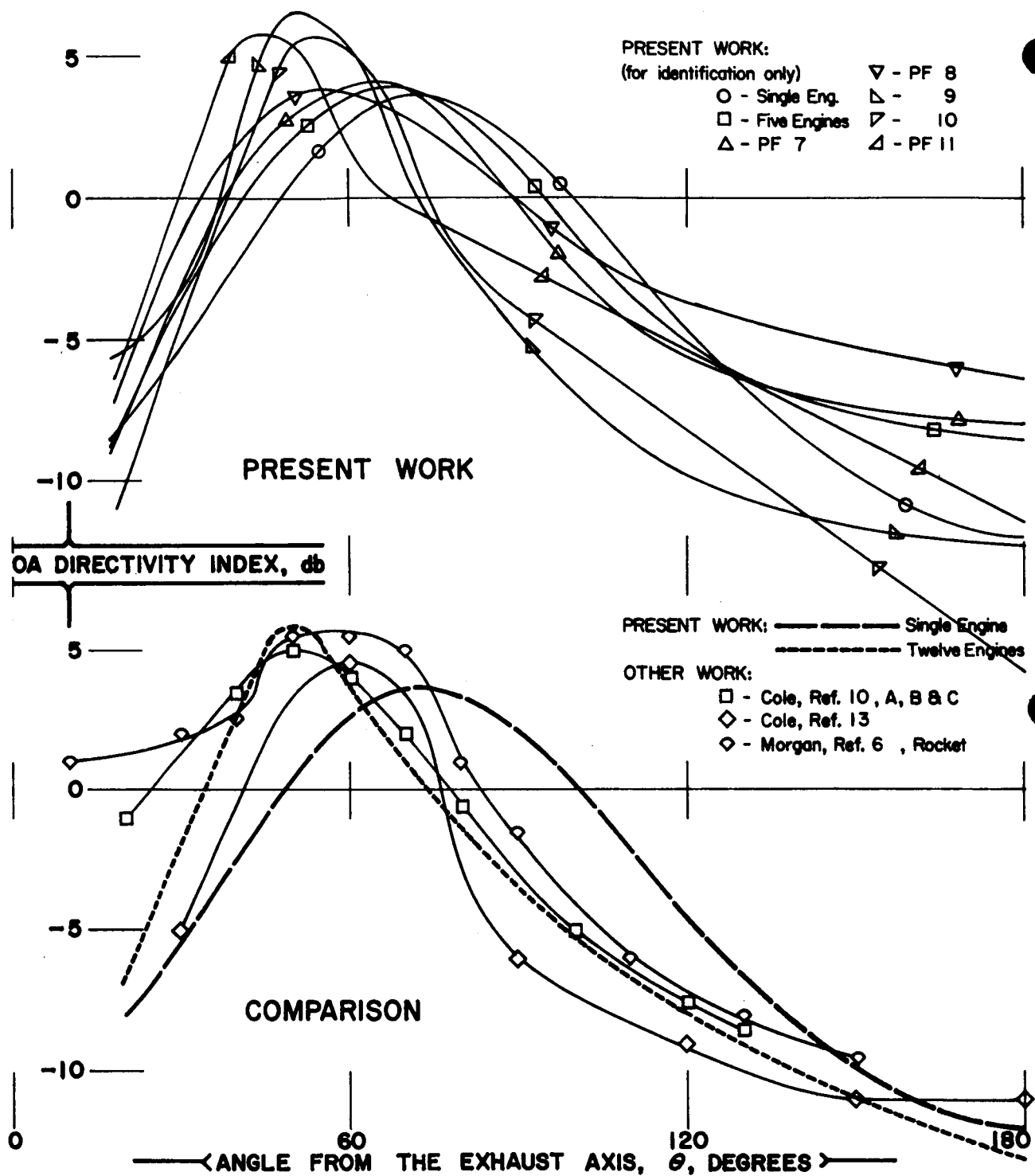


Fig. VI-6 Comparison of the Overall Directivity Indices

In Fig. VI-7, the directivity indices from four 1/3-octave bands are plotted using the 11 firings of the present work. These four bands cover a frequency range which encompasses the PWL spectrum peak of each firing. The agreement is quite good at many angles and very close for all angles in the 3150-cps band.

The data at 20 deg is distinguished by the wide scatter particularly at the lower frequencies. This method does not offer a great deal of promise considering the observed wide scatter.

D. APPARENT SOURCE LOCATION

The concept of a specific area in the exhaust stream that contains the major sources in a given frequency band has been proven useful by many investigators. It is recognized that, in reality most of the exhaust stream contributes to some extent to the power level of each frequency band.

The distribution of the 1/3-octave band SPL along the stream boundary given in Appendix A demonstrates this fact. What is usually meant by "source location" is the axial location of the peak of this distribution. This point should not be interpreted as the actual location of the major source, since an effect of refraction in the stream on the directivity has been shown (Ref 17).

The apparent source location has been determined by the traverse of a microphone along the stream boundary during a firing. The method of data reduction is discussed in Chapter IV. This moving microphone method shows the variation of SPL with distance but with the variation as a function of time superimposed. From the data in Appendix A, it can be seen that this is somewhat of a problem at the lower frequency because it is difficult to select the peak accurately.

The apparent source locations are plotted in Fig. VI-8 as the Strouhal number as a function of the axial distance from the nozzle exit plane in nozzle diameters. The exit velocity and the effective diameter are used as parameters. The correlation of the data from the various cluster configurations is fair, but this group is displaced from the single-engine curves. The reason for this disparity is not known unless it is that the exit velocity and effective diameter are not good correlation parameters. The use of the exit diameter of a single engine was tried but this resulted in much larger scatter.

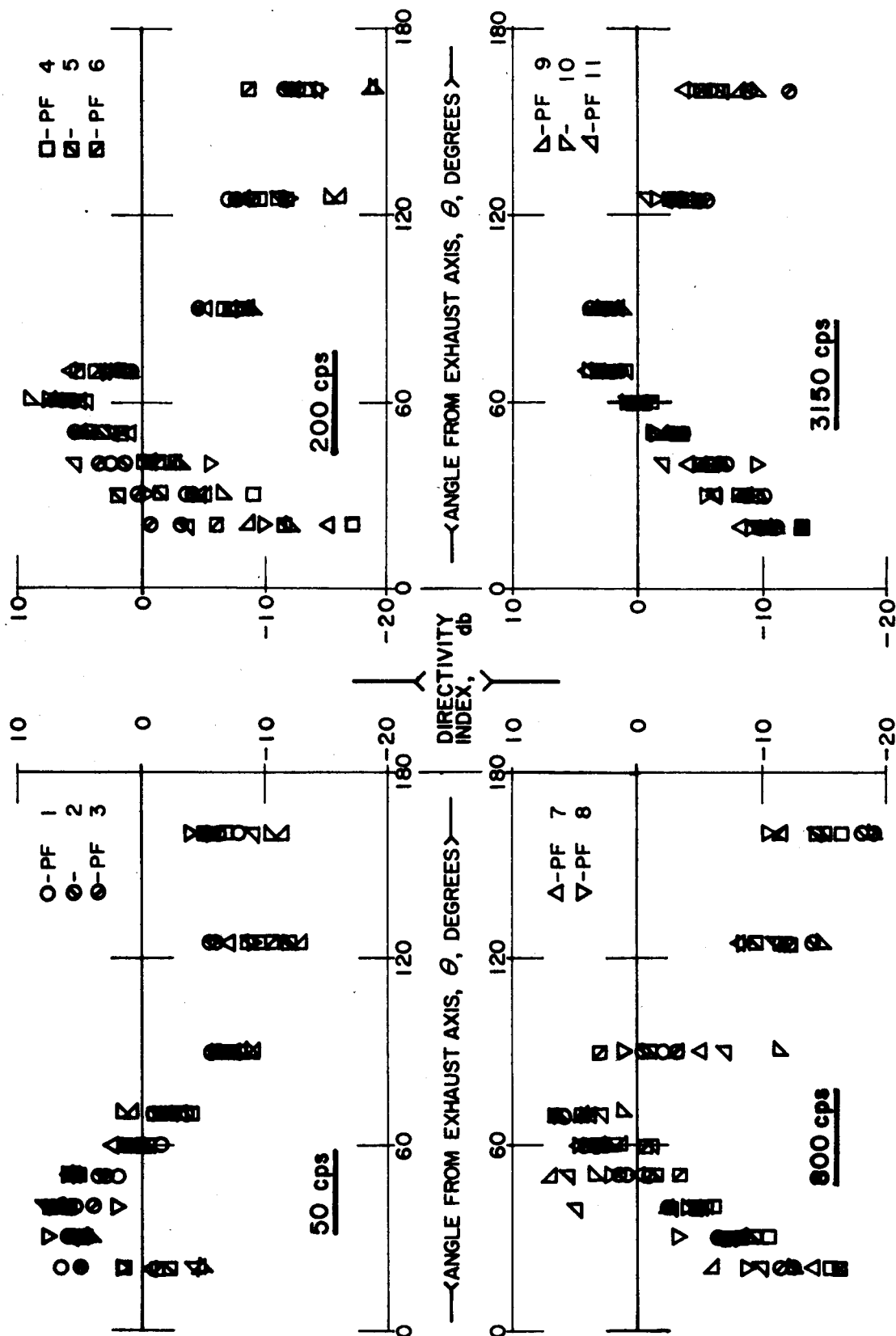


Fig. VI-7 1/3-Octave Band Directivity Index Comparison for Selected Frequencies

Overalls:

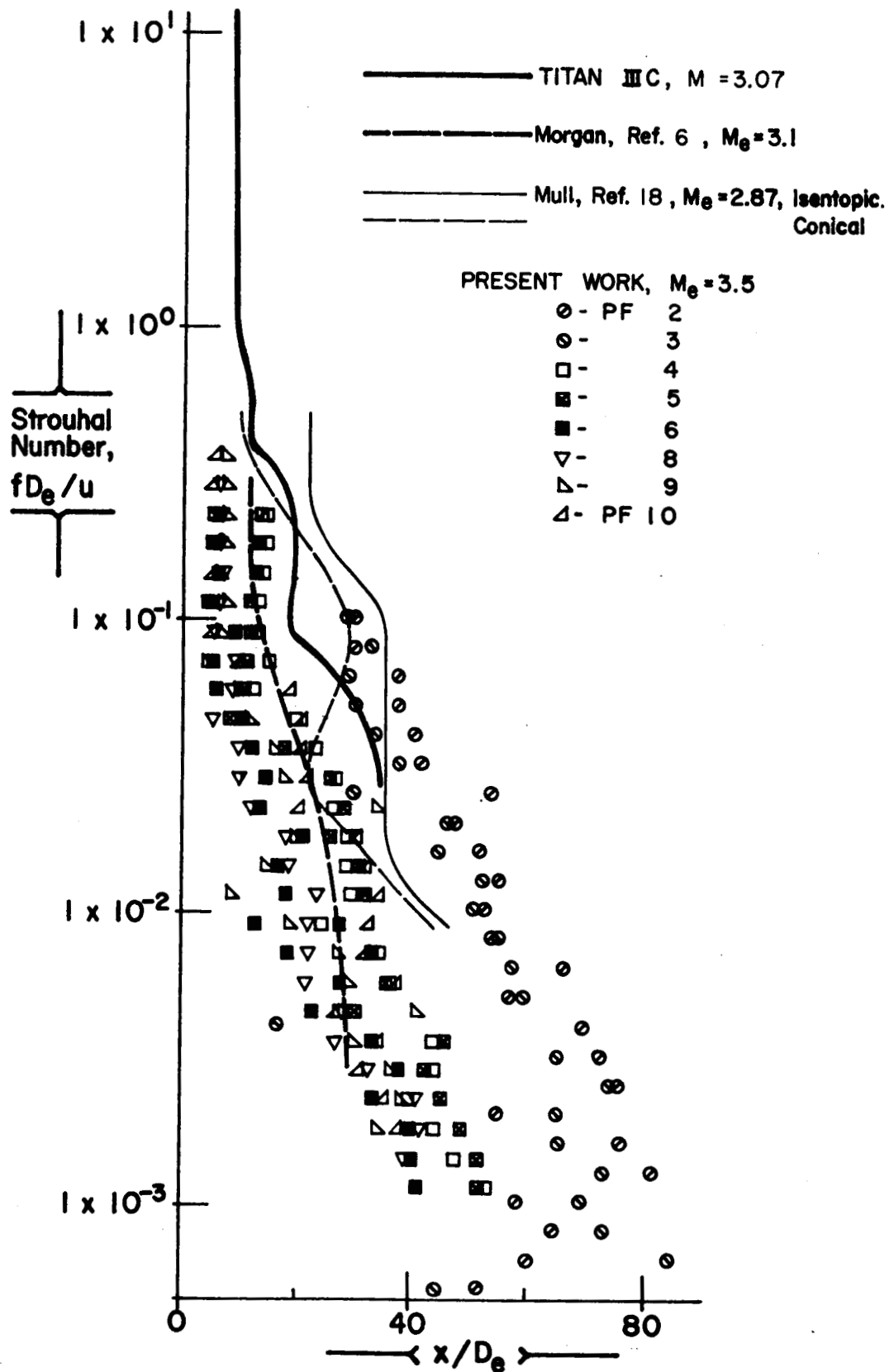


Fig. VI-8 Apparent Source Location Data Compared with Other Results

Apparent source location data from three other sources are included for comparison in Fig. VI-8 from the indicated sources. The Titan IIIC data were obtained with a microphone at the top of the umbilical tower. The SPL in each 1/3-octave band was plotted as a function of liftoff distance, enabling the source distribution to be calculated. Although the vehicle has two solid rocket motors (SRMs), the nozzle diameters of a single SRM has been used in plotting the data since the exhaust streams show little interaction. The data from Morgan (Ref 6) were taken using a line of stationary microphones along the exhaust stream boundary. The exit Mach number is given for reference.

The data acquired by Mull (Ref 18) was obtained by a single microphone traversing the boundary of the exhaust of a supersonic, cold, air jet.

There is fair agreement between Morgan's results and the present cluster data and between the other sources and the single-engine measurements. In general, the correlation is not a satisfactory one; it has too much scatter. A correlation technique using the subsonic parameters used for the power spectrum analysis might prove more useful if sufficient data on all the exhaust stream conditions could be obtained.

The overall source locations at the top of Fig. VI-8 are simply the apparent location produced by a traverse with no filtering. This information was not available for all the references but, for those shown, indicates that the apparent location of the overall noise is about 10 effective diameters from the nozzle exit plane.

E. NEAR FIELD

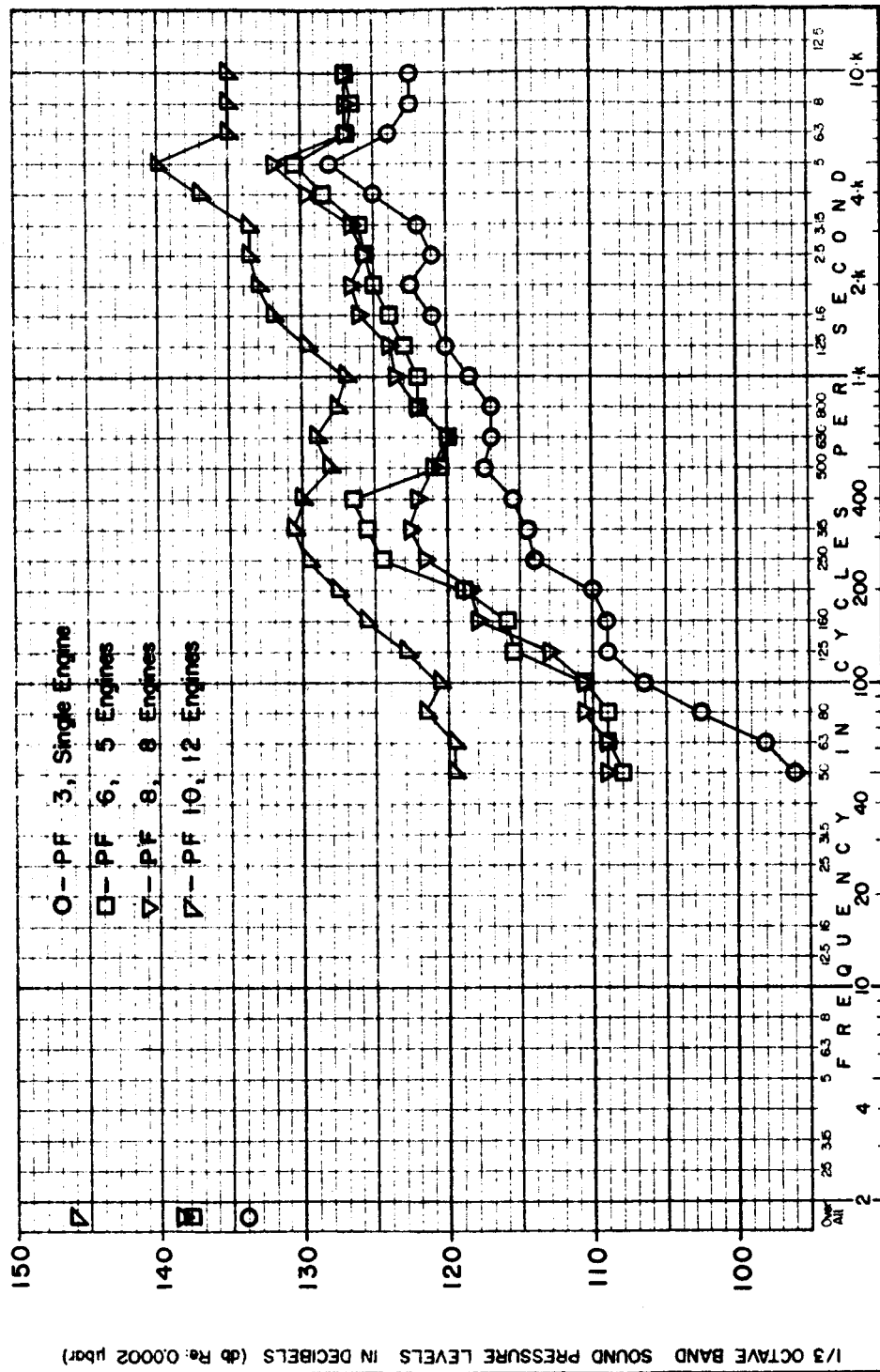
The data taken in the near field have proven the least amenable to correlation. The near-field radiation characteristics, varying source to receiver distances, and effects of reflecting surfaces are all troublesome factors.

The near-field data in this study were taken at the nozzle exit plane and at two places upstream of this point. The exit plane microphone was suspended in the air adjacent to the exhaust stream. The two other pickups were placed above a "simulated vehicle skin" surface. These two microphones were spaced three effective nozzle diameters and sixteen effective nozzle diameters from the engine exit plane. This means, for example, that the physical distance from the exit was larger for the eight-engine clusters than for the five-engine clusters. The sound pressure level spectrums for two different clusters would be expected to be equal if the following conditions are met for each frequency band:

- 1) The ratio of the effective source to receiver distances are equal to the ratio of the effective nozzle diameters, or for the twelve- and eight-engine clusters, $r_{12}/r_8 = D_{e12}/D_{e8}$;
- 2) The near-field directivity functions are the same for both clusters;
- 3) The ratio of the acoustic power is equal to the ratio of the effective diameters squared.

For condition 1) to be met, the major sources would have to be located at the nozzle exit plane. This has been previously demonstrated to be incorrect. Condition 2) is difficult to assess accurately. If the directional effects observed in the far field are indicative of the near-field case, then Fig. VI-6 and VI-7 both show, that for angles close to the upstream axis, there is a marked change in directivity with clustering configuration. Finally, condition 3) is met when considering the overall power level but not in the various frequency bands.

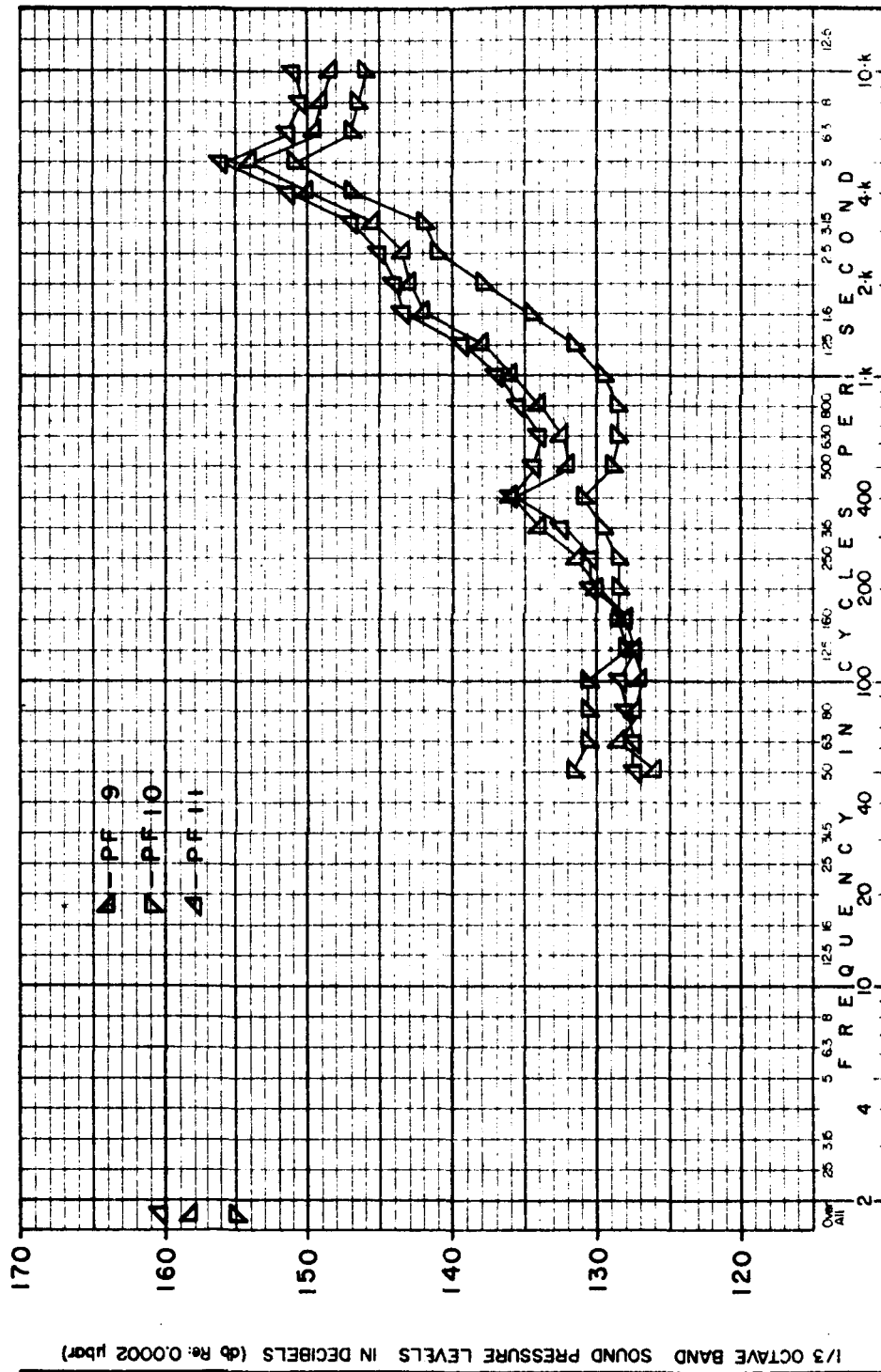
Figure VI-9 is a plot of the SPL spectrums at the $x/D_e = 16$ position for four program firings. It is obvious that the scatter is wide and in the light of the foregoing discussion is to be expected.

Fig. VI-9 Near-Field SPL Spectra at 16 D_e from NEP

It is of interest to note that, if a pair of near-field measurements of one firing are used to obtain the apparent source locations by the amplitude correlation method, the results give a source distribution much closer to the engine exit than does the traversing microphone. One possible explanation of this finding has to do with the distribution of acoustic energy in the exhaust stream in a given frequency band. Sources of acoustic energy in a given frequency band are distributed along the exhaust stream. Therefore, sources close to the exit plane (although less intense than the major source) can make the major contribution to the near field because of the small source-to-receiver distances. This can be demonstrated if the power level distribution is taken to be the same as the SPL distribution given in Appendix A.

There is an effect of the cluster configuration as demonstrated in Fig. VI-10. The SPL spectra at the exit plane are plotted for the three twelve-engine clusters. The extremely high peak in the 5-kc band is present in all the near-field spectra. This was demonstrated in Ref 1 to be a pure tone component with strong radiation along the stream axis.

Finally, Fig. VI-11 demonstrates, that for cluster configurations, the near-field levels may not increase as the number of engines in the cluster increases. These measurements taken at the nozzle exit plane show the spectrum from the twelve-engine firing (Firing No. 10) to be lower in some frequency bands than the five- and eight-engine cluster spectrums. This phenomenon is apparently associated with the directivity and source location as previously discussed.



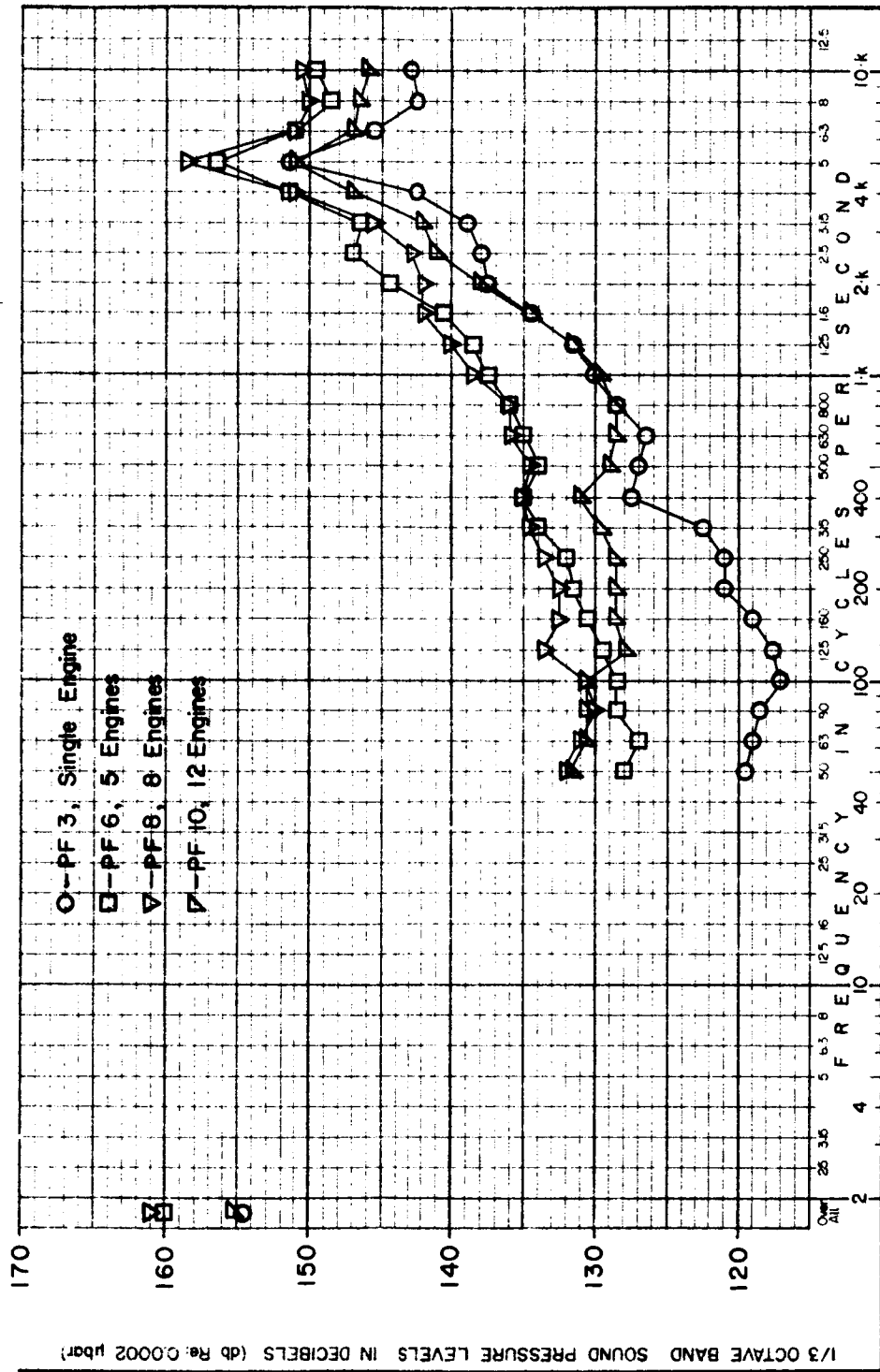


Fig. VI-11 Near-Field SPL Spectra at the NEP

VII. CONCLUSIONS

The following conclusions result from the study of the data from both Phase I and Phase II and from comparison with the results of the referenced sources.

The results of the present study indicate that the acoustic efficiency is about 1/4% for most of the clusters and the single engine. There is an effect attributed to clustering which reduces the total acoustic power produced by some of the clusters from that which would be expected based on the single-engine efficiency.

Comparison with other data shows a wide variation in the measured efficiency for sources with similar mechanical powers.

The power spectra from the present work can be correlated by using the exit velocity and an effective diameter. This correlation technique does not work well when the data from other investigators are used. A velocity and diameter based on the subsonic portion of the stream was used to correlate the present results, and agreement with the generalized power spectrum for subsonic jets was found.

The overall directivity is a function of the number of nozzles in the cluster (or the peak frequency of the power spectrum), with the peak in the directivity index curve shifting from 70 deg for the single engine to 50 deg for the twelve-engine cluster.

The directivity index curves compared with other data show a fair agreement when the sizes of the clusters or single nozzles are similar.

A plot of the 1/3-octave band directivity curves shows a surprising similarity for the different clusters at some frequencies but poor similarity at others. The greatest data scatter occurs at angles close to the exhaust axis.

The apparent source locations are not well correlated using the effective diameter of the cluster. There is good agreement between the single-engine source locations and such different sources as the Titan IIIC data.

The near-field measurements were designed to determine the adequacy of the effective diameter as a correlating dimension for the cluster configurations. The correlation is very poor, indicating that other parameters must be considered.

The effect of the ground plane absorption is evident in the data and, as demonstrated in the Phase I report (Ref 1), has proven a source of difficulty in other measurement programs.

VIII. RECOMMENDATIONS

In correlating the available acoustic data produced by high-speed flows, it becomes apparent that the large number of variables is a hindrance to this approach. In rockets, the composition of the exhaust gases, the degree of expansion (exit static pressure), and the amount of afterburning in the exhaust are typical of the variables whose effects are difficult to define and may significantly influence the radiated acoustic field. For the supersonic rocket exhaust stream, very little correlation exists between the aerodynamic characteristics of the flow and the related acoustic sources. Many of the correlation parameters that have been proposed use variables that their proponents confess are difficult to relate to the acoustic source mechanism. The approach used in this work of using parameters in the subsonic region of the exhaust may have some merit if the approach is proven to be generally applicable and if this subsonic velocity and diameter can be related to other known exhaust stream variables. For these reasons two specific recommendations in this area are enumerated:

- 1) To measure the acoustic field produced by rockets where the development of the exhaust stream is known with a degree of accuracy. This will probably require aerodynamic measurements in the exhaust plume and would permit an accurate determination of the significant correlation parameters;
- 2) Further study of existing acoustic data should be made to determine the merit of using the subsonic parameters in correlating the power spectrums, apparent source location, and near-field noise. Some research to determine necessary engine characteristics will be required for most of the existing data.

The phenomenon of the ground absorption discussed at some length in the Phase I report (Ref 1) has proven a source of difficulty in interpreting and using the data from many tests, including the present work, demonstrating the need for a better understanding of this effect. The particular relationship between the source and receiver heights and the ground plane impedance should be investigated using both theoretical and experimental techniques.

IX. REFERENCES

1. E. B. Smith: Acoustic Scale-Model Tests of High-Speed Flows. Martin-CR-66-13. Martin Company, Denver, Colorado, March 1966.
2. W. J. Galloway: "Frequency Analysis of Short Duration Random Noise." Sound, November-December 1962.
3. C. M. Harris: "Absorption of Sound in Air versus Humidity and Temperature." JASA, Vol 40, July 1966.
4. R. Lee et al.: Research Investigation of the Generation and Suppression of Jet Noise. General Electric Company Report. Navy Bureau of Weapons Contract No. 59-6160-C, January 1961.
5. S. H. Guest: Acoustic Efficiency Trends for High Thrust Boosters. NASA TN D-1999, July 1964.
6. W. V. Morgan, and K. J. Young: Studies of Rocket Noise Simulation with Substitute Gas Jets and the Effect of Vehicle Motion on Jet Noise. ASD-TDR-62-787, March 1963.
7. J. Sugamele and L. C. Sutherland: Acoustic Model Rocket Studies. Boeing Company Report No. D5-4457, March 1960.
8. T. J. Hargest and M. J. Porter: "Preliminary Note on the Noise of Multiple Jets," National Gas Turbine Establishment. MEM 342, August 1960.
9. R. C. Potter and M. J. Crocker: Acoustic Prediction Methods for Rocket Engines Including the Effects of Clustered Engines and Deflected Exhaust Flow. NASA CR-566, November 1964.
10. J. N. Cole et al.: Noise Radiation from Fourteen Types of Rockets in the 1,000 to 130,000 Pounds Thrust Range. WADC TR 57-354, December 1957.
11. J. K. Manhart et al.: An Acoustic Study of the KIWI-B Nuclear Rocket. NASA CR-370, January 1966.
12. W. H. Mayes et al.: Near Field and Far Field Noise Surveys of Solid Fuel Rocket Engines for a Range of Nozzle Exit Pressure. NASA TN D-21, August 1959.

13. J. N. Cole et al.: Effects of Various Exhaust Blast Deflectors on Acoustic Noise Characteristics of 1000-pound-thrust Rocket. WADD TR 60-6, September 1960.
14. A. R. Anderson and F. R. Johns: "Characteristics of Free Supersonic Jets Exhausting into Quiescent Air." Jet Propulsion, January 1955.
15. C. M Harris, ed: Handbook of Noise Control. McGraw-Hill Book Company, Inc., 1957.
16. R. Lee and W. Semrau: Method of Predicting Overall Directivity Pattern of Suppressor Nozzles. General Electric Company Report R 58 AGT 947, December 1958.
17. J. Atvars et al.: Refraction of Sound by Jet Flow or Jet Temperature. UTIAS TN-109, May 1965.
18. H. R. Mull and J. C. Erickson, Jr.: "Effect of Jet Structure on Noise Generation by Supersonic Nozzles." JASA, Vol 31, February 1959.

X. BIBLIOGRAPHY

- Barnett, N. E.: Experimental Study of Sound Power Radiated from Cold Model Jets and Ground Silencing Arrangements. AFAPL-TR-65-55 (AD621-634), Vol I, 1965.
- Barrett, Robert E.: Techniques for Predicting Localized Vibratory Environments of Rocket Vehicles. NASA TN D-1836, October 1963.
- Bond, D. A.: A Summary of Model and Full Scale Acoustic Data for Prediction of Missile Lift-Off Noise Environments. Northrup Norair Report NOR-64-215, September 1964.
- Bolt, Beranek, and Newman, Inc: 100 FW3 Solid Fuel Motor Static Firing - Acoustic and Vibration Spectra. Aero Mem. No. 8.14, November 1962.
- Bolt, Beranek, and Newman, Inc: DVXL 5-1 Solid Fuel Motor Static Firing - Acoustic and Vibration Spectra. Report No. 1035, September 1963.
- Data Acquisition Report for Solid Propellant Rocket Motor Static Firings. Test Report 212. Datacraft, Inc. NASA Contract NAS8-11760, 23 March 1966.
- Dow, R. H.: Sound Level Measurements XLR87-AJ-1 and XLR-AJ-1 Liquid Rocket Engines. AGC, Tech. Mem. 129 LRP, 21 May 1957.
- Dyer, Ira: Distribution of Sound Sources in a Jet Stream. JASA, Vol 31, July 1959.
- Eldred, K. M. et al.: Suppression of Jet Noise with Emphasis on the Near Field. ASD-TDR-62-578, February 1963.
- Ffowcs Williams, J. E.: The Mechanism of Noise Generation by Supersonic Flows. Rept No. 1140. NASA Contract NAS1-3217, June 1964.
- Ffowcs Williams, J. E.: "The Mach Wave Field Radiated by Supersonic Turbulent Shear Flows." J. Fluid Mech. 21, No. 4, 641-657, 1965.
- Harris, C. M.: "Absorption of Sound in Air in the Audio-Frequency Range." JASA, Volume 35, January 1963.

- Howes, W. L.: Ground Reflection of Jet Noise. NACA TN 4260, April 1958.
- Howes, W. L.: Similarity of Far Noise Fields of Jets. NASA TR R-52, 1959.
- Ingard, U.: "On the Reflection of a Spherical Sound Wave from an Infinite Plane." JASA, Vol 23, No. 3, May 1951.
- Ingard, U.: "A Review of the Influence of Meteorological Conditions on Sound Propagation." JASA, Vol 25, No. 3, May 1953.
- Lassiter, L. W. and Heitkotter, R. H.: Some Measurements of Noise from Three Solid-Fuel Rocket Engines. NACA TN 3316. December 1954.
- Lighthill, M. J.: "Jet Noise." AIAA J., Vol I, No. 7, July 1963.
- Mollo-Christensen, E. and Narasimha, R.: "Sound Emission from Jets at High Subsonic Velocities." Jour. of Fluid Mech. November 1959.
- Mollo-Christensen, E. et al.: Experiments on Jet Flows and Jet Noise Far Field Spectra and Directivity Patterns. MIT Report ASRL-TR-1007. February 1963.
- Mollo-Christensen, E. et al.: Measurements of Near Field Pressures of Subsonic Jets. MIT Report ASRL TR 1009. April 1963.
- Morgan, W. V. et al.: The Use of Acoustic Scale Models for Investigating Near Field Noise of Jet and Rocket Engines. WADD TR 61-178. April 1961.
- Mull, H. R. and Erickson, J. C., Jr.: Survey of Acoustic Near Field of Three Nozzles at a Pressure Ratio of 30. NACA TN 3978. April 1957.
- Results of Sound Pressure Level Measurements during AS-201 Launch, Parts I and II. NASA TR-305. 15 March 1966.
- Nyborg, W. L. and Mintzer, D.: Review of Sound Propagation in the Lower Atmosphere. WADC TR 54-602. May 1955.
- Parkin, P. H. and Scholes, W. E.: "The Horizontal Propagation of Sound from a Jet Engine Close to the Ground, at Radlett." J. Sound Vib., Vol I, 1964.

- Parkin, P. H. and Scholes, W. E.: "The Horizontal Propagation of Sound from a Jet Engine Close to the Ground, at Hatfield." J. Sound Vib., Vol II, 1965.
- Peverley, R. and Smith, E. B.: Advanced Rocket Engine Jet Characteristics and Effects Study, Final Report. Martin-CR-64-81, Martin Company, Denver, Colorado, 1964.
- Ribner, H. S.: On the Strength Distribution of Noise Sources Along a Jet. University of Toronto, Institute of Aerophysics. UTIA Rept 51. April 1958.
- Ribner, H. S.: The Noise of Aircraft. University of Toronto, Institute of Aerospace Studies. UTIAS Review 24, August 1964.
- Ribner, H. S.: "Noise Generation Mechanisms." Canadian Aeronautics and Space Jour, January 1966.
- Wiener, F. M. and Keast, D. M.: "Experimental Study of the Propagation of Sound over Ground." JASA, Vol 31, No. 6, June 1959.
- Wilhold, G. A., Guest, S. H., and Jones, J. H.: A Technique for Predicting Far Field Acoustic Environments Due to a Moving Rocket Sound Source. NASA TN D-1832. August 1963.

Martin-CR-66-75

APPENDIX A

DATA TABULATION

Table A-1 Program Firing Test Log

Firing No.	Date	Time	Temp (°F)	Bar (in Hg)	R.H. (%)	Wind		Data Sample Time (sec)	Acoustic Measurement Successfully Acquired
						Vel. (mph)	Dir.		
1	Dec 6, 1965	15:50	60	24.15	16	2	N	3.5	12
2	Dec 8, 1965	13:30	62	24.01	10	2	N	4.0	13
3	Dec 22, 1965	09:39	49	23.70	31	5	N	4.0	13
4	Jan 7, 1966	14:55	57	24.15	24	6	N	3.1	11
5	Jan 11, 1966	11:13	49	23.82	11	4	N	4.0	13
6	Jan 13, 1966	11:50	37	24.04	18	5 to 8	S	4.0	13
7	Jan 26, 1966	13:53	46	24.10	16	5	S	3.5	10
8	Jan 28, 1966	14:18	39	24.00	22	5	S	4.0	13
9	Aug 18, 1966	14:15	83	24.33	37	4 to 13	N	3.0	13
10	Aug 30, 1966	11:26	86	24.17	26	3	S	2.5	13
11	Sept 7, 1966	14:17	81	24.37	20	2	S	3.0	11

Table A-2

1/3-Octave-Band Sound Level in Decibels (in db re. 10^{-13} watts)

Freq	Program Firing Number										
	1	2	3	4	5	6	7	8	9	10	11
50	142.5	141	142	157.5	158	157	159.5	159	163.5	164	161.5
63	144	143	145	159	160	159.5	162.5	161.5	164.5	165	163
80	148.5	146.5	148.5	160.5	162.5	161.5	163.5	163.5	167.5	166.5	165
100	149	148.5	150.5	162	163	161.5	164	163	167.5	167	165
125	150	150.5	152.5	162.5	162.5	162	162.5	164.5	167.5	168	166.5
160	152.5	152.5	154.5	163.5	164.5	164	163.5	165	169	169	167
200	151.5	152.5	153	165	164	164	164.5	167	172	172	166
250	149.5	152.5	152.5	163	161.5	162.5	162.5	163	170.5	171	165
315	146	149	149.5	161.5	161	161.5	161.5	164	170	170	165.5
400	146.5	147	150.5	157	159	160	158.5	163	172	172.5	167
500	153	151	154.5	160.5	161	160.5	162.5	161	170.5	172.5	167
630	156.5	155.5	158	163	163	163	164	160	166	167	160.5
800	159.5	158	160	165.5	165	165	165.5	162	165	165.5	160.5
1000	159.5	160	160	165	165	164.5	166	164.5	165.5	165.5	160.5
1250	156	159.5	157.5	162	163.5	163.5	165	165	165.5	166.5	162
1600	156.5	156.5	158	161	161.5	162.5	162.5	163.5	166.5	167.5	164
2000	159.5	158	161	164	163.5	162.5	164.5	162	166	167.5	164
2500	156.5	160.5	158.5	162	163	163	163	164	162.5	164	163
3150	159.5	158.5	161	162.5	162	162.5	163	164	164	164.5	161.5
4000	157.5	158.5	159.5	161.5	161	162	162.5	163.5	161	162.5	162
5000	158	158.5	160.5	162.5	161	161.5	162.5	163.5	161	162	162
6300	157.5	158	160	162	159.5	160.5	161.5	162.5	160	160.5	160
8000	156.5	157	160	162	158	160	161	161.5	160.5	160.5	160.5
<u>10000</u>	<u>156.5</u>	<u>156.5</u>	<u>160</u>	<u>162</u>	<u>157</u>	<u>159.5</u>	<u>159.5</u>	<u>160.5</u>	<u>158</u>	<u>159</u>	<u>159.5</u>
OA	169.5	170	171.5	176	176	176	177	177	181	181.5	178

Martin-CR-66-75

Table A-3 1/3-Octave-Band Sound Pressure Levels in Decibels
(db re: 0.0002 μ bar)

Program Firing No. 1

Single Engine

Sample Time 3.5 Seconds

Center Freq. cps	* 20° 120'	30° 120'	40° 120'	50° 120'	60° 120'	70° 120'	90° 120'	125° 120'	160° 120'	D _e	3 D _e	16 D _e
50	99	98	96.5	94.5	91	90	86	86.5	84.5	124	114	106.5
63	100	99.5	98	98.5	94	92.5	88	88	85	123	113	104.5
80	105	104.5	103	101.5	98.5	96	90.5	89.5	87.5	122	113	105.5
100	104	105	103.5	103	100.5	98	92	91.5	87.5	121.5	112.5	107.5
125	101	104.5	103	105	103.5	102	95	92	89.5	121	112.5	110.5
160	94	102.5	103.5	110.5	107	103.5	96.5	94	90	121	113.5	111
200	90	98	104	107	107	103.5	97	94.5	89	121	115	112
250	90.5	96	101	100	105.5	104.5	96	93	88.5	121	115.5	114
315	85	91	96	99.5	101	100	93.5	90.5	86.5	122	117	114.5
400	92	95.5	99.5	101	98.5	100	96	90.5	86	125	120.5	114
500	93	98	103	106	106.5	108.5	102	91	87	127.5	123	117
630	98.5	102	105	109	110.5	113.5	105	93.5	89	125.5	121.5	116
800	97	102.5	107	110.5	113.5	116	107.5	97.5	90.5	126.5	122.5	116.5
1000	98.5	101.5	105.5	110.5	113	115.5	107	99.5	91.5	128	123	116.5
1250	96	98.5	103	112	108	110.5	105	99	92.5	131	125.5	118.5
1600	95.5	98	101	106.5	108.5	111	108	97	93	132	128	120.5
2000	96	100	103.5	108	111.5	114.5	111.5	103.5	94.5	134.5	132	122.5
2500	95.5	98.5	101.5	104.5	107.5	110.5	109	103	93.5	136	132.5	123
3150	100	101	102.5	106.5	110.5	113	112	105	97.5	137.5	134	125.5
4000	100	100.5	102	105.5	107	111.5	109	104.5	98	139.5	135	127.5
5000	102	103	104.5	106.5	108.5	111	109	106.5	102	143.5	140	133
6300	103	103.5	104	107	108	111	109	106	101	142.5	139	132
8000	103	103.5	103	105	107	110	107.5	103.5	99.5	143	138.5	131
<u>10000</u>	<u>103</u>	<u>103.5</u>	<u>103</u>	<u>105</u>	<u>106.5</u>	<u>110</u>	<u>107.5</u>	<u>104.5</u>	<u>100</u>	<u>143</u>	<u>139.5</u>	<u>130.5</u>
OA	113.5	115	117	120.5	122	124	120	114.5	109	150	146.5	139

*Extrapolated Data, See Text

Martin-CR-66-75

Table A-4 1/3-Octave-Band Sound Pressure Levels in Decibels
(db re: 0.0002 μ bar)

Program Firing No. 2

Sample Time 4.0 Seconds

Single Engine

Center Freq. cps	20° 120'	30° 120'	40° 120'	50° 120'	60° 120'	70° 120'	90° 120'	125° 120'	160° 120'	D _e	3 D _e	16 D _e
50	95.5	96.5	96	94	90.5	87	85	85	85	117	107	98.5
63	97	99	98.5	96	92.5	90	88	87	86	116.5	107	98.5
80	99.5	102	102.5	99.5	97.5	94.5	90	89.5	88	116	109	102.5
100	101.5	104	104.5	101.5	100.5	97.5	93	91	88.5	116	111	106.5
125	102	104.5	104.5	105.5	103.5	101.5	95	92	90.5	117.5	113	110.5
160	101.5	103	104	108	108	104	95.5	93.5	91	118	114	110.5
200	99.5	98.5	104	108	108	104	98	95	91	119.5	117	111
250	95	95.5	101	102.5	109	106.5	98.5	94	90.5	121	118	115
315	88.5	91.5	96.5	98.5	105	104	97.5	93	90	121.5	119.5	115
400	88	93	96	99.5	100	102	95	92	88.5	124	121.5	114
500	91.5	97	101	105.5	103	106.5	98.5	90.5	89	126.5	122.5	117.5
630	95	99.5	104.5	107	108	111.5	104	91.5	90	128	124.5	118
800	95.5	100.5	105.5	109.5	111.5	114	107.5	94	90	129.5	125.5	118
1000	93	99.5	104.5	109.5	112	116	109.5	97.5	90.5	131.5	126.5	119.5
1250	92.5	98	102	114	110	114	110.5	99	92.5	133	131.5	121.5
1600	92	96.5	100	104.5	106	111	109.5	99.5	93.5	137	135.5	122.5
2000	94.5	97	102.5	106.5	110	111	111.5	98.5	93.5	138.5	135	123.5
2500	94	97.5	102	106	108.5	112.5	115	103	92.5	140	135	123.5
3150	95.5	98.5	102.5	105.5	108.5	110.5	112.5	103.5	97.5	140	136	121.5
4000	93.5	97	101.5	104.5	107	110.5	112.5	105	96.5	142	136.5	123.5
5000	95.5	97.5	102.5	104.5	107.5	111	111.5	106	98.5	144.5	142.5	124
6300	95	98	102	105	107	109	112	105.5	99.5	144	137	122.5
8000	94.5	97	101.5	104	106	108	110.5	104.5	98	144.5	137.5	121.5
<u>10000</u>	<u>95</u>	<u>97</u>	<u>101.5</u>	<u>103.5</u>	<u>105.5</u>	<u>108</u>	<u>110</u>	<u>105</u>	<u>99</u>	<u>144.5</u>	<u>136.5</u>	<u>121</u>
OA	110.5	113	116	120	121	123.5	122.5	114	108	152	147	133.5

Martin-CR-66-75

Table A-5 1/3-Octave-Band Sound Pressure Levels in Decibels
(db re: 0.0002 μ bar)

Program Firing No. 3

Sample Time 4.0 Seconds

Single Engine

Center Freq. cps	20° 120'	30° 120'	40° 120'	50° 120'	60° 120'	70° 120'	90° 120'	125° 120'	160° 120'	D _e	3 D _e	16 D _e
50	97	98	96	95	93.5	89	86.5	86	85.5	119.5	107.5	96
63	99.5	101	100	98	95.5	92	89.5	87.5	86.5	119	108.5	98
80	103	105	103.5	101.5	99.5	96.5	91	91	88.5	118.5	109	102.5
100	104.5	107	105	103	102.5	100	94.5	90.5	89	117	111.5	106.5
125	105.5	107	103.5	107.5	106.5	103.5	97	92.5	90	117.5	112.5	109
160	104	109.5	105	109	109.5	104.5	97.5	94	90.5	119	113	109
200	102.5	103.5	106.5	108.5	108	104	98.5	94	91	121	116.5	110
250	99.5	99	104.5	101.5	110	105	97	93	91.5	121	117	114
315	93	92.5	98.5	100	108.5	100.5	95	92	90.5	122.5	119.5	114.5
400	93	96.5	99.5	103.5	108	103	96.5	95	89.5	127.5	124.5	115.5
500	94	103	103.5	111.5	106	110	99.5	95	88	127	126	117.5
630	98	104	104	108	111	115	104.5	95	88	126.5	123	117
800	99	104	106	109.5	114	117	107.5	98	92.5	128.5	124.5	117
1000	96.5	103.5	105.5	111.5	114	115.5	109.5	100	94.5	130	125.5	118.5
1250	96.5	99	104	114	108.5	109	109	101	96	131.5	130	120
1600	97.5	99.5	101.5	105.5	110	113.5	109	100	97	134.5	133	121
2000	99.5	102	105	108	112	114.5	115	102	96	137.5	134	122.5
2500	98.5	100	103	105.5	107.5	111.5	112	104.5	97	138	134	121
3150	100	101.5	104.5	107.5	110.5	112.5	115	105.5	99	139	138	122
4000	99.5	101.5	103	105.5	111	111	113	107	100.5	142.5	140	125
5000	102.5	103	104	106.5	109	111	114	109	102.5	151.5	143.5	128
6300	99.5	101.5	104	106.5	109.5	111	113	108	101	145.5	140	124
8000	98.5	101	102.5	105.5	109	111	113.5	107	101	142.5	138	122.5
<u>10000</u>	<u>99.5</u>	<u>101</u>	<u>103</u>	<u>105.5</u>	<u>109</u>	<u>111</u>	<u>113.5</u>	<u>107.5</u>	<u>101</u>	<u>143</u>	<u>138</u>	<u>122.5</u>
OA	114	117	117.5	121.5	123	125	123.5	116.5	110.5	154.5	148.5	134

Martin-CR-66-75

Table A-6 1/3-Octave-Band Sound Pressure Levels in Decibels
(db re: 0.0002 μ bar)

Program Firing No. 4

Sample Time 3.1 Seconds

Five Engines

Center Freq. cps	20° 120'	* 30° 120'	* 40° 120'	50° 120'	60° 120'	70° 120'	90° 120'	125° 120'	160° 120'	D _e	1.3 D _e	7.1 D _e
50	109	112	113.5	113.5	109	103.5	99.5	98	100.5	129	120.5	108.5
63	108	112.5	115.5	116	111.5	105.5	102	100	102	127.5	120.5	108.5
80	109.5	114	116.5	117	113	108.5	103	101	101	128.5	121	111.5
100	111	114.5	117	118	115.5	112	105.5	102	101	127.5	121.5	116
125	110.5	113.5	115.5	117	117	115.5	106.5	102	101.5	128.5	122	118.5
160	98	105.5	111.5	116.5	121	118	107	103	102	129	123	118.5
200	98	106	112.5	118	122	119	108.5	104	102	130.5	126	121
250	103	107.5	111.5	113.5	117	120	107.5	102.5	101.5	132	127	122.5
315	101	103	106.5	110.5	115.5	118	107	102	101	132	129	124.5
400	101	105.5	109	111	110.5	110	105	100.5	99.5	133.5	130.5	123.5
500	98.5	106	111	114	112.5	117	106.5	100	98	133.5	131	124.5
630	100	104.5	108.5	112	116	119.5	112	100	97	133.5	130	124
800	100	105	109.5	114	118.5	122	114.5	103	99	134	129.5	124
1000	99.5	104.5	109	114	118.5	121	115	105	100.5	135	131	125.5
1250	99.5	104.5	109	112.5	114.5	117	114	106.5	102	136.5	135	126
1600	99	102.5	105.5	108.5	112	115.5	112.5	105.5	102.5	138.5	136.5	127
2000	101	104	107.5	110.5	115	117.5	117.5	105	102	142.5	137	129.5
2500	100.5	103.5	106	108.5	111	115.5	115	108.5	103.5	145	139	129
3150	102	104	106.5	109	111.5	116	115	108.5	106	144	141	128.5
4000	101.5	103.5	105.5	108	110.5	114	113.5	110.5	109.5	149	146	133
5000	105.5	107.5	109	110	111	114.5	114.5	111.5	110	156.5	152	137
6300	102	105	107.5	109.5	111	115	114.5	110	108.5	150	144.5	130.5
8000	101	104	106.5	109	111	115.5	114	109.5	108.5	147.5	143	129.5
<u>10000</u>	<u>102</u>	<u>104.5</u>	<u>106.5</u>	<u>109</u>	<u>111.5</u>	<u>115</u>	<u>114.5</u>	<u>109.5</u>	<u>108</u>	<u>149</u>	<u>143.5</u>	<u>128.5</u>
OA	119	122.5	125	127.5	129.5	130.5	126	120	118.5	159.5	155	142

*Interpolated Data, see text.

Martin-CR-66-75

Table A-7 1/3-Octave-Band Sound Pressure Levels in Decibels
(db re: 0.0002 μ bar)

Program Firing No. 5

Sample Time 4.0 Seconds

Five Engines

Center Freq. cps	20° 120'	30° 120'	40° 120'	50° 120'	60° 120'	70° 120'	90° 120'	125° 120'	160° 120'	D _e	3 D _e	16 D _e
50	106	113	115.5	113	109	107	100	99.5	102	128	115.5	109
63	105.5	113.5	118	115.5	111.5	107	102	101	102	127.5	115.5	109
80	109.5	115.5	120.5	118.5	114.5	109.5	102	102	102	128	116	109.5
100	109.5	116	121	118	115	111.5	104.5	102.5	101	128	118.5	110.5
125	107.5	116.5	118.5	116	116	115.5	105	103	101	128.5	120	116.5
160	104.5	114.5	114	117	121.5	119.5	105.5	104	102	129.5	121	118.5
200	102.5	112.5	114	118	121	117.5	106	105	102	131	124.5	119
250	100	107	111	113.5	116	117.5	105	104	105.5	132	126	124.5
315	100	104	110	110.5	116	117	105	103	101.5	134	129	125.5
400	101.5	103.5	111	111	112	115	104.5	102	100.5	135.5	132	126.5
500	99	104.5	114.5	115	112	116.5	106	100.5	98	133.5	130	120
630	99.5	105.5	113.5	114	115.5	119.5	111	102	97	134.5	129.5	121
800	99	105.5	109.5	113.5	117	121.5	114	105.5	100	135.5	130	122.5
1000	99	104.5	110	114	117.5	121	115	107.5	102	137	131.5	122
1250	99	102.5	109.5	116.5	114	118	115	107.5	103	138	134	123.5
1600	98.5	102	107	110	112	116	114	106.5	103	140.5	136.5	124
2000	101	103	106.5	110	113.5	117	117	109	103.5	144.5	137.5	125.5
2500	101	103	106	109.5	111.5	116	116	110	104	147	139	126
3150	102	103.5	106	108.5	111.5	115.5	114.5	109.5	106.5	145.5	137.5	125.5
4000	101.5	103	106	108	110.5	113	113	109.5	107.5	151	142	128
5000	103.5	104.5	106.5	108	110	113	112.5	110.5	108	155.5	148	130.5
6300	99.5	102.5	105.5	107	108.5	112	111.5	108.5	106	150	142.5	126.5
8000	98.5	101	104	105.5	107.5	110	110	107	105	148	139	126
<u>10000</u>	<u>98</u>	<u>100.5</u>	<u>104.5</u>	<u>104</u>	<u>107</u>	<u>109.5</u>	<u>109</u>	<u>106.5</u>	<u>104.5</u>	<u>148</u>	<u>140</u>	<u>126.5</u>
OA	117	124.5	128	128	129	130.5	125.5	120	117	159.5	152	138

Martin-CR-66-75

Table A-8 1/3-Octave-Band Sound Pressure Levels in Decibels
(db re: 0.0002 μ bar)

Program Firing No. 6

Sample Time 4.0 Seconds

Five Engines

Center Freq. cps	20° 120'	30° 120'	40° 120'	50° 120'	60° 120'	70° 120'	90° 120'	125° 120'	160° 120'	D _e	3 D _e	16 D _e
50	106	112.5	114	112	108	105.5	99.5	96.5	102	128	115	108
63	105.5	113.5	116.5	116	111.5	108	100.5	99	104	127	116	109
80	108.5	113.5	118.5	118	114.5	109.5	102	99	103.5	128.5	117	109
100	108	113.5	119	117.5	114.5	110.5	104	100.5	102.5	128.5	119.5	110.5
125	107.5	115.5	118	117	115	115	106	101	102.5	129.5	120	115.5
160	104	117.5	115	114.5	119	119	106.5	101.5	107.5	130.5	120.5	116
200	108	116	113	115.5	120	119.5	107	102.5	105.5	131.5	124	119
250	103.5	110.5	112.5	114.5	116	119	108	101.5	102.5	132	125	124.5
315	102	110	111	112	115.5	117.5	107.5	100.5	102.5	134	128.5	125.5
400	100.5	109	112	113	113	115.5	107.5	99	101.5	135	131	126.5
500	96.5	108.5	115.5	110.5	111.5	115.5	110.5	99	98	134	129	120.5
630	95	108	114.5	108.5	112	118	115.5	100	97.5	135	129	120
800	94	106.5	111	111.5	114.5	119.5	118	103.5	100.5	136	129.5	122
1000	95	106	109	112.5	116	119.5	116	105.5	102.5	137.5	131.5	122
1250	94.5	106	109	113	114.5	118	116	106	102.5	138.5	133.5	123
1600	95	105	109.5	111.5	112.5	115.5	115.5	105.5	102.5	140.5	135.5	124
2000	97.5	104	107	110	112.5	116	116	106.5	104	144.5	137.5	125
2500	99.5	103.5	106.5	109	111.5	116	116	108.5	105.5	147	138.5	125.5
3150	99.5	104.5	107	109.5	111.5	115	115.5	108	107.5	146.5	139	126
4000	101.5	106	107	109	110.5	114	114.5	110	109	151.5	142	128.5
5000	103	107.5	107.5	109	111	114	113.5	110.5	110	156.5	149	130.5
6300	101	106	107	108.5	110	113	113	109.5	108.5	151	143	127
8000	100	105	106.5	107.5	109	112.5	112	108.5	108	148.5	139.5	126.5
10000	<u>99.5</u>	<u>105.5</u>	<u>106</u>	<u>107</u>	<u>108.5</u>	<u>111</u>	<u>111.5</u>	<u>108</u>	<u>107.5</u>	<u>149.5</u>	<u>141</u>	<u>127</u>
OA	118	124.5	127	127	128	130	127	119.5	119	160	152	138

Martin-CR-66-75

Table A-9 1/3-Octave Band Sound Pressure Levels in Decibels
(db re: 0.0002 μ bar)

Program Firing No. 7

Eight Engines - Saturn IB Config.

Sample Time 3.5 Seconds

Center Freq. cps	20° 120'	30° 120'	40° 120'	50° 120'	60° 120'	70° 120'	90° 120'	125° 120'	160° 120'	D _e	3 D _e	16 D _e
50	109	115	116	115.5	112	106.5	102	102.5	104.5	126	111	109.5
63	110.5	115.5	118.5	119	117.5	107.5	104	104	105	126.5	112.5	110.5
80	111	115	119	121.5	118.5	110	104.5	103	106	128	114	111
100	109.5	116	120	121	119.5	111	107	104.5	104.5	128	117.5	109.5
125	106.5	115	116.5	117	116.5	116	107.5	105.5	103.5	127.5	119	113.5
160	102	117.5	116	114.5	116	119.5	107.5	106	103	128	120	119.5
200	99.5	110	114	115.5	119.5	120.5	109.5	106.5	103	130	125	119.5
250	98.5	103.5	108	110.5	116.5	119.5	108.5	105	103	132	125	123.5
315	99.5	104	107	109.5	114	119	107.5	103.5	103.5	133	127.5	124.5
400	99	105	109.5	113	114	112.5	105	102.5	100	134.5	130	123.5
500	100.5	109	113.5	117	118	117.5	107	101.5	99.5	133	129	121
630	101	108.5	112.5	115.5	118	120	111.5	101	103.5	133.5	129	121
800	101.5	109	113	115.5	120.5	121.5	114	106	103.5	135.5	129	123
1000	101	108.5	112.5	115.5	119	121	117	109.5	104.5	137.5	131	123
1250	100.5	105.5	113.5	118.5	119	118.5	116	110	103.5	137.5	131.5	123.5
1600	101	104.5	108.5	111.5	117.5	116	114	107.5	103.5	142	133.5	126.5
2000	102.5	106	110	112.5	116.5	118.5	116.5	109.5	105.5	143	133.5	126
2500	103.5	105	107.5	110.5	114	116.5	115.5	110	106.5	146	135.5	127
3150	105	107	109	110	112.5	117.5	114.5	110.5	109.5	146.5	137.5	127
4000	105.5	106.5	108	110	112.5	115	114.5	110.5	110.5	152.5	139.5	129.5
5000	107	108	109	110	112	115	114	111	111	157	141	131.5
6300	104.5	107	108.5	109	110	114.5	113.5	109.5	109	151.5	138.5	127
8000	104	106.5	108	109	110	114	112.5	109	109	150	136.5	127
<u>10000</u>	<u>103.5</u>	<u>105.5</u>	<u>107</u>	<u>108</u>	<u>110</u>	<u>112.5</u>	<u>111</u>	<u>108</u>	<u>108</u>	<u>150</u>	<u>136.5</u>	<u>127</u>
OA	119	125.5	127.5	129.5	130.5	131	126.5	121	119.5	160.5	148	139

*Interpolated Data, See Text

Martin-CR-66-75

Table A-10 1/3-Octave-Band Sound Pressure Levels in Decibels
(db re: 0.0002 μ bar)

Program Firing No. 8

Eight Engines, Circular Config.

Sample Time 4.0 Seconds

Center Freq. cps	20° 120'	30° 120'	40° 120'	50° 120'	60° 120'	70° 120'	90° 120'	125° 120'	160° 120'	D _e	3 D _e	16 D _e
50	110.5	116.5	111	115	110.5	107.5	103	100	105	132	112	109
63	110.5	117	115	118.5	115	108.5	104.5	101	105.5	131	113.5	109
80	112.5	117	117	121.5	117	112	104	101.5	107	130	116	110.5
100	112.5	118	117	120.5	116	112.5	105.5	102.5	105	130.5	117.5	110.5
125	112	118.5	116.5	118	119	119	107.5	103.5	104	133.5	119	113
160	109.5	119.5	114	118	122	119	107.5	104.5	103	132.5	120	118
200	107	116.5	111	122	124.5	120	109	105	102.5	132.5	123.5	118.5
250	102	111	110.5	118	119.5	116.5	108.5	103.5	101.5	133.5	124	121.5
315	101	109	109	116	119	120.5	108	103	101.5	134.5	126.5	122.5
400	101.5	108	114.5	120	118.5	116	106	101	100	135	129	122
500	101.5	108	111.5	118	117	113	104.5	103	99	134.5	128	121
630	102	108.5	111.5	113.5	114.5	114.5	109.5	101	102	136	128	120
800	103	108.5	108	114	116.5	116	113	103.5	101.5	136	129	122
1000	102.5	107	107.5	116	118	118.5	116	107.5	103	138.5	131	123.5
1250	102	106.5	106.5	118	117	118.5	117.5	110	104	140	132	124
1600	102	107	105.5	114	114.5	117	116	110	105.5	142	134.5	126
2000	103	105.5	103.5	112.5	112.5	113.5	115.5	109	106	142	135	126.5
2500	103.5	106.5	103	111.5	114	116	117.5	111.5	107	143	135	125.5
3150	105	108.5	104.5	112.5	114.5	116	116.5	112.5	109.5	145.5	136	126.5
4000	106.5	108.5	104.5	112.5	113	113.5	116	114	111	151	140.5	129.5
5000	108	109	105	111.5	113	114	116	113.5	111.5	158.5	146.5	132
6300	105.5	108	104	111.5	112.5	113	115	112	109.5	151	138	127
8000	104	107	103	110.5	112	113	113.5	111.5	109	150	137	127
<u>10000</u>	<u>103.5</u>	<u>106.5</u>	<u>102</u>	<u>109.5</u>	<u>111.5</u>	<u>112</u>	<u>112.5</u>	<u>110</u>	<u>108.5</u>	<u>150.5</u>	<u>136.5</u>	<u>127</u>
OA	121.5	127.5	125.5	131	131	130	127	122.5	120	161	149.5	138.5

Martin-CR-66-75

Table A-11 1/3-Octave Band Sound Pressure Levels in Decibels
(db re: 0.0002 μ bar)

Program Firing No. 9

Twelve Engine Clusters

Sample Time 3.0 Seconds

Center Freq. cps	20° 120'	30° 120'	40° 120'	50° 120'	60° 120'	70° 120'	90° 120'	125° 120'	160° 120'	D _e	3D _e	16D _e
50	109.5	118	120.5	119	114	114.5	104.5	100.5	102	126	109.5	110
63	111	117	121.5	120.5	116	114.5	106	101.5	102	128.5	111.5	109.5
80	112	118	125	124	120	116.5	106	101	103.5	127.5	112	109.5
100	112.5	117.5	124	124.5	120	117.5	108	102	101.5	127	116.5	108.5
125	112	117.5	122	123	121	121	109	102	101	127.5	118	112.5
160	118.5	120.5	122.5	124.5	124	122.5	109	103	101	128	118.5	117.5
200	113.5	117	119.5	126.5	129.5	125.5	111	106	103.5	130	124	120
250	115	113.5	118	126	125	125.5	111.5	106.5	104.5	131.5	125	124
315	117.5	113	117.5	126	124.5	124	116	107.5	105.5	134	128	125.5
400	110	112.5	117.5	130	124.5	126	114.5	107.5	110	136	129	125
500	110.5	111.5	121.5	130.5	121.5	120	111	105	113.5	132	127.5	120
630	110	107	113	122	117.5	120.5	112.5	104.5	110.5	132.5	126.5	120
800	109	106.5	112.5	122	116.5	119	112	102.5	103.5	134	126	117
1000	105.5	105.5	114.5	122.5	118	120	112.5	102.5	100	136	126.5	117.5
1250	102.5	105.5	111	119.5	119	120.5	114.5	106	99.5	138	129	120
1600	102.5	106	111.5	118	118.5	121	118	107.5	101.5	142	131.5	123.5
2000	103.5	106	110	117.5	115.5	120	118.5	109	103.5	143	132.5	124
2500	102.5	104.5	107.5	113.5	114.5	116	114.5	108	102.5	143.5	133	123.5
3150	103.5	105.5	109	112	114.5	117.5	116	110	106	145.5	132.5	124.5
4000	104	105	108	111	112	114.5	113.5	109.5	107	150	136	126
5000	104	105.5	108	110.5	111	113.5	113	110	106.5	154	138	126
6300	103	103.5	106.5	108.5	109.5	112.5	112	109	105.5	149.5	134	122
8000	103.5	103.5	106	109	110	113	112	109	106	149	133	122
<u>10000</u>	<u>100.5</u>	<u>102.5</u>	<u>104</u>	<u>107.5</u>	<u>108</u>	<u>111</u>	<u>109.5</u>	<u>107</u>	<u>104</u>	<u>148.5</u>	<u>131.5</u>	<u>120</u>
OA	125.5	127.5	132.5	137.5	134.5	134.5	126.5	120.5	119	158.5	144	136

Martin-CR-66-75

Table A-12 1/3-Octave-Band Sound Pressure Levels in Decibels
(db re: 0.0002 μ bar)

Program Firing No. 10

Twelve Engine Circular Canted

Sample Time 2.5 Seconds

Center Freq. cps	20° 120'	30° 120'	40° 120'	50° 120'	60° 120'	70° 120'	90° 120'	125° 120'	160° 120'	D _e	3D _e	16D _e
50	109	118	120	120	114	115.5	105	102	103.5	131.5	118.5	119.5
63	110.5	118	121.5	120.5	116	117	106	102.5	104	130.5	121	119.5
80	111.5	115.5	123.5	123	119	118	106.5	104	104	130.5	120.5	121.5
100	111.5	117.5	122.5	123.5	119.5	119	107.5	105	103	130.5	120.5	120.5
125	110.5	118	123	122	121	122.5	109.5	105.5	102.5	128	121.5	123
160	113	118.5	119.5	123.5	124	124	109	106.5	102.5	128.5	122	125.5
200	110	115.5	119	125.5	131	123	110.5	107	103	128.5	128.5	127.5
250	106	113	117	125	123.5	128	111	107.5	102	128.5	131	129.5
315	105	112	117	124.5	124	126	112	107	101	129.5	130.5	130.5
400	107	111.5	119	126.5	125	129	113.5	107.5	107	131	128.5	130
500	102.5	108	119	132.5	123	123	112.5	106	106	129	127	128
630	103.5	105.5	113	122.5	119.5	122.5	113	105	100	128.5	124	129
800	103	106	111.5	119	118	121	113.5	105.5	101.5	128.5	124	127.5
1000	102	106.5	113	122	116.5	120	113.5	108.5	100	129.5	124	127
1250	102	107	113	120	118.5	121.5	116	111.5	100.5	131.5	125	129.5
1600	102.5	107	112.5	120	119.5	121.5	118.5	111.5	103.5	134.5	127	132
2000	103	107	110.5	118.5	119	122.5	118.5	112.5	104.5	138	129.5	133
2500	102	105.5	109.5	114	115	119	114.5	111	102	141	132.5	133.5
3150	103.5	106	109.5	113.5	115.5	118.5	116	112	104	142	135	133.5
4000	104.5	105.5	109.5	111.5	112.5	116	113	111	105	147	140	137
5000	105.5	107	108.5	111	111.5	115	112.5	111.5	105.5	151	143	140
6300	103	104.5	107	110	110	114.5	111	109	102	147	137.5	135
8000	103	104	106.5	110.5	110.5	114.5	111.5	109	102	146.5	135	135
<u>10000</u>	<u>100.5</u>	<u>102.5</u>	<u>105</u>	<u>109</u>	<u>108.5</u>	<u>113</u>	<u>110</u>	<u>107.5</u>	<u>100.5</u>	<u>146</u>	<u>135.5</u>	<u>135</u>
OA	121.5	127	131.5	137	135.5	136	127	122.5	117	155	147	146

Martin-CR-66-75

Table A-13 1/3-Octave-Band Sound Pressure Levels in Decibels
(db re: 0.0002 μ bar)

Program Firing No. 11

Twelve Engines Circular

Sample Time 3.0 Seconds

Center Freq. cps	* 20° 120'	30° 120'	40° 120'	50° 120'	60° 120'	70° 120'	90° 120'	125° 120'	160° 120'	D _e	3D _e	16D _e
50	107.5	116.5	119.5	117	111	108.5	105	99.5	102.5	127.5	114.5	108
63	109.5	116	120.5	119.5	114.5	109.5	105.5	101	103	127.5	116.5	108
80	112.5	116.5	122.5	121.5	117	111	106.5	101.5	103.5	128	116	108.5
100	112	118	122.5	122	116.5	112.5	106	103	102.5	128.5	117	107.5
125	113.5	121	124	122.5	116	114.5	108	104	101.5	127.5	119	111.5
160	114.5	120	122.5	124	118	118.5	107.5	104	101	128	121	116.5
200	112.5	118	121.5	118.5	120.5	119	109	105	102	130.5	129	118
250	108.5	115.5	120	120.5	118	119	109.5	104	101.5	130.5	129	118.5
315	108.5	115.5	118.5	124	115	116	109.5	105.5	101.5	132.5	126.5	121
400	105.5	110	126	123	115.5	116	109.5	106	105	136	129	121
500	100.5	106	124	126	112	112	107	104	107	134.5	129	119.5
630	100	103	118	116.5	109	110	109	102	102	134	128.5	119.5
800	100.5	103.5	115.5	116	109.5	108.5	112	101.5	100	135.5	128	117
1000	99	103.5	115.5	114.5	112.5	113	109.5	104	100.5	137	130	118
1250	100	104	113	114	114.5	114.5	113	108	101.5	139.5	130.5	121
1600	100	104.5	111.5	112.5	114	115	117.5	109	103	143.5	132	124
2000	101.5	105.5	110.5	111.5	111.5	114.5	118.5	109.5	104.5	144	132.5	124.5
2500	103	106.5	109.5	112	112	113.5	115	110.5	106.5	145	133	123.5
3150	103	105.5	109.5	109.5	112	112.5	113.5	111	105	147	134	125
4000	107	107.5	110.5	111	110.5	113	114	111.5	109.5	151.5	137.5	126.5
5000	106	107	110	111	111.5	111	113	113	107.5	156	139.5	127.5
6300	106	106	108	109.5	108.5	110.5	111.5	109	105.5	151.5	134	124
8000	106.5	105.5	108.5	110	110	112	111.5	110	106	150.5	133.5	124.5
<u>10000</u>	<u>105</u>	<u>105</u>	<u>107.5</u>	<u>110</u>	<u>108.5</u>	<u>111.5</u>	<u>110</u>	<u>110</u>	<u>105</u>	<u>151</u>	<u>132.5</u>	<u>123.5</u>
OA	122.5	128	133.5	133.5	128.5	128	126	122	118.5	160.5	145.5	135.5

* Extrapolated Data, See Text

FIGURE A-1a

SPL DISTRIBUTION TRAVERSE MICROPHONE

PROGRAM FIRING NO. 2

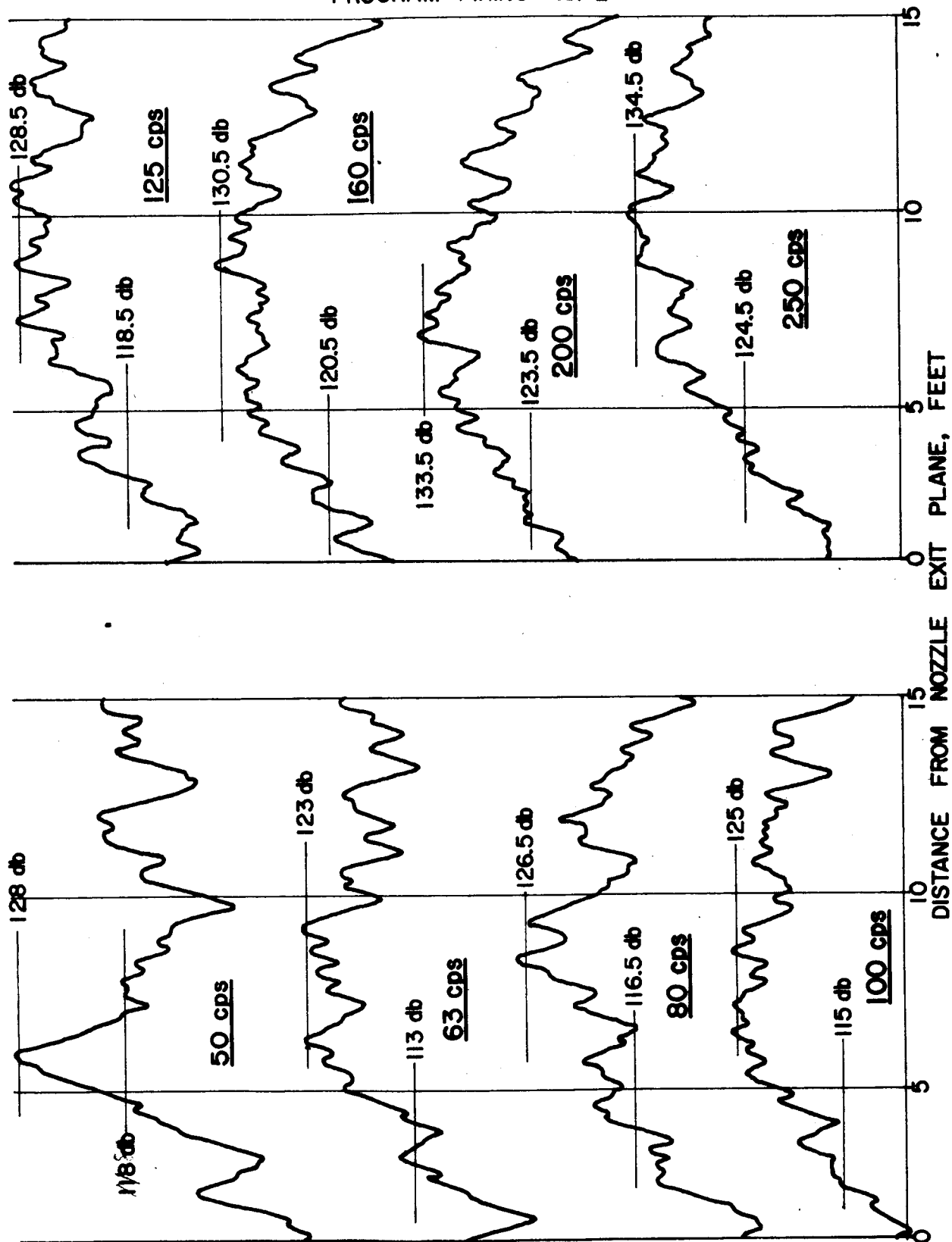


FIGURE A-1b

SPL DISTRIBUTION TRAVERSE MICROPHONE

PROGRAM FIRING NO. 2

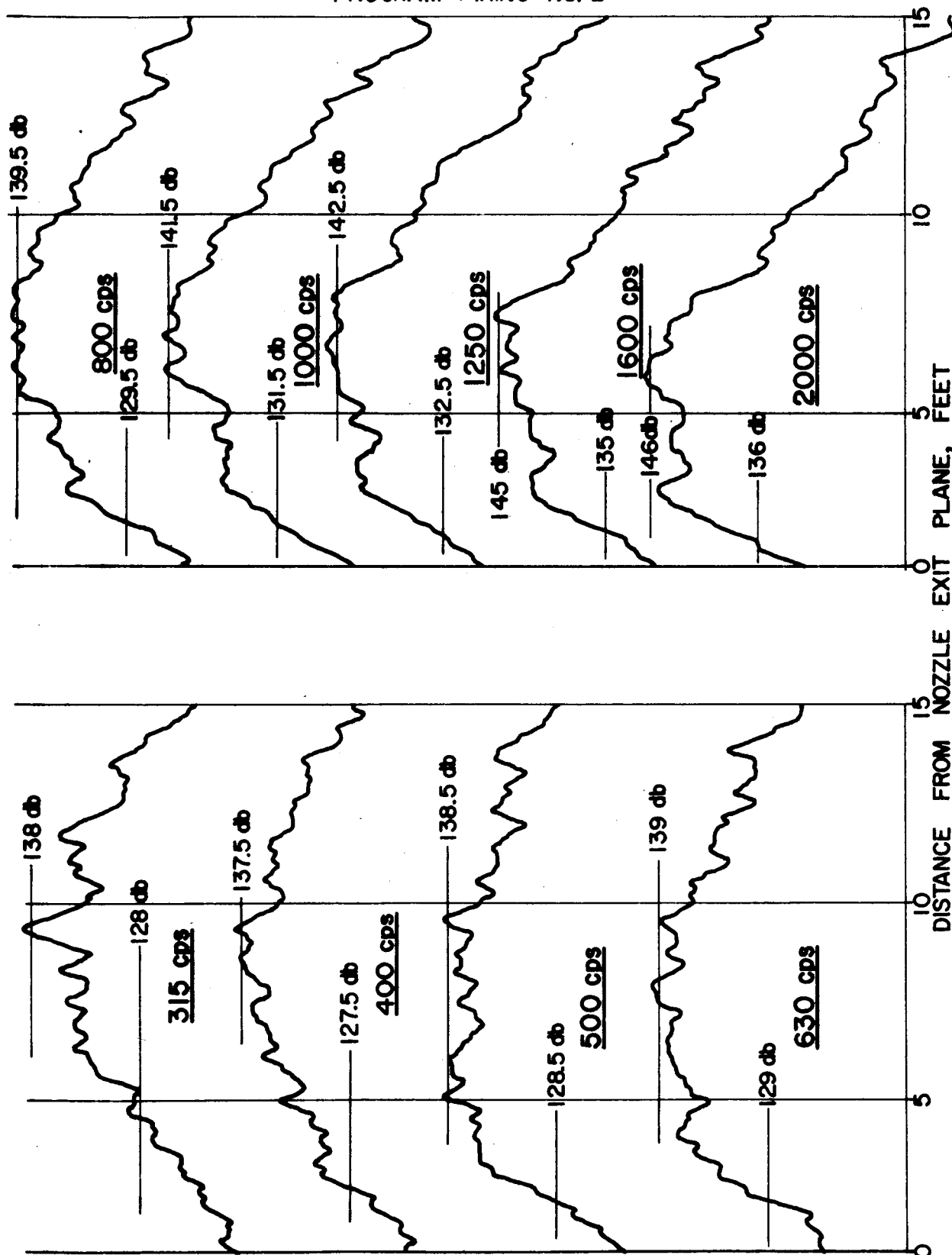


FIGURE A-1c

SPL DISTRIBUTION TRAVERSE MICROPHONE

PROGRAM FIRING NO. 2

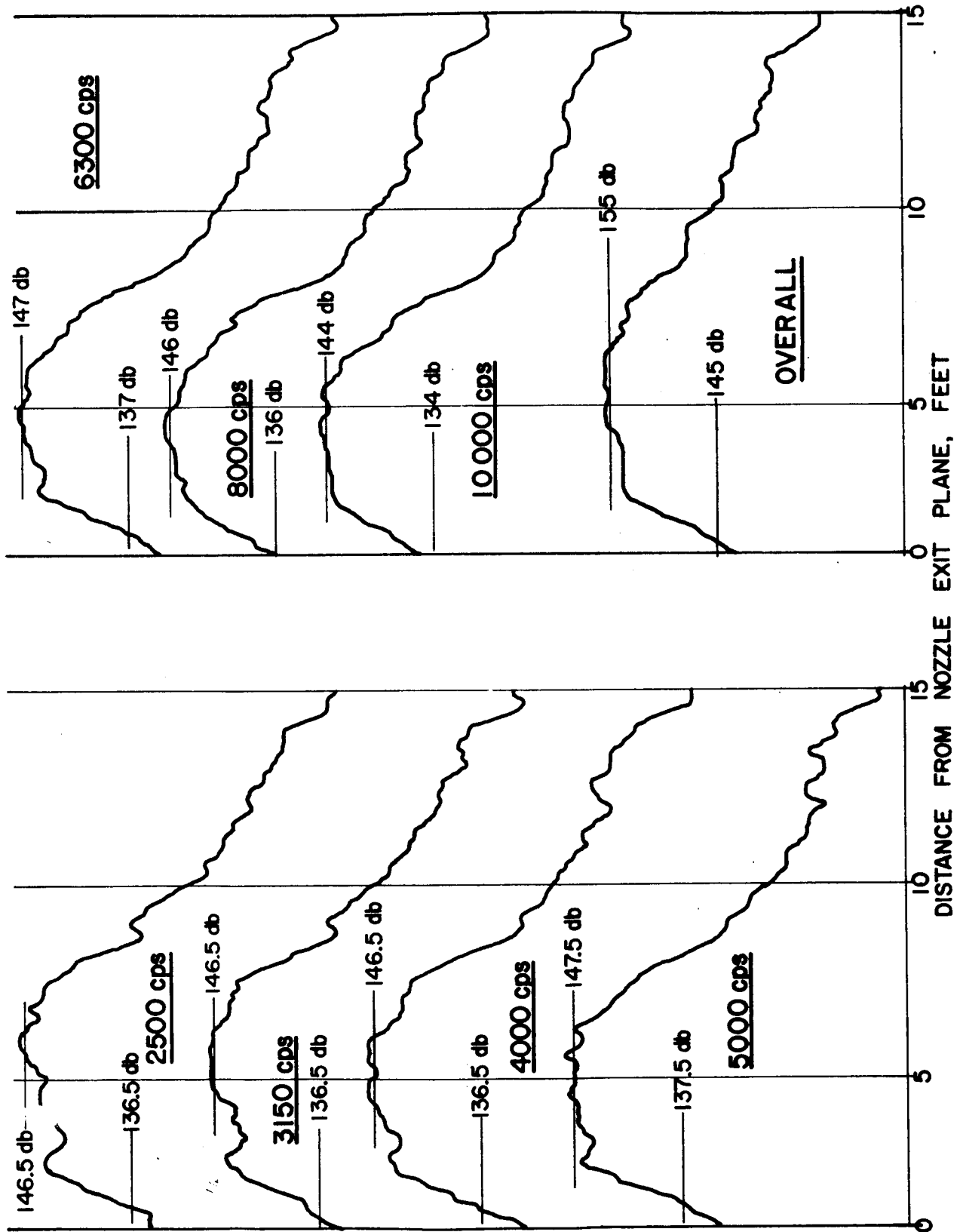


FIGURE A-2a

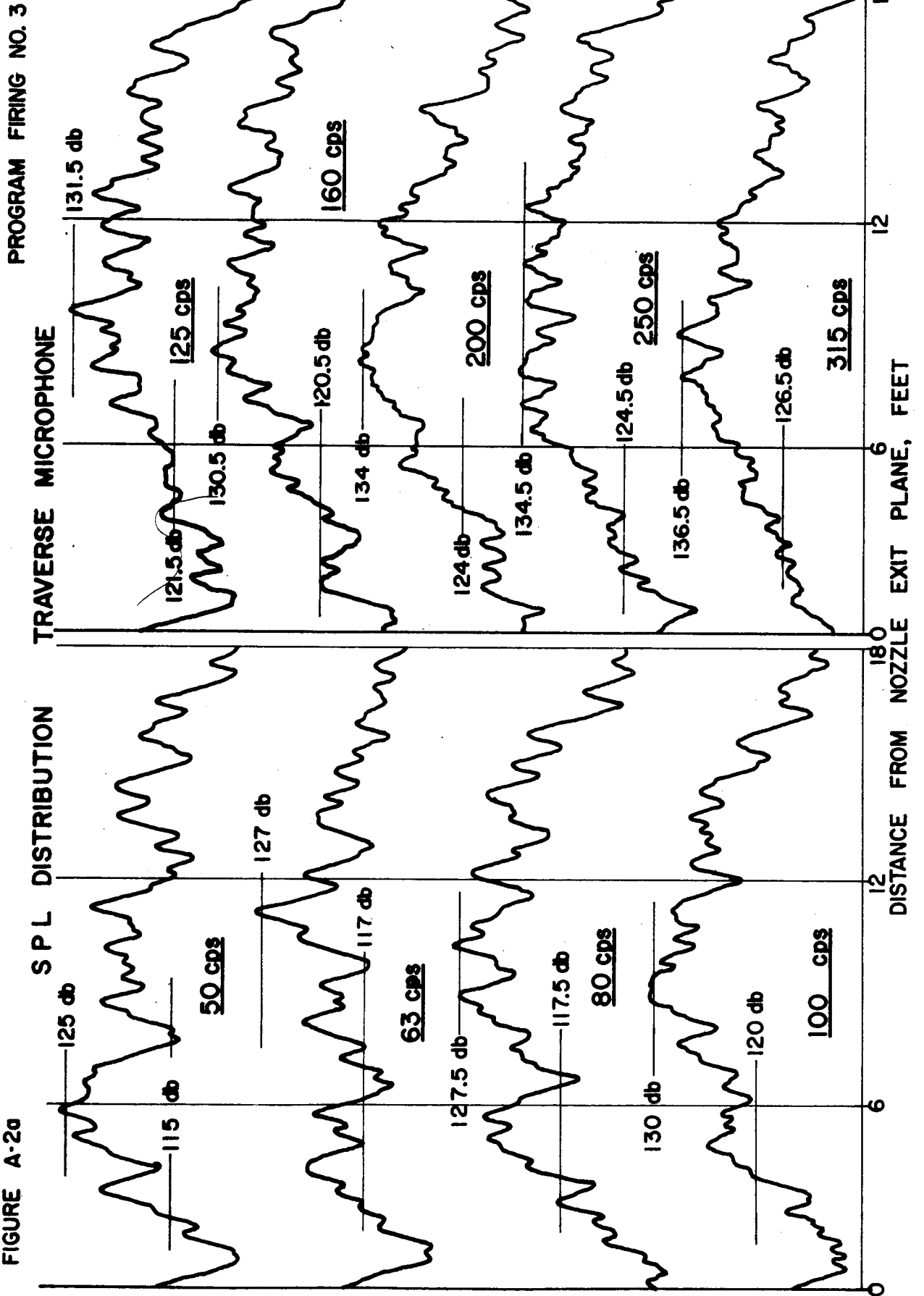


FIGURE A-2b

PROGRAM FIRING NO. 3

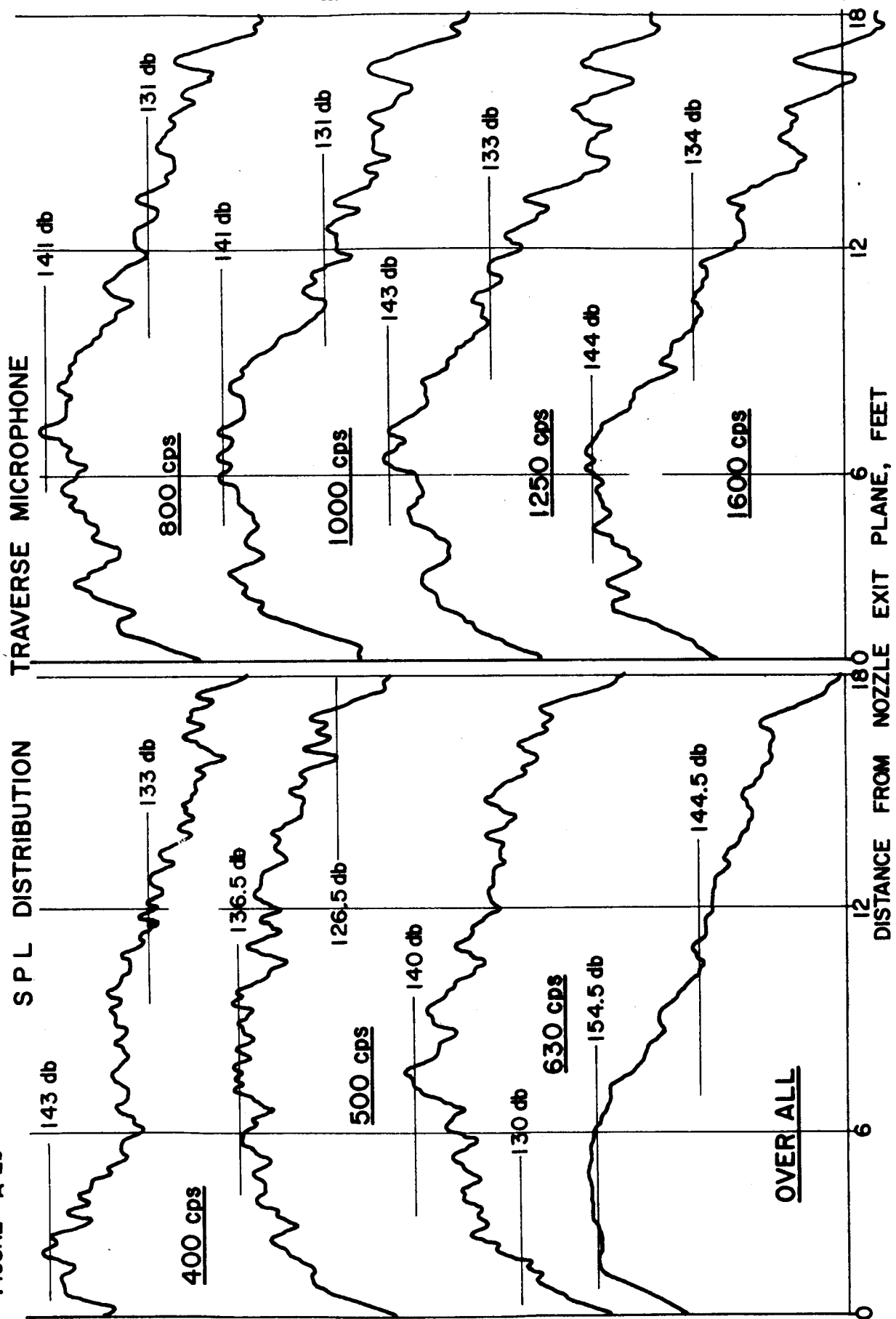


FIGURE A-2c

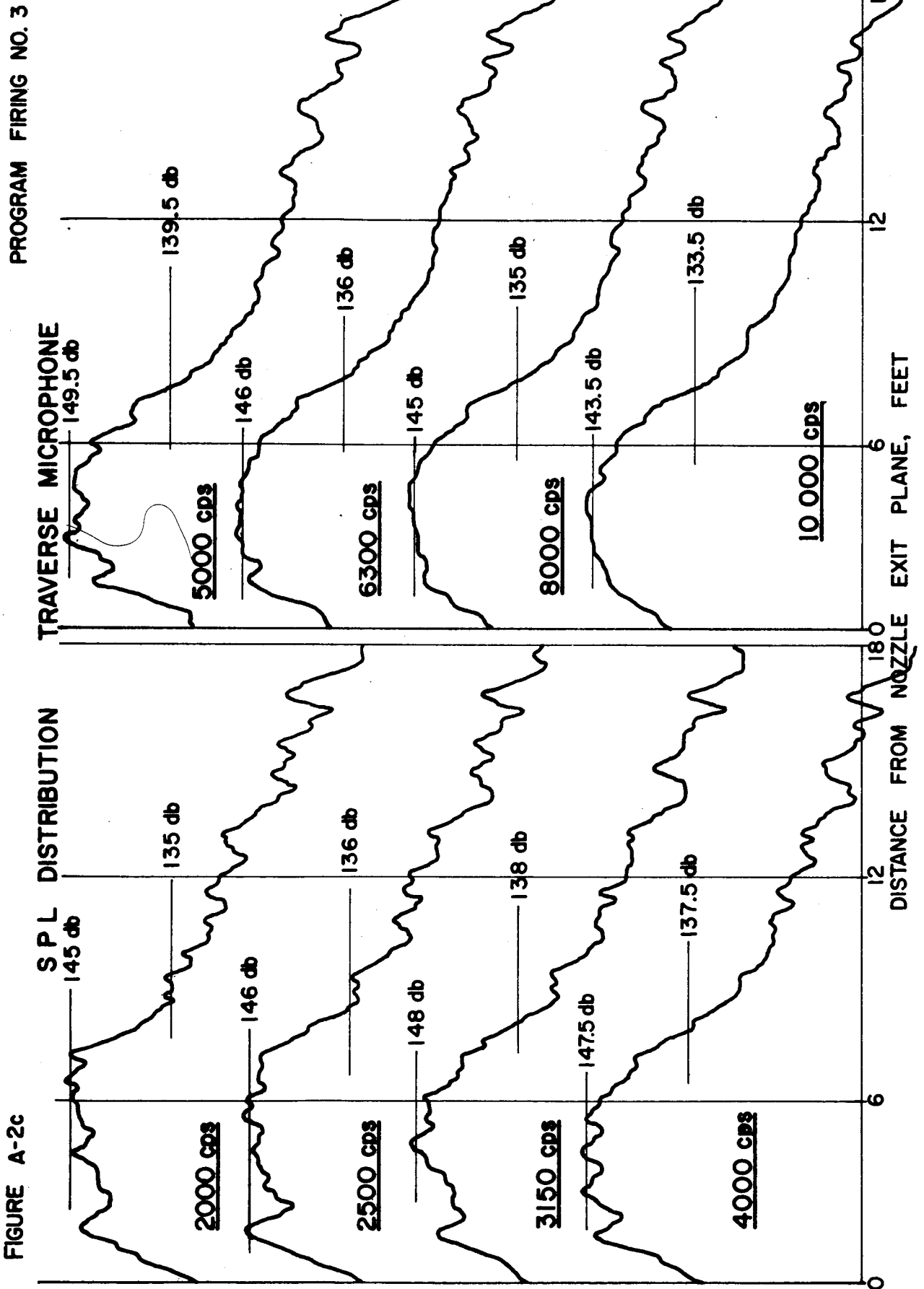
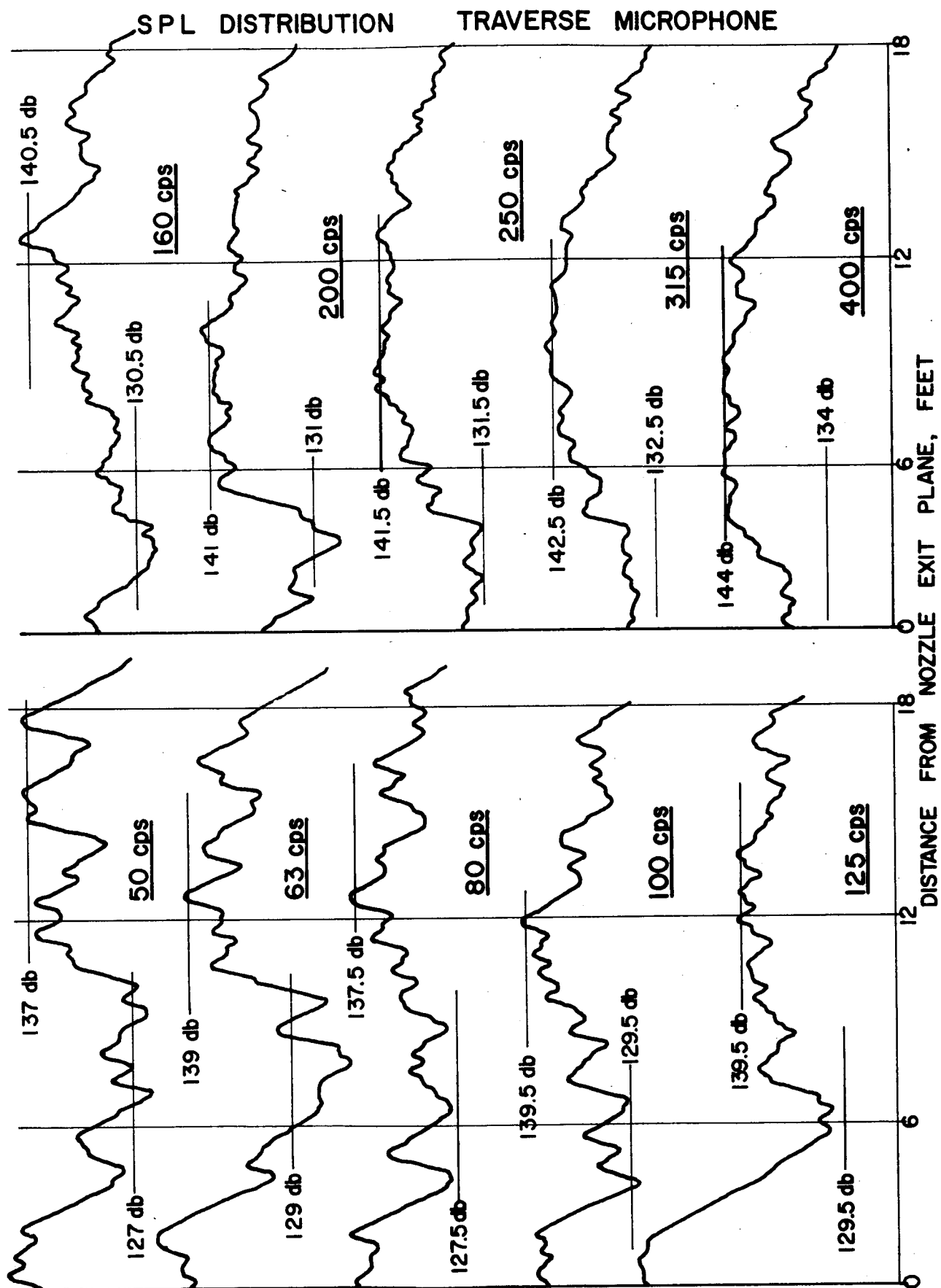


FIGURE A-3a

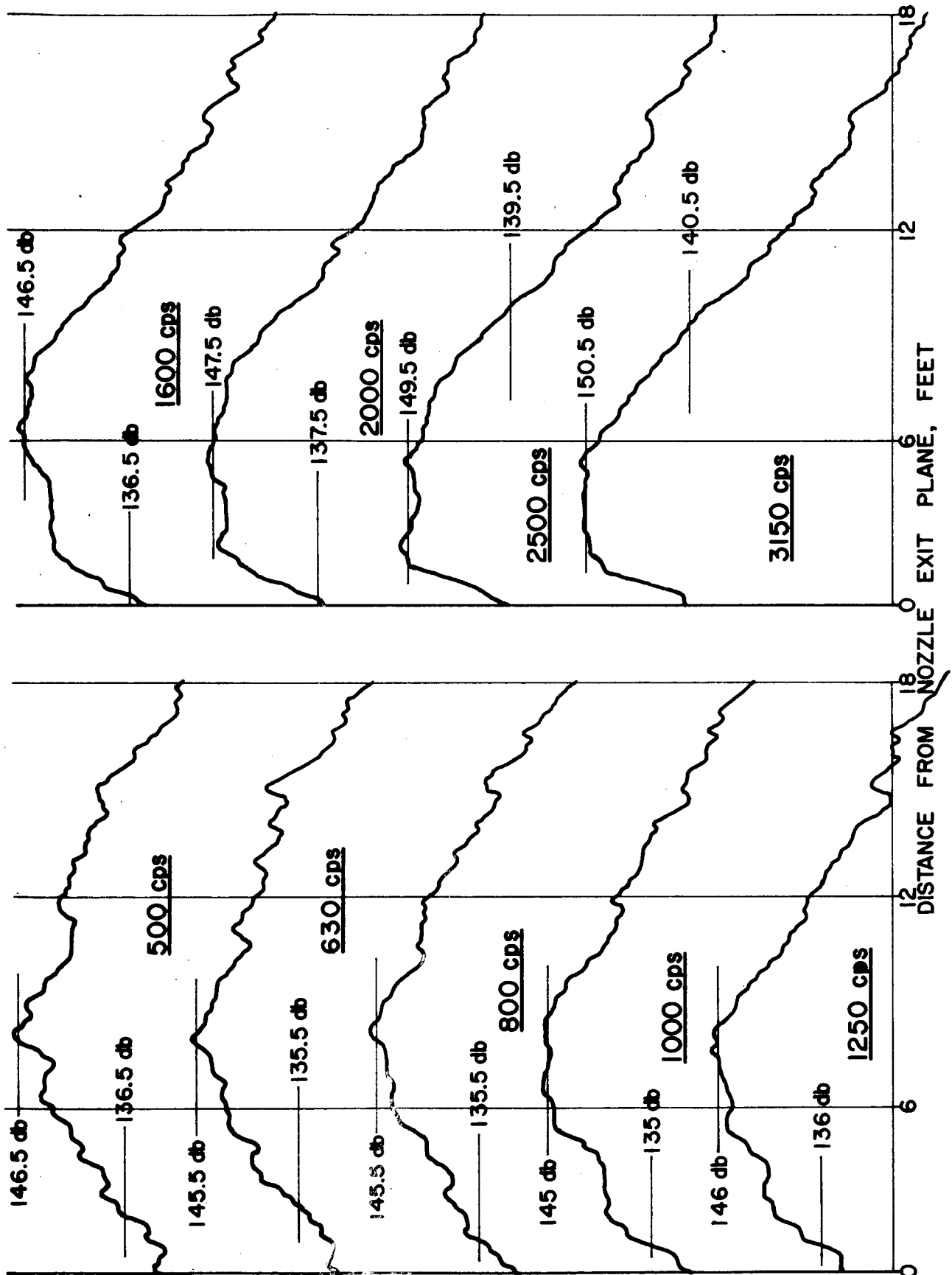


PROGRAM FIRING NO. 4

FIGURE A-3b

SPL DISTRIBUTION

TRAVERSE MICROPHONE



PROGRAM FIRING NO. 4

FIGURE A-3c

SPL DISTRIBUTION

TRAVERSE MICROPHONE

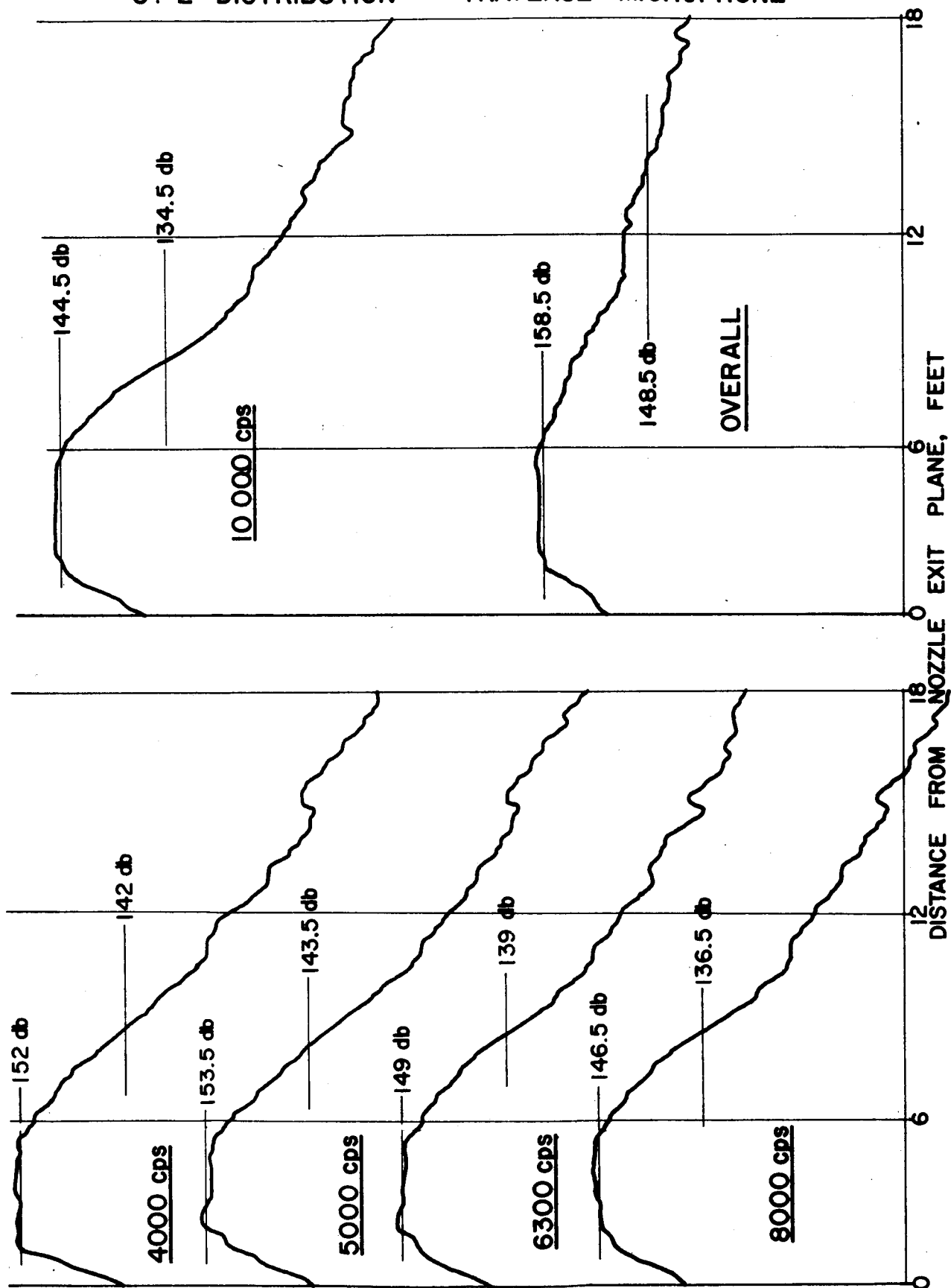


FIGURE A-4a

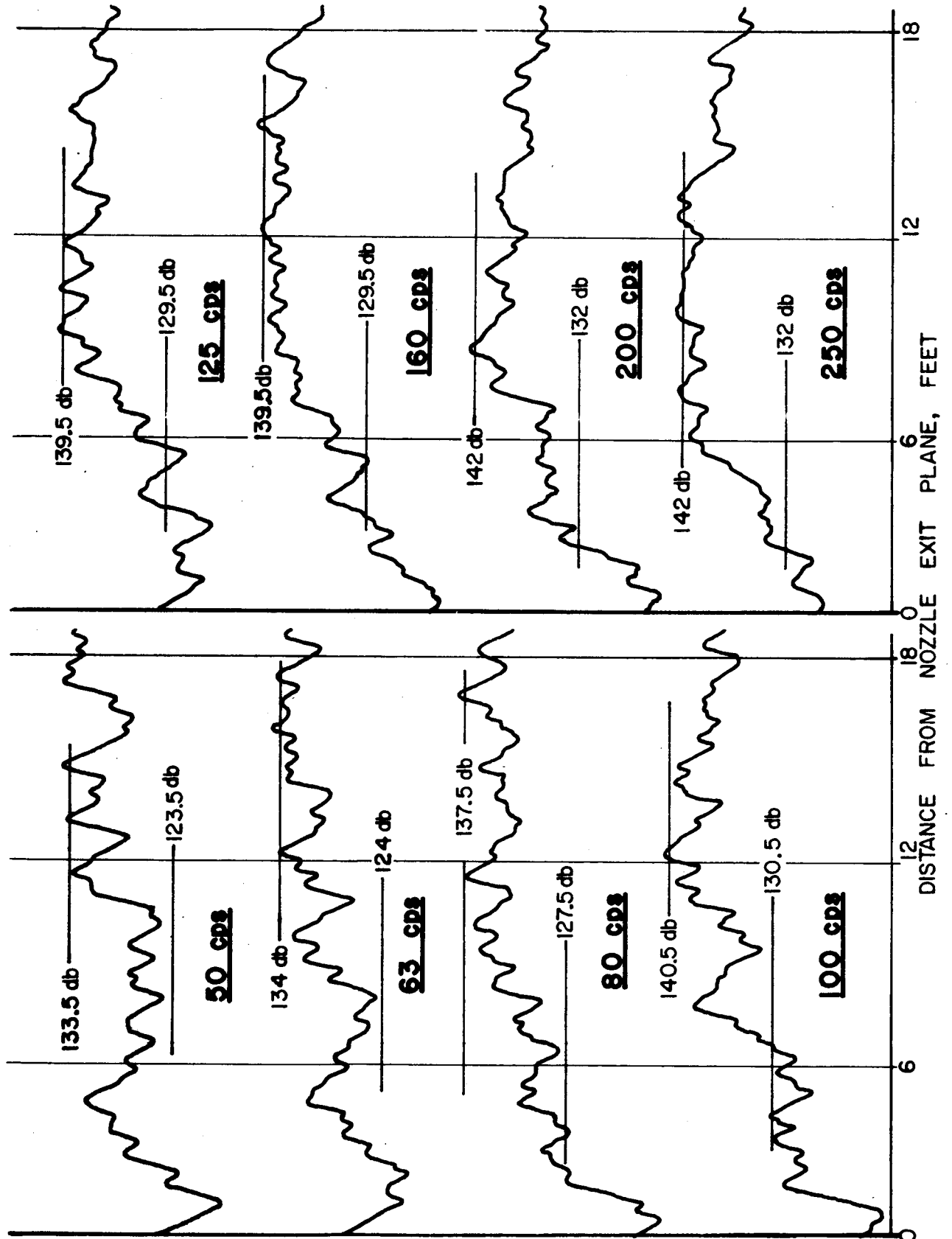
SPL DISTRIBUTION TRAVERSE MICROPHONE
PROGRAM FIRING NO. 5

FIGURE A-4b

SPL DISTRIBUTION TRAVERSE MICROPHONE
PROGRAM FIRING NO. 5

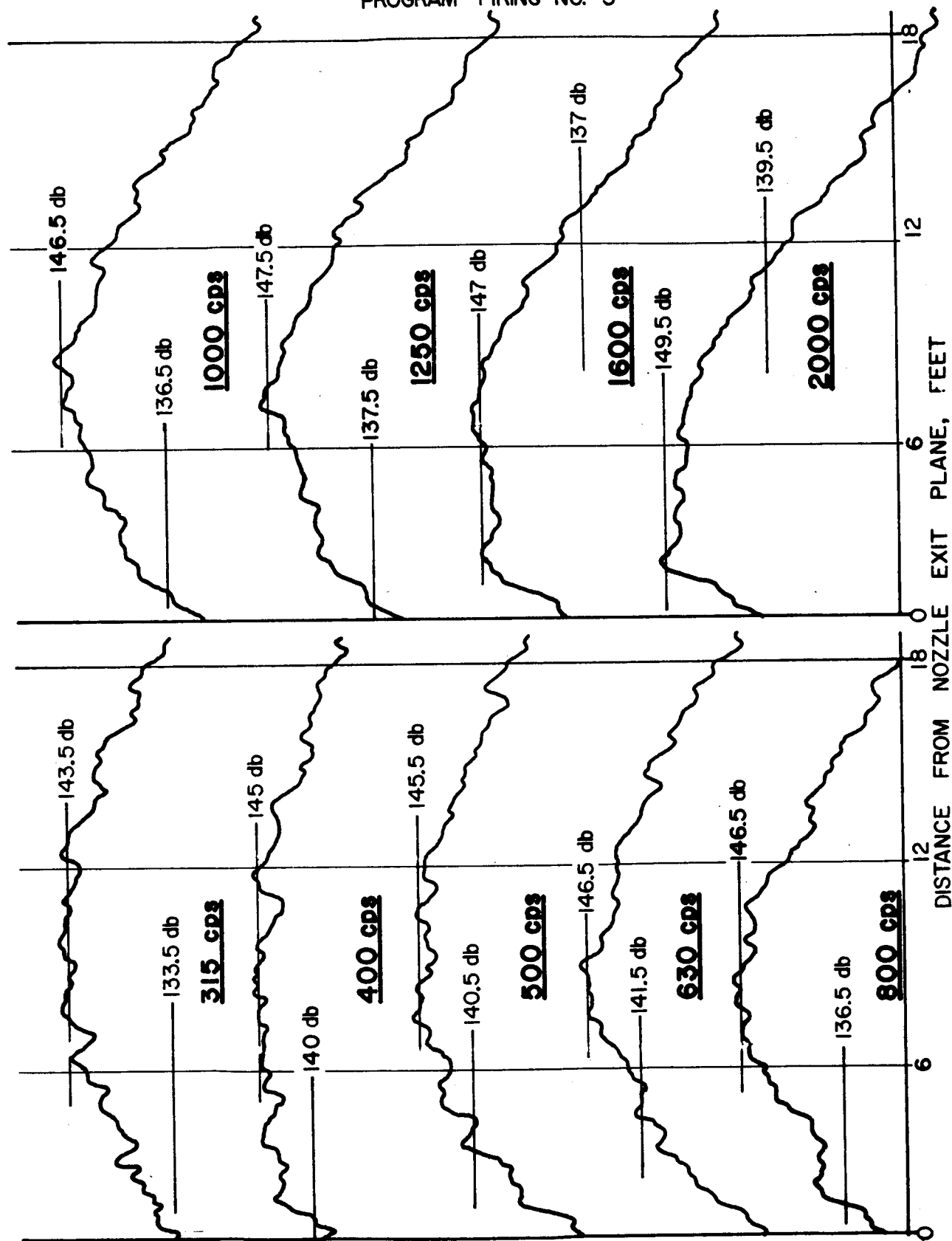
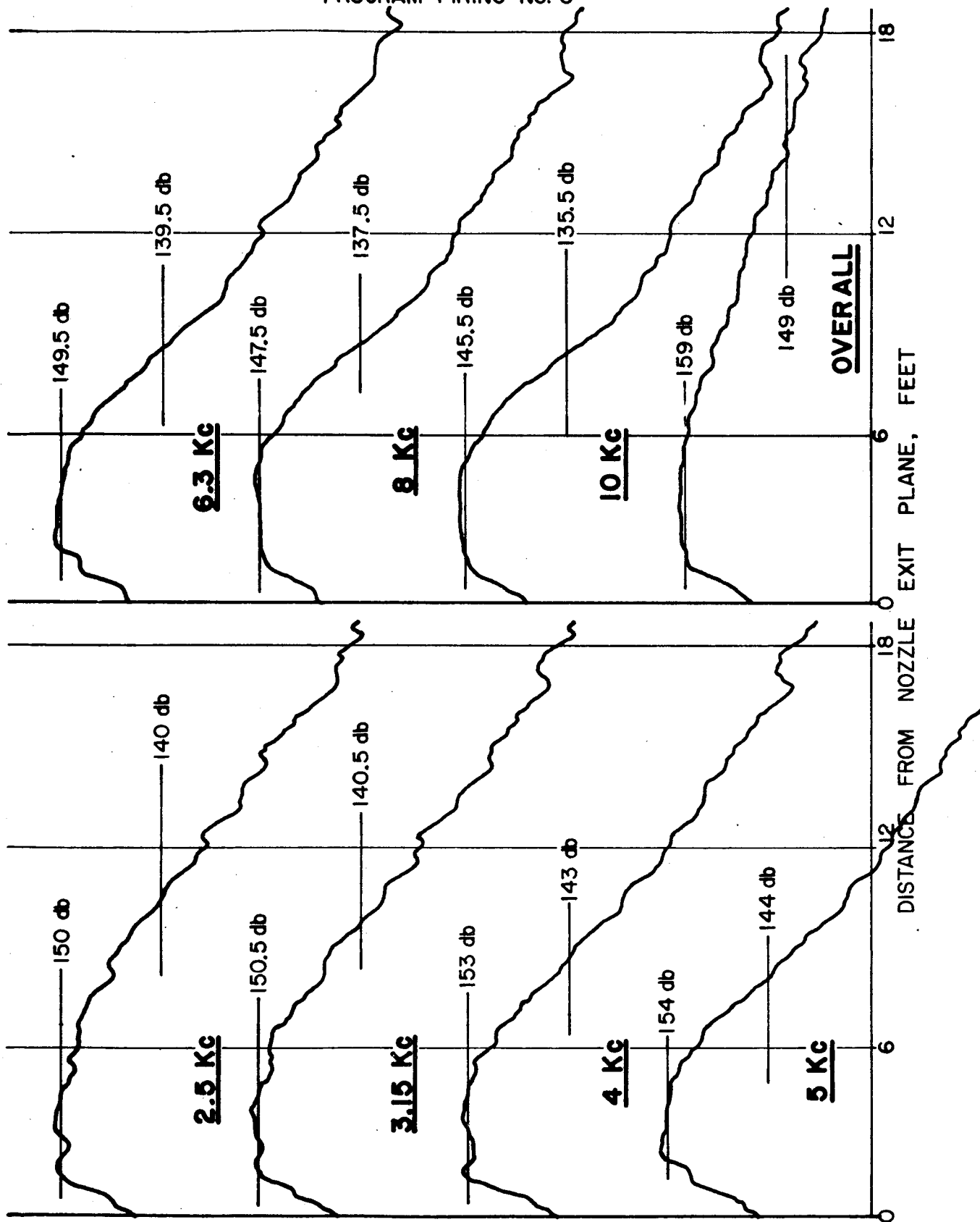


FIGURE A-4c

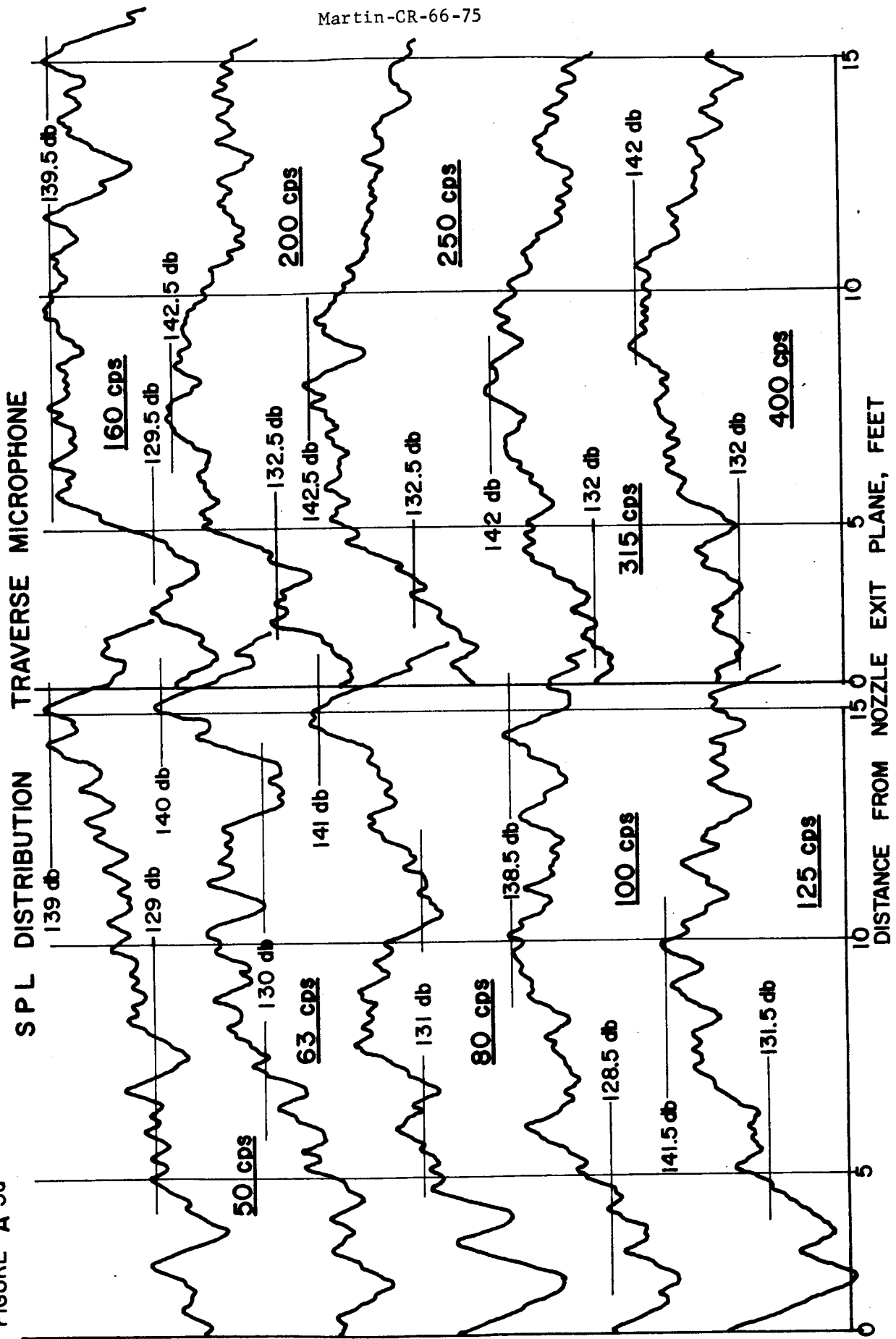
SPL DISTRIBUTION TRAVERSE MICROPHONE

PROGRAM FIRING NO. 5



PROGRAM FIRING NO. 8

FIGURE A-5a



PROGRAM FIRING NO. 8

FIGURE A-5c

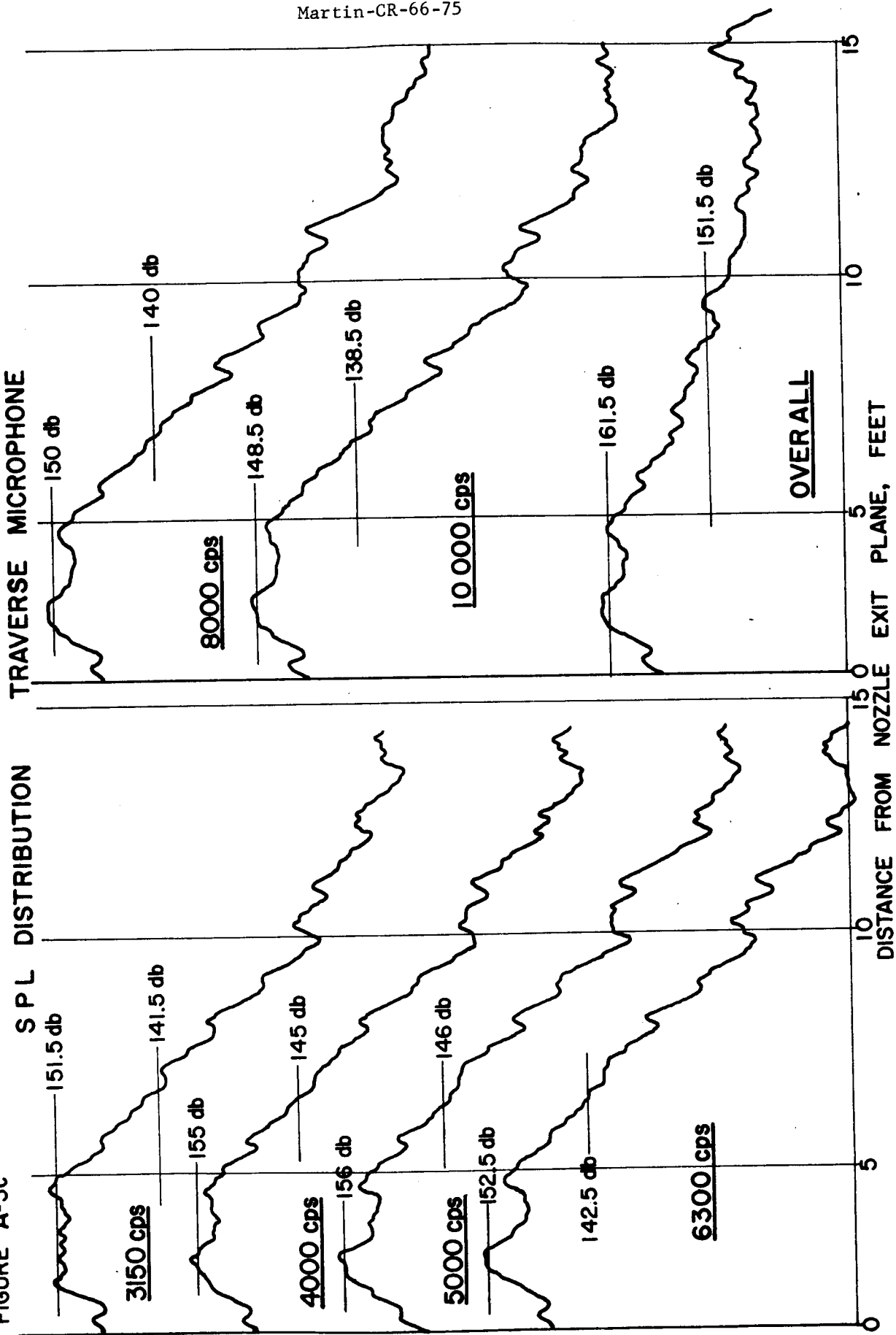


FIGURE A-6a

SPL DISTRIBUTION

TRAVERSE MICROPHONE

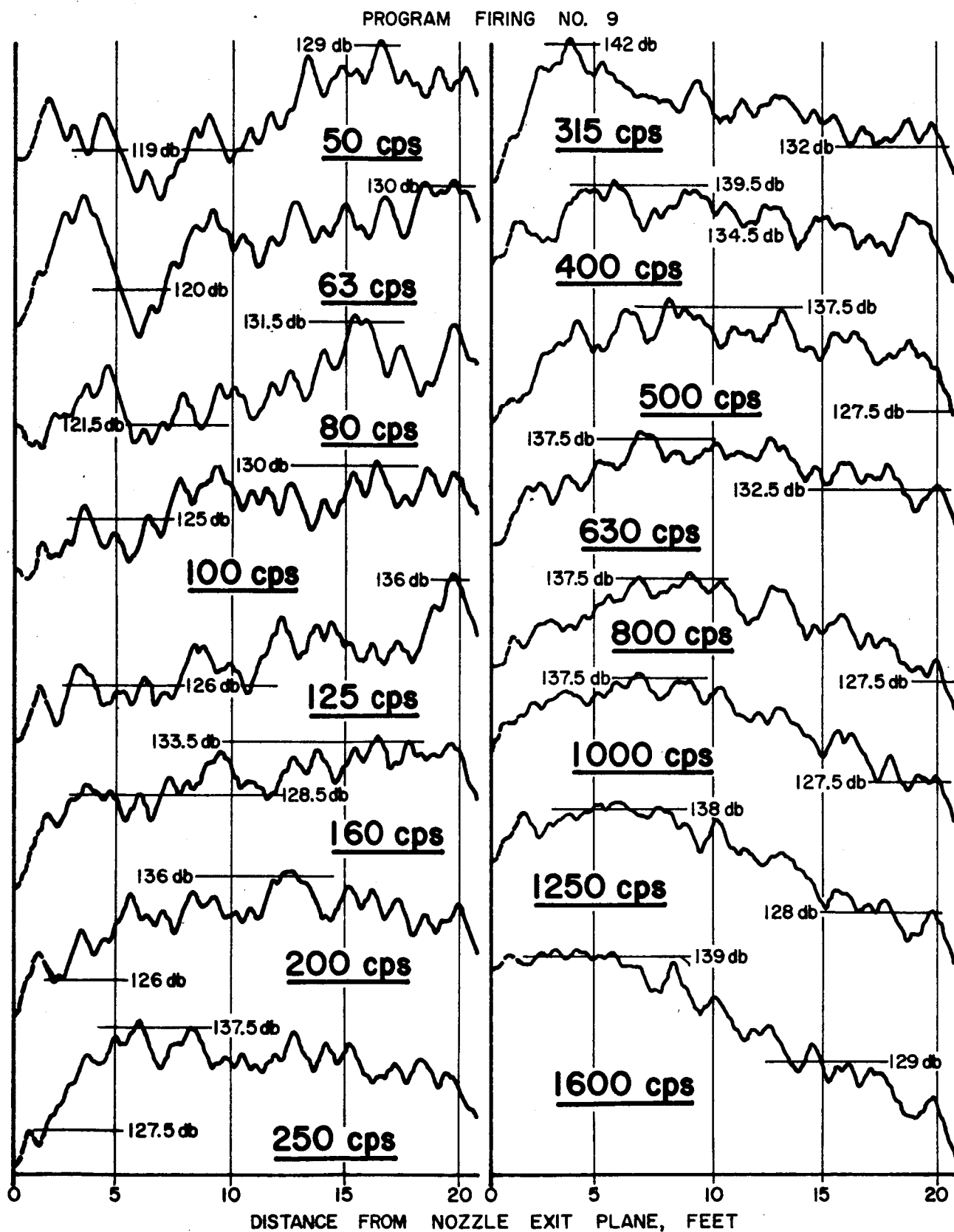


FIGURE A-6b

SPL DISTRIBUTION

TRAVERSE MICROPHONE

PROGRAM FIRING NO. 9

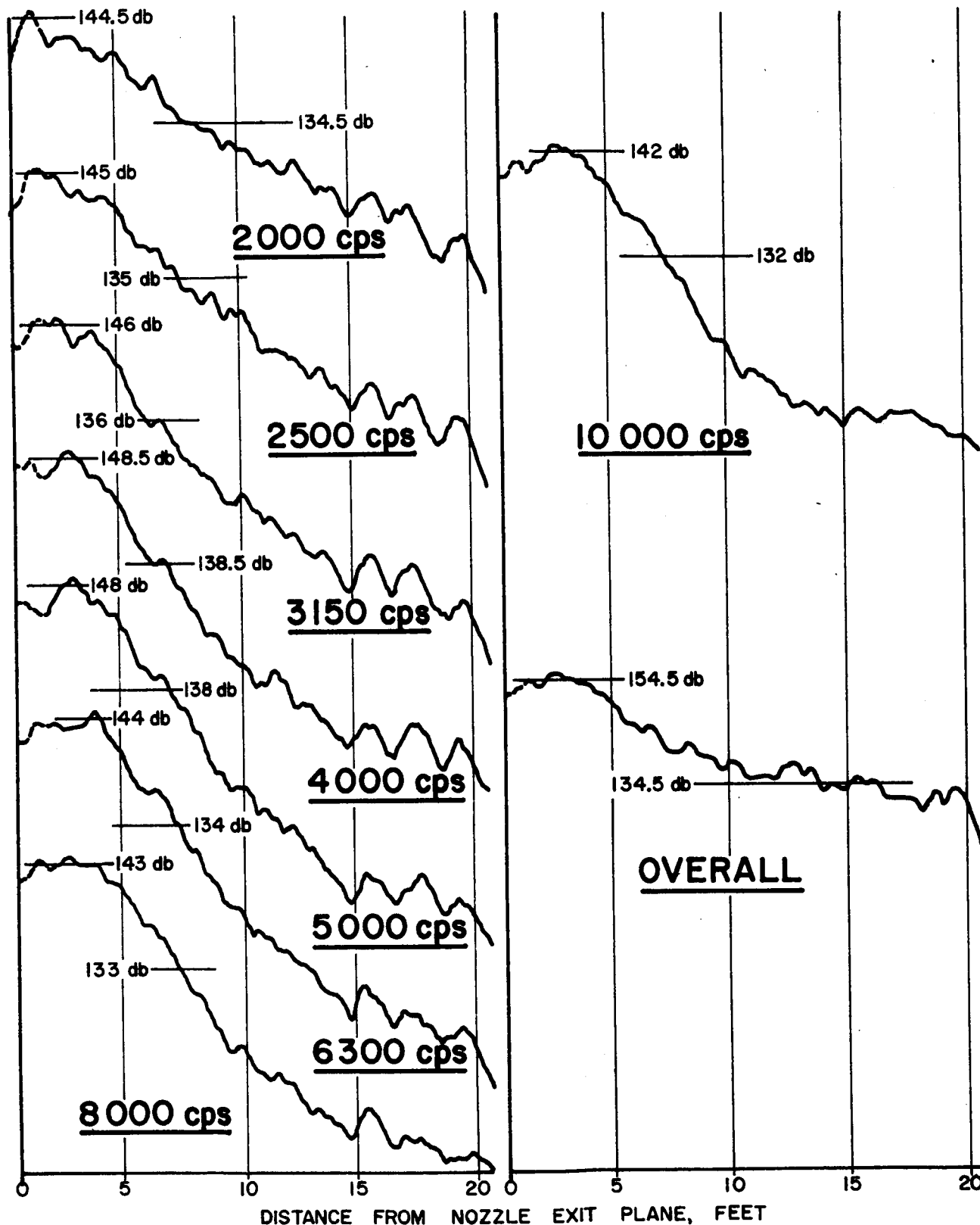


FIGURE A-7a

SPL DISTRIBUTION

TRAVERSE MICROPHONE

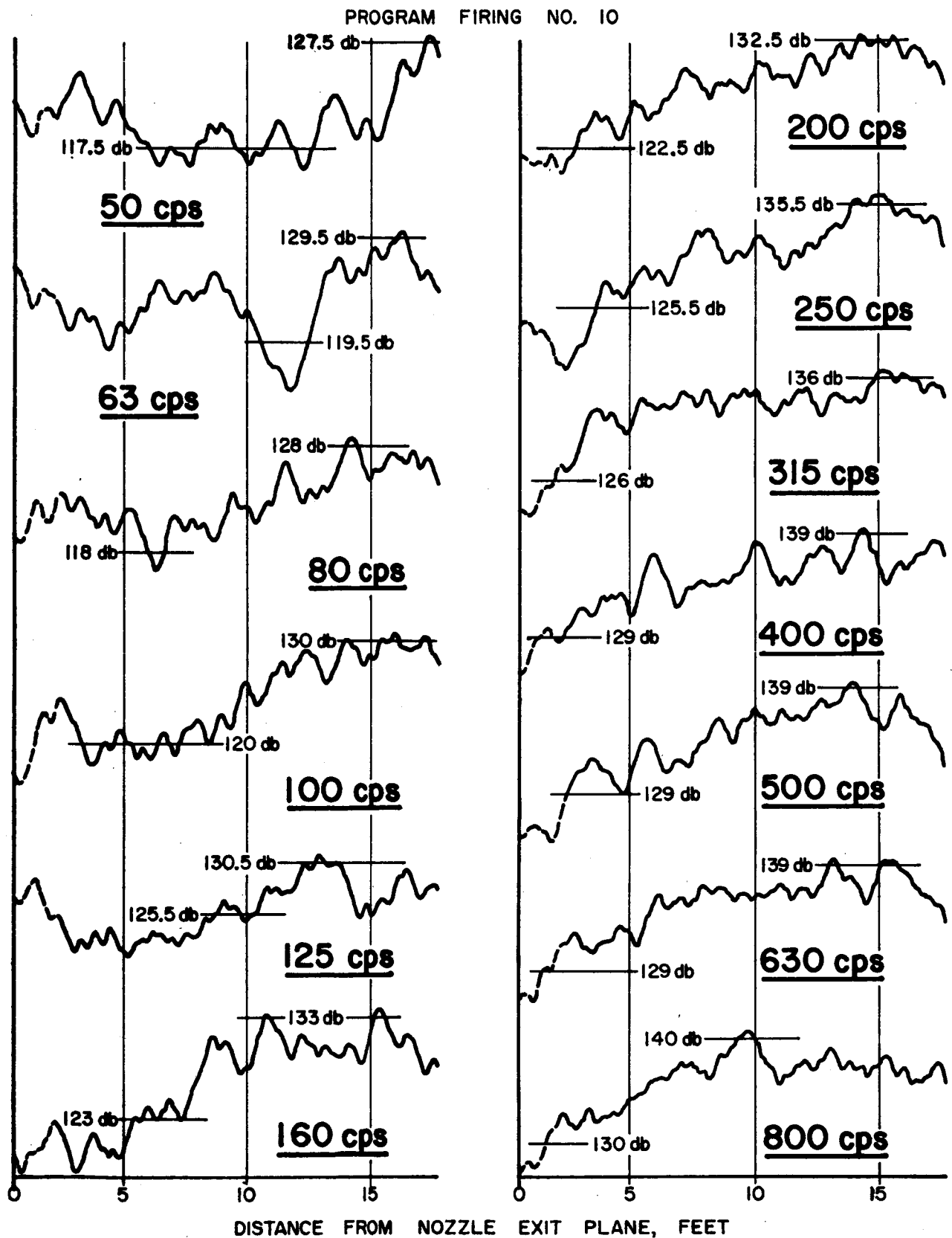
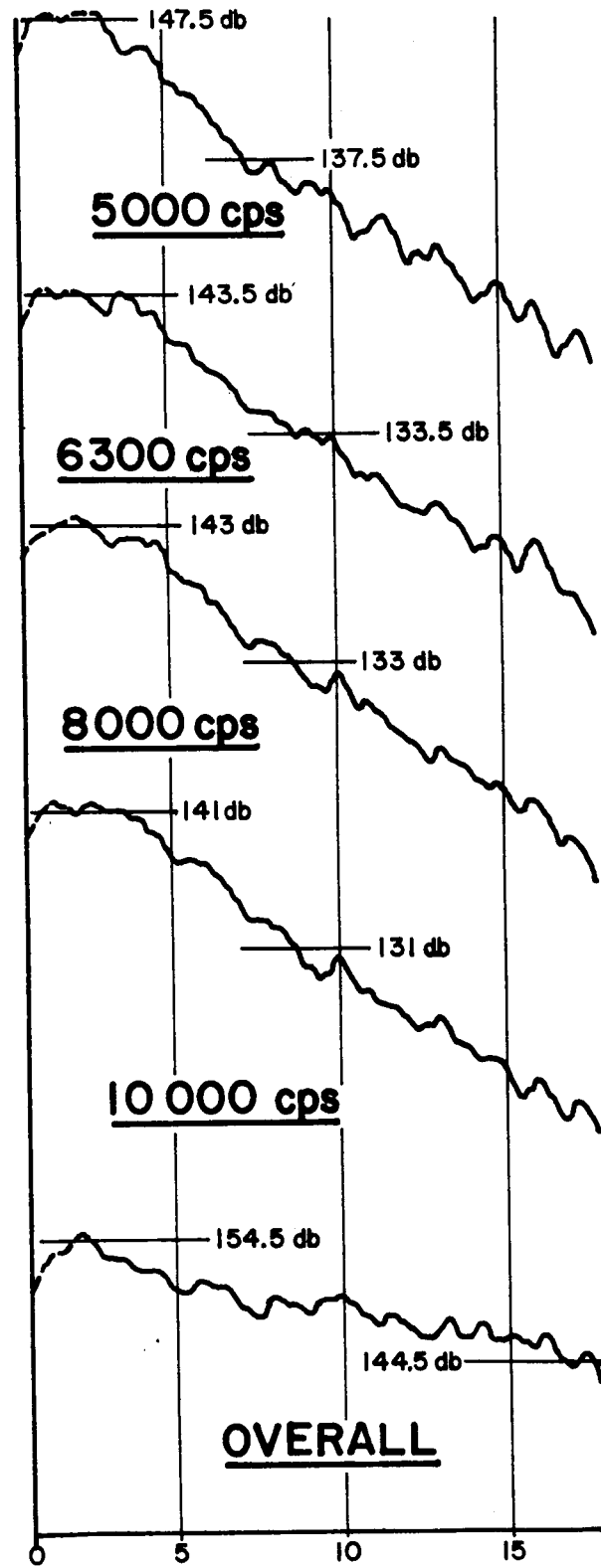
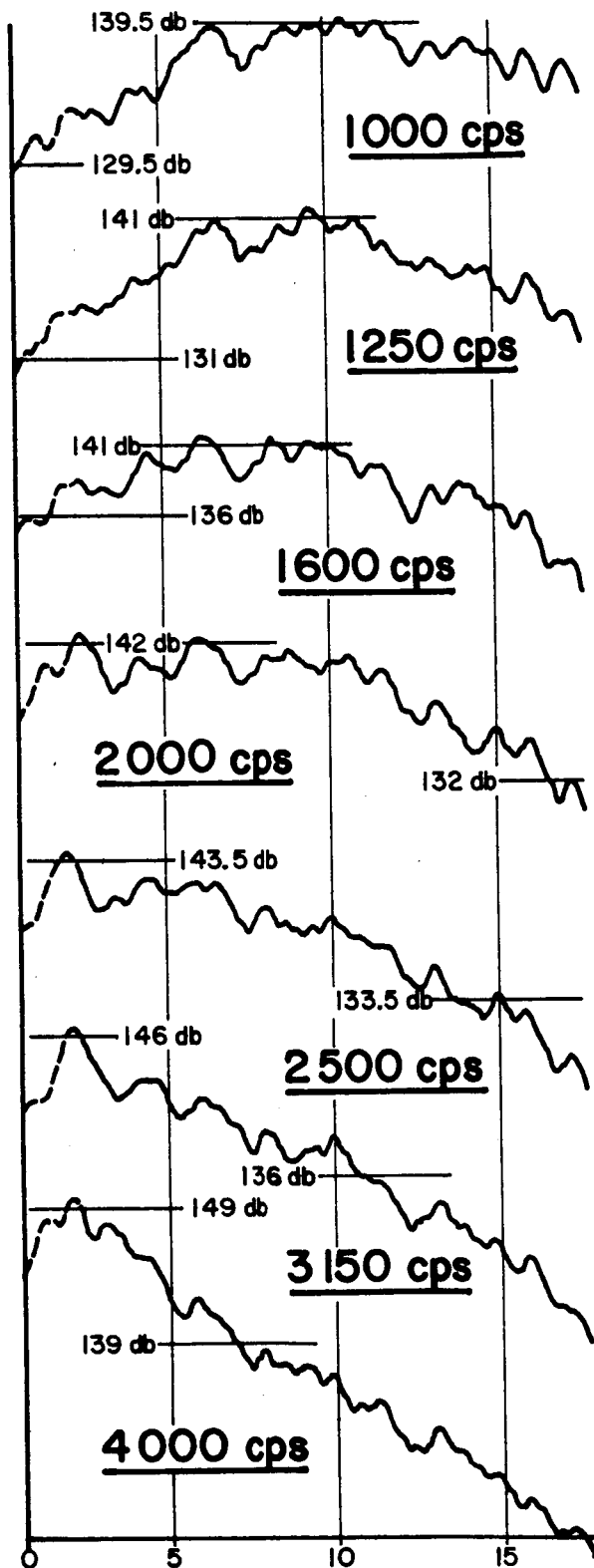


FIGURE A-7b

SPL DISTRIBUTION

TRAVERSE MICROPHONE

PROGRAM FIRING NO. 10



DISTANCE FROM NOZZLE EXIT PLANE, FEET